

Seismic Performance of Flat Plate Structures in Punching Shear Modelled with Non-Layered and Layered Shell Elements

by

Kashfia Nazneen

MASTER OF SCIENCE IN CIVIL ENGINEERING (STRUCTURAL)



DEPARTMENT OF CIVIL ENGINEERING
BANGLADESH UNIVERSITY OF ENGINEERING AND TECHNOLOGY

June, 2023

Seismic Performance of Flat Plate Structures in Punching Shear Modelled with Non-Layered and Layered Shell Elements

by

Kashfia Nazneen

A thesis submitted to the Department of Civil Engineering,
Bangladesh University of Engineering and Technology (BUET), Dhaka
in partial fulfilment of the requirements for the degree
of

MASTER OF SCIENCE IN CIVIL ENGINEERING (STRUCTURAL)




DEPARTMENT OF CIVIL ENGINEERING
BANGLADESH UNIVERSITY OF ENGINEERING AND TECHNOLOGY

June, 2023

The thesis titled “SEISMIC PERFORMANCE OF FLAT PLATE STRUCTURES IN PUNCHING SHEAR MODELLED WITH NON-LAYERED AND LAYERED SHELL ELEMENTS” submitted by Kashfia Nazneen, Roll No.: 0417042353, Session: April 2017, has been accepted as satisfactory in partial fulfillment of the requirement for the degree of Master of Science in Civil Engineering (Structural) on 11th June, 2023.

BOARD OF EXAMINERS



11/06/2023

Dr. Raquib Ahsan
Professor
CE, BUET, Dhaka.

Chairman
(Supervisor)



Dr. Abu Siddique
Professor and Head
CE, BUET, Dhaka.

Member
(Ex-Officio)



Dr. Tahsin Reza Hossain
Professor
CE, BUET, Dhaka.

Member



Dr. Sk. Sekender Ali
Ex-Professor
Department of Civil Engineering,
Bangladesh University of Engineering and Technology, Dhaka;
Flat 9A, Concord Bithi Villa, Plot-42B, Road-41, Gulshan-2,
Dhaka.

Member
(External)

CANDIDATE'S DECLARATION

It is hereby declared that except for the contents where specific references have been made to the work of others, the studies contained in this thesis is the result of investigations carried out by the author. No part of this thesis has been submitted to any other University or other educational establishment for a Degree, Diploma or other qualification (except for publication).

Signature of the Candidate

Kashfia Nazneen

KASHFIA NAZNEEN

DEDICATION

This thesis is dedicated to my beloved parents

ACKNOWLEDGEMENT

First and foremost, the author wishes to convey gratitude to Almighty Allah for enabling her to complete this thesis.

The author wishes to express her sincere appreciation and heartfelt thanks to her thesis supervisor, Professor Dr. Raquib Ahsan, Department of Civil Engineering, Bangladesh University of Engineering and Technology (BUET), for his constant guidance, supervision, keen interest, and resource management in ensuring the successful completion of the project. His valuable advice has been incredibly beneficial to the author.

The author wants to extend her gratitude to Dr. Abu Siddique, Dr. Tahsin Reza Hossain, and Dr. Sk. Sekender Ali, members of the thesis defense committee, for their advice and support in reviewing this thesis.

A very special debt of gratitude is owed to the author's mother, who died before this thesis could be completed. This would not have been possible without her encouragement, support, and love. Additionally, the author wishes to express her gratitude to her father and sisters for their unwavering support and cooperation throughout this study. Finally, the author would like to express her gratitude to her husband, father-in-law, and mother-in-law for having faith in her and encouraging her to continue pursuing this research.

ABSTRACT

The seismic performance of flat plate structures is a critical area of research in the field of structural engineering. Nonlinear analysis through modeling software considers the nonlinear behavior of materials, such as concrete and steel, which allows for a more realistic prediction of the structural response to extreme lateral loading conditions. This research aims to study the nonlinear effect on punching shear due to seismic loading in flat plates using layered shell models and compare them with thick shell models. Three types of aspect ratios type A (53 m \times 29.26 m), type B (53 m \times 22.4 m) and type C (38.41 m \times 29.26 m) have been used in this research, with a panel size of 6.4 m \times 6.858 m. Number of stories, material properties and slab thickness have been varied to generate total 36 model types.

All models have been designed using layered shell slab and thick shell slab to perform parametric study using the nonlinear static analysis procedure. Three earthquake hazard levels Maximum Considered Earthquake (MCE), Design Basis Earthquake (DBE) and Serviceability Earthquake (SE) have been taken into consideration to analyze the seismic performance of structures. The buildings are designed as dual system frame structure with special moment resisting frame in moderate seismic zone (Zone 2) as per BNBC 2020. 'Displacement Coefficient Method' according to ASCE 41 has been used to determine nonlinear behavior of the structures, such as - maximum displacement, base shear capacity, hinge formation and punching shear stress.

The layered shell models exhibit higher stiffness than thick shell models in linear static analysis resulting in lower displacement and drift. Nonlinear static analysis also indicates better performance of layered shell models including higher base shear capacity, a smaller number of plastic hinges and lower plastic rotation. None of the models exhibited punching failure as the observed punching shear stresses were considerably lower than the slab capacity. The stress resultants obtained from layered shell models are much higher than the thick shell models. The results of this research will provide insights into a preferable analytical modeling technique for seismic design using layered shell elements and aid researchers in understanding punching shear behavior in seismic analysis of flat plate structures.

TABLE OF CONTENTS

CANDIDATE’S DECLARATION	iii
DEDICATION	iv
ACKNOWLEDGEMENT	v
ABSTRACT.....	vi
TABLE OF CONTENTS.....	v
LIST OF TABLES	viii
LIST OF FIGURES	viii
LIST OF TECHNICAL SYMBOLS AND TERMS.....	xii
LIST OF ABBREVIATIONS	1
Chapter 1	2
INTRODUCTION	2
1.1 General	2
1.2 Background of the Study	2
1.3 Objectives of the Research	3
1.4 Organization of the Thesis	3
Chapter 2	5
LITERATURE REVIEW.....	5
2.1 Introduction	5
2.2 Flat Plate Structures.....	5
2.2.1 Modes of Failure of Flat Plates	6
2.2.2 Previous Study on Flat Plate Structures	7
2.2.3 Provisions of Flat Plate as Per Various Design Codes.....	13
2.3 Earthquake Trend in Bangladesh.....	14
2.4 Seismic Design Concept.....	19
2.5 Earthquake Hazard Level	21
2.5.1 Serviceability Earthquake (SE)	21
2.5.2 Design Earthquake (DE)	21
2.5.3 Maximum Earthquake (ME)	22

2.6	Seismic Design Method.....	22
2.6.1	Response Spectrum Analysis (RSA).....	23
2.6.2	Non-Linear Time History Analysis (NTHA).....	24
2.6.3	Nonlinear Static Analysis (NSA).....	24
2.7	Elements of Nonlinear Analysis.....	30
2.7.1	Shell Element	30
2.7.2	Nodes	42
2.7.3	Hinges	43
2.8	Available Lateral-Force-Resisting Systems	45
2.8.1	Bearing Wall System.....	46
2.8.2	Building Frame System.....	46
2.8.3	Moment-Resisting Frame.....	47
2.8.4	Dual System	47
2.9	Structural Performance Levels	47
2.9.1	Immediate Occupancy Structural Performance Level (S-1)	49
2.9.2	Damage Control Structural Performance Range (S-2).....	49
2.9.3	Life Safety Structural Performance Level (S-3)	49
2.9.4	Limited Safety Structural Performance Range (S-4)	50
2.9.5	Collapse Prevention Structural Performance Level (S-5).....	50
2.10	Global Building Acceptability Limits.....	50
2.11	Remarks	52
Chapter 3.....		54
NUMERICAL MODELLING		54
3.1	Introduction	54
3.2	Linear Static Analysis	54
3.2.1	Design Codes	54
3.2.2	Material Specifications.....	54
3.2.3	Loading Criteria	54
3.2.4	Load Combinations	57
3.2.5	Boundary Conditions	59
3.2.6	Model Element Details.....	59
3.2.7	Base Model	61
3.2.8	Model Variations.....	63

3.3	Nonlinear Static or Pushover Analysis (NLSA).....	66
3.3.1	Hinge Assignment.....	66
3.3.2	Gravity Load	67
3.3.3	Pushover Load.....	67
3.3.4	Response Spectrum	68
3.3.5	Analysis Procedure.....	69
3.4	Remarks.....	70
Chapter 4	71
RESULTS AND DISCUSSIONS		71
4.1	Introduction	71
4.2	Model Validation.....	71
4.3	Structural Performance from Linear Static Analysis	80
4.3.1	Base Model Analysis	80
4.3.2	Comparison Between Model Variations	85
4.4	Structural Performance from Nonlinear Static Analysis.....	94
4.4.1	Plastic Hinge	94
4.4.2	Base Shear and Maximum Top Displacement.....	98
4.4.3	Capacity curve.....	101
4.4.4	Slab Displacement at Different Earthquake Level.....	104
4.4.5	Slab Performance Check	105
4.4.6	Punching Shear	110
4.5	Remarks.....	119
Chapter 5	121
CONCLUSIONS AND RECOMMENDATIONS		121
5.1	Conclusions	121
5.2	Recommendations for Future Study.....	122
REFERENCES.....		123
APPENDIX A.....		126
MODEL DETAILS.....		126
A.1	Reinforcement Details	126
APPENDIX B		133
DUAL SYSTEM CHECK		133

LIST OF TABLES

Table 2.1: Methods of Analysis of Flat Plate Structure Followed by Different Codes (Khan, 2018)	14
Table 2.2: List of Major Regional Earthquakes (BNBC, 2020), (<i>NCEI Hazard Earthquake Search</i> , n.d.).....	17
Table 2.3: Modeling Parameters and Numerical Acceptance Criteria for Nonlinear Procedures—Two-Way Slabs and Slab–Column Connections (ASCE 41-17, 2017)51	51
Table 3.1: Considered Loads.....	55
Table 3.2: Structural Configurations of Building Models	66
Table 4.1: Material Property and Dimensions of Slabs Tested by Elstner and Hognestad (1956).....	72
Table 4.2: Reinforcement Details of Slabs Tested by Elstner and Hognestad (1956)73	73
Table 4.3: Punching Shear Stress Comparison	79
Table 4.4: Drift Check for Earthquake (Layered Shell in X-Direction)	82
Table 4.5: Drift Check for Earthquake (Layered Shell in Y-Direction)	82
Table 4.6: Drift Check for Earthquake (Thick Shell in X-Direction).....	83
Table 4.7: Drift Check for Earthquake (Thick Shell in Y-Direction).....	83
Table 4.8: Plastic Hinge States at Target Displacement (Layered Shell)	95
Table 4.9: Plastic Hinge States at Target Displacement (Thick Shell).....	97
Table 4.10: Base Shear and Corresponding Maximum Top Displacement (As Per ASCE 41-13).....	98
Table 4.11: Slab Displacement at Different Earthquake Level.....	104
Table 4.12: Modeling Parameters and Numerical Acceptance Limit for All Models	105
Table 4.13: Performance Level of Slab Based on Global Acceptance Limit (Layered Shell)	107
Table 4.14: Performance Level of Slab Based on Global Acceptance Limit (Thick Shell)	109
Table 4.15: Punching Shear for MCE Level Earthquake.....	114
Table 4.16: Punching Shear for DBE Level Earthquake	117
Table 4.17: Punching Shear for SE Level Earthquake.....	118

LIST OF FIGURES

Figure 2.1: Punching Shear Failure (Nilson et al., 2009).....	6
Figure 2.2: Plate Boundaries and Fault Zones Surrounding Bangladesh (BNBC, 2020)	15
Figure 2.3: Earthquake Magnitudes in Different Areas of Bangladesh (BNBC, 2020)	16
Figure 2.4: Seismic Zoning Map of Bangladesh (BNBC, 2020).....	23
Figure 2.5: Determination of Performance Point According to Capacity Spectrum Method (Zameeruddin and Sangle, 2016).....	26
Figure 2.6: Determination of Target Displacement by Displacement Coefficient Method (FEMA 273, 1997).....	28
Figure 2.7: Component Force vs. Deformation Curve (a) Type 1 Curve, (b) Type 2 Curve, (c) Type 3 Curve (Fema 356, 2000).....	30
Figure 2.8: Shell Section Material Angle (CSI, 2016).....	33
Figure 2.9: Four-Layer Shell, Showing The Reference Surface, The Names Of The Layers, And The Distance And Thickness For Layer “C” (CSI, 2016).....	34
Figure 2.10: Positive and Negative Faces of Shell Element in ETABS (CSI, 2023).	37
Figure 2.11: Distribution of Internal F11 Force (CSI, 2023).....	38
Figure 2.12: The Positive Directions for Shell Element Internal Forces F11, F22, F12, V13 and V23 (CSI, 2023).	39
Figure 2.13: Direct and Shearing Stress Components of Shell Elements in ETABS (CSI, 2023).....	40
Figure 2.14: The Points Where ETABS Reports the Shell Element Internal Stress Values for the Positive 1 Face Internal Stresses (CSI, 2023).	41
Figure 2.15: The Positive Directions for Shell Element Internal Stresses S11, S22, S12, S13, S23, the Principal Stresses (S-Max And S-Min) and the Positive Directions for the Maximum Transverse Shear Stresses, S-Max-V (CSI, 2023).....	41
Figure 2.16: Nodes in Shell Element (a) Four-Node Quadrilateral Shell Element (b) Three-Node Triangular Shell Element (CSI, 2016).....	42
Figure 2.17: Lateral-Force-Resisting Systems: (a) Steel Moment-Resisting Frame; (b) Reinforced Concrete Moment-Resisting Frame; (c) Braced Steel Frame; (d)	

Reinforced Concrete Shear Walls; (e) Steel Frame Building with Cast-In-Place Concrete Shear Walls; (f) Steel Frame Building with In-Filled Walls of Nonreinforced Masonry. (Taranath, 2004).....	45
Figure 2.18: The A-B-C-D-E Curve for Force vs. Displacement and Moment vs. Rotation.....	48
Figure 2.19: Slab Rotation (a) Relationship between Interstorey Drift D_r , Column Rotation Ψ_{col} and Contribution of the Slab Ψ_{slab} to the Interstorey Drift Ratio Ψ_{isd} ..	52
Figure 3.1: Four-Node Shell Element	60
Figure 3.2: Slab Layer Properties	61
Figure 3.3: Plan of Base Building Model Type-A	62
Figure 3.4: 3d View of Base Building Model Type A.....	63
Figure 3.5: Building Type-B	64
Figure 3.6: Building Type-C	65
Figure 4.1: Maximum Deflection of Slab A-1a for Varying Mesh Size.....	72
Figure 4.2: Test Slab Used by Elstner and Hognestad (1956)	73
Figure 4.3: Maximum Deflection Observed in Plate A-1a	73
Figure 4.4: Maximum Deflection Observed in Plate A-7b.....	74
Figure 4.5: Load vs. Deflection for Plate A-1a.....	74
Figure 4.6: Load vs. Deflection for Plate A-7b.....	75
Figure 4.7: Observed Stress in Layered Shell FE Model A-1a (a) V13 (b) V23 (c) S_{maxV}	77
Figure 4.8: Observed Stress in Layered Shell FE Model A-7b (a) V13 (b) V23 (c) S_{maxV}	79
Figure 4.10: Story Height vs. Lateral Displacement (Base Model).....	80
Figure 4.11: Story Height vs. Story Drift (Base Model).....	81
Figure 4.12: Story Height vs. Story Shear (Base Model)	84
Figure 4.13: Story Height vs. Stiffness (Base Model)	84
Figure 4.14: Height vs. Lateral Displacement (Type A) (a) Layered Shell (X-Direction), (b) Layered Shell (Y- Direction), (c) Thick Shell (X- Direction), (d) Thick Shell (Y- Direction).....	87

Figure 4.15: Height vs. Story Drift (Type A) (a) Layered Shell (X- Direction), (b) Layered Shell (Y- Direction), (c) Thick Shell (X- Direction), (d) Thick Shell (Y- Direction)	89
Figure 4.16: Height vs. Story Shear (Type A) (a) Layered Shell (X- Direction), (b) Layered Shell (Y- Direction), (c) Thick Shell (X- Direction), (d) Thick Shell (Y- Direction)	91
Figure 4.17: Height vs. Story Stiffness (Type A) (a) Layered Shell (X- Direction),	94
Figure 4.18: Plastic Hinge Formation at DBE Level Earthquake (Model A.L.9.7) ..	95
Figure 4.19: Base Shear Capacity Chart (X-Direction)	100
Figure 4.20: Base Shear Capacity Chart (Y-Direction)	100
Figure 4.21: Capacity Curve (Base Shear vs. Displacement) for Layered Shell Models (a) X- Direction, (b) Y- Direction.	102
Figure 4.22: Capacity Curve (Base Shear vs. Displacement) for Thick Shell Models (a) X- Direction, (b) Y- Direction	103
Figure 4.23: Punching Shear Results for Model A.L.8.10 (Layered Shell) (a) SE (X- Direction), (b) DBE (X-Direction), (c) MCE (X-Direction), (d) SE (Y-Direction), (e) DBE (Y-Direction), (f) MCE (Y-Direction)	112
Figure 4.24: Punching Shear Results for Model A.T.8.10 (Thick Shell) (a) SE (X- Direction), (b) DBE (X-Direction), (c) MCE (X-Direction), (d) SE (Y-Direction), (e) DBE (Y-Direction), (f) MCE (Y-Direction)	113
Figure 4.25: Punching Shear at MCE Level for Layered Shell Models (X-Direction)	115
Figure 4.26: Punching Shear at MCE Level for Layered Shell Models (Y-Direction)	115
Figure 4.27: Punching Shear at MCE Level for Thick Shell Models (X-Direction)	116
Figure 4.28: Punching Shear at MCE Level for Thick Shell Models (Y-Direction)	116

LIST OF TECHNICAL SYMBOLS AND TERMS

- a_h = Expected horizontal peak ground acceleration (in g) for design
- b_o = Punching perimeter
- C_d = Deflection Amplification Factor
- C_t and m = Constants that are obtained from Table 6.2.20 of BNBC (2020)
- C_s = Normalized acceleration response spectrum
- D = Effect of dead load
- d = Effective depth of slab
- f_c' = Concrete strength
- E_v = Vertical seismic load effect
- F_a = Site Coefficient
- F_v = Site Coefficient
- g = Acceleration due to gravity
- h_n = Height of building in metres from foundation or from top of rigid basement
- I = Structural Importance Factor
- K_d = Wind Directionality Factor
- K_{zt} = Topographic Factor
- PF1 = Modal participation factor for the first natural mode
- Q_D = Action caused by dead loads;
- Q_L = Action caused by live load
- Q_S = Action caused by effective snow load
- R = Response Reduction Factor
- S = Site dependent soil factor
- S_1 = Spectral response acceleration parameter at a one second period, obtained from response acceleration contour maps
- S_a = Spectral response acceleration (in units of g)
- S_d = Spectral displacement
- S_{DS} = Design short-period spectral response acceleration parameter, adjusted for site class, for determining level of seismicity
- S_{D1} = Design spectral response acceleration parameter at a one-second period, adjusted for site class, for determining level of seismicity

S_s = Spectral response acceleration parameter at short periods, obtained from response acceleration contour maps

T = Fundamental building period

T_B = Lower limit of the period of the constant spectral acceleration branch

T_C = Upper limit of the period of the constant spectral acceleration branch

T_D = Lower limit of the period of the constant spectral displacement branch

T_e = Effective fundamental period

V = Base shear

V_b = Basic wind speed

V_y = Effective yield strength

W = Total seismic weight of the building defined

Z = Seismic Zone Coefficient

Δ_{roof} = Roof displacement

α_1 = Modal mass coefficient for the first natural mode

α_s = 40 for interior columns, 30 for edge columns, 20 for corner columns

β = Coefficient used to calculate lower bound for S_a .

δ_y = Effective yield displacement

η = Damping correction factor

Ω_o = System Overstrength Factor

$\Phi_{1, \text{roof}}$ = Roof level amplitude of the first

Φ_{v_c} = Punching shear stress capacity in MPa

LIST OF ABBREVIATIONS

ACI=American Concrete Institute

ASCE=American Society of Civil Engineers

BNBC=Bangladesh National Building Code

CP=Collapse Prevention

DBE=Design Based Earthquake

FEMA=Federal Emergency Management Agency

IO=Immediate Occupancy

LS=Life Safety

MCE=Maximum Considered Earthquake

NSA=Nonlinear Static Analysis

NTHA=Nonlinear Time History Analysis

RSA=Response Spectrum Analysis

SE=Serviceability Earthquake

Chapter 1

INTRODUCTION

1.1 General

Flat plate system is becoming extensively popular in building construction owing to its distinct advantages- aesthetics and speedy construction. However, seismic events such as earthquakes can cause significant damage to flat plate structures, leading to the loss of life and property. Therefore, studying the seismic performance of flat plate structures is crucial to improve their safety and resilience against earthquakes.

Advancements of technology have revolutionized structural engineering, allowing for faster and more efficient analysis and design of structures through cutting-edge design software in accordance with new design codes. Nonlinear analysis through the software can identify potential failure mechanisms that may not be captured by traditional analysis methods, enabling engineers to design more resilient structures that can withstand the effects of seismic loads and avoid catastrophic failure during an earthquake. Additionally, nonlinear analysis can be used to evaluate retrofitting strategies for existing structures and optimize the design of flat plate structures for seismic loads. The two main types of shell elements used in the slab analysis are non-layered and layered elements, each with its own advantages and disadvantages. This research focuses on the seismic performance of flat plate structures using nonlinear static analysis with both non-layered and layered shell elements.

1.2 Background of the Study

In recent times, numerous nonlinear finite element modellings have been done for determining failure behavior of flat plate systems. During past earthquakes, many flat plate building structures have performed poorly due to inadequate resistance for its sudden brittle failure called “punching shear failure” under lateral loading (Agrahari, 2019). Most researchers incorporated parametric studies using non-layered shell element to investigate punching shear capacity of slab-column connections. Influence of reinforcement was studied on punching shear behavior of flat slab. The effects of load eccentricity, opening size and location on punching strength were also investigated. The layered finite element model for reinforced concrete plates and shells

was first applied in incremental-variable elasticity technique for determining the load-deflection curve by Hand et al. (1973). Layered shell element has also been used to create hypo elastic concrete material model to study the influence of the distribution of transverse shear strain on the punching shear failure mode and to capture nonlinear behavior of slab and extract in-plane force/stress data. However, the number of research works done to capture the nonlinear effect of punching shear using layered slab is limited. The focus of the present research is to study the nonlinear effect of punching shear due to seismic loading in flat plates using layered shell model and compare this approach with thick shell (non-layered) model to understand the difference between the obtained results for more reliable seismic design.

1.3 Objectives of the Research

The main objectives of this study are:

- i. To assess seismic performance of flat plate structures by drift, displacement, stiffness, story shear and plastic hinge formation at different earthquake levels by modelling slab with layered shell and thick shell element.
- ii. To observe and compare punching shear stress of layered shell and thick shell flat plate slabs.
- iii. To conduct parametric study by varying story height, building aspect ratio, slab thickness and column size for observing punching shear failure mechanism of flat plates under seismic loading.

1.4 Organization of the Thesis

The thesis paper is organized into total five chapters. Apart from chapter one, the following chapters are organized as follows:

Chapter 2: A literature review is summarized the background study on nonlinear static analysis procedure, response modification factor and performance under seismic loads of shear wall structures, flat plate structures and shear wall - flat plate structural systems.

Chapter 3: This chapter presents the numerical modeling of numerous building structures namely shear wall-flat plate structural system (SW-FP). Basic design consideration for linear static analysis and modeling criteria, hinge properties and

loading criteria for non-linear static analysis/pushover analysis have been discuss in this chapter.

Chapter 4: This chapter presents model validation, structural performance from linear static analysis (LSA) and nonlinear static analysis (NLSA). Result output, structural performance of linear static model, nonlinear behavior of SW-FP structural system models are summarized and compare with respect to different parameters are shown in this chapter.

Chapter 5: This chapter summarizes the research and lists out the conclusions based on the outcome of the numerical results and recommend scopes for future studies.

Chapter 2

LITERATURE REVIEW

2.1 Introduction

Historical documentation of punching failures of flat plates during major earthquakes confirms the necessity to improve the performance of flat plate structural systems. One of the most critical issues for these systems is the failure of slabs in the vicinity of a column in shear by developing a failure surface in the form of a truncated cone or pyramid. This mode of failure, known as a punching shear failure, is commonly the major contributor of flat plate building collapse. Shear in beam is analogous to punching shear in slabs in two dimensions. Since the failure is a sudden rupture which is not much restrained by the main reinforcement, the shear tends to decrease the ultimate load of the structure below its flexural capacity.

A diverse range of tests have been conducted to assess the punching shear strength of slabs. A number of theories have been suggested to predict the strength observed in these tests. This chapter outlines the experimental studies and analytical methods adopted by different researchers including the requirements of various building codes.

2.2 Flat Plate Structures

The term "flat plate" refers to a particular kind of structural system where slabs of uniform thickness are supported directly on columns without the use of beams. Flat plates are often utilized in structures with relatively small gravity loads. According to BNBC (2020), the term "flat plate" is attributed to slabs without drop panels, column capital or brackets.

Punching failure of slabs adjacent to columns due to excessive load concentration is a prime concern for flat plates. A benefit of the flat plate system is the addition of an edge beam at the panel's edge to lessen the deflection of the external panel of the plate. Flat plates' main drawback is its weakness against lateral stresses. Hence, if they are to be utilized in high-rise constructions, specific elements like shear walls and structural walls must be installed.

With the collaboration of all the floors in the structure, the slab beam columns system functions collectively as a three-dimensional system to withstand lateral loads in

addition to gravity loads. However, a thorough three-dimensional assessment of the structure is difficult. Due to the flexibility of the slab, slab moments are transferred indirectly as opposed to planer frames, where beam moments are directly carried to columns. Additionally, slab moments generated by gravity can transfer from loaded to unloaded spans; which must be taken into consideration.

2.2.1 Modes of Failure of Flat Plates

There are two failure modes of slab–column connections in a flat plate slab, flexural and punching shear.

a) Flexural Failure

Gravity loads acting on slab tends to bend the slab in the central area, leading to flexural failure. Flexural failure may appear in the slabs with a low level of flexural reinforcement ratio. The defining characteristic of this kind of failure mode is the occurrence of significant plastic deflection prior to the failure of the brittle punching (Jafarian and Raji, 2022).

b) Punching Shear Failure

A typical flat plate punching shear failure is characterized by the punching of a column through a portion of the surrounding slab.

Figure 2.1 shows an example of a punching shear failure.

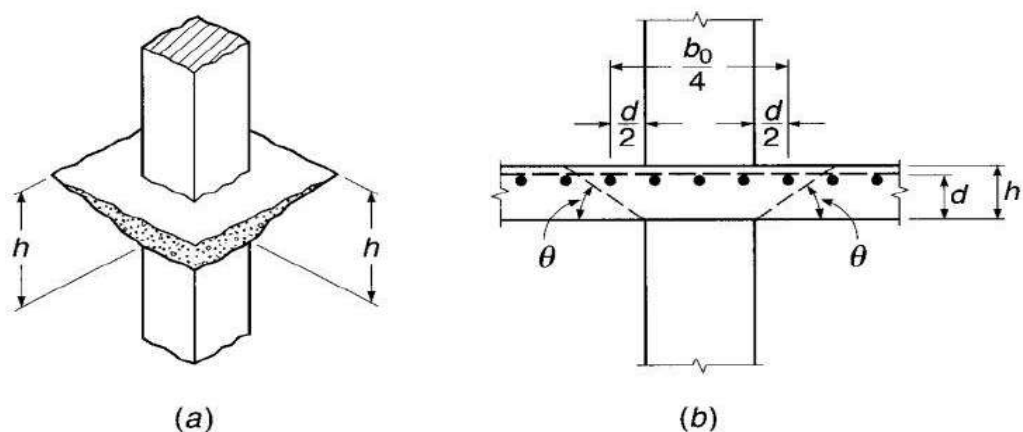


Figure 2.1: Punching Shear Failure (Nilson et al., 2009)

Diagonal tension cracks form in a two-way slab system with a concentrated load or at a slab-column connection encircling the load or column. into compression area of the slab and encounter resistance near the load similar to the shear-compression condition.

While the slab continues to take load, such cracks extend and finally the punching failure occurs with the punching out a solid of upheaval as a pyramid shape of concrete in the vicinity of column which is shown in

Figure 2.1. This type of failure is catastrophic since no external, visible signs can be seen prior to the occurrence of the failure.

In-depth investigation has been made to determine how slab-column connections behave. The type and intensity of loading determine the failure mode. The punching shear strength of the connection between the slab and column is crucial and is greatly influenced by the gravity shear ratio. When lateral loads and unbalance moments are present, the method of moment transfer from slab to column becomes extremely complicated. These unbalanced moments cause additional shear and torsion at the connections, which are subsequently transmitted into the column and cause excessive slab cracking, which further reduces the slab's stiffness (Alam, 2018).

When determining the thickness of flat plates at the column-slab intersection, this sort of failure is one of the most important factors to consider. Hence, the accurate estimate of punching shear strength is a major concern for engineers designing flat plates.

2.2.2 Previous Study on Flat Plate Structures

The establishment and advancement of flat plate system can be attributed to a multitude of significant research studies, which have greatly contributed to enhancing its overall design and construction.

One of the earliest influential studies was conducted by Hillerborg (1956), a Swedish engineer. He proposed a theory for predicting the behavior of reinforced concrete slabs without beams or columns, which he called the "strip method". This method involved dividing the slab into narrow strips, each behaving as a beam. Hillerborg's research showed that by using this method, the behavior of flat plate slabs could be accurately predicted, and the amount of reinforcement required could be optimized.

In the early 20th century, analysis procedures for structures were simple and used basic structural models and loading types. However, as modal analysis and response spectrum analysis (RSA) procedures became more prevalent, the importance of understanding vibration modes and natural periods in controlling seismic demands became apparent. In the 1960s and 1970s, the advent of computer programs and

dynamic analysis solvers led to the establishment of detailed dynamic analysis procedures, which involved directly solving the governing equations of motion (Mazhar et al., 2016). This also led to the use of nonlinear modeling for more accurate structural idealization compared to linear elastic models. With more ground motion records becoming available, the use of these advanced analysis procedures has become more widespread.

Determining the failure behavior of flat plate systems has been the subject of numerous nonlinear finite element modeling in recent years. Studying the seismic performance of flat plate structures through nonlinear analysis offers several advantages over traditional linear analysis methods. Nonlinear analysis takes into account the inelastic behavior of structures under seismic loads and provides more accurate predictions of their response. This is particularly important for flat plate structures, which are prone to failure under seismic loads.

As punching shear failure is one of the most common observed failure mode in flat plate slabs, researchers have been working on developing and improving the design for punching shear failure in flat plate slabs for many years. Nonlinear analysis can predict the potential for punching shear failure, which traditional linear analysis may not identify. Most researchers incorporated parametric studies using non-layered shell element to investigate punching shear capacity of slab-column connections. Both material and geometrical aspects of concrete, such as its strength and the effect of reinforcing, are explored in these researches. These investigations incorporated various methods such as the truss model approach, the equivalent frame method, fracture mechanics, plasticity model, assumed deflection method etc.

Nowadays, the design of flat plate slabs to resist punching shear generally follows the guidelines specified by the building code. These guidelines consider various factors such as the size of the column, slab thickness, compressive strength of the concrete, and the quantity and spacing of shear reinforcement. The research and development of punching shear failure design for flat plate slabs has had a significant impact on the development of these guidelines.

During the late 1980s and 1990s, the importance of nonlinear modeling and analysis increased significantly with the emergence of performance-based seismic engineering (PBSE) as a well-accepted methodology for evaluating and designing building

structures for seismic events (ATC-40, 1996). This methodology focuses on predicting structural performance to provide decision-makers with key information about structural safety and risk. Performance is characterized in terms of expected damage to various structural and nonstructural components and building contents. As structural damage implies inelastic behavior, traditional design and analysis procedures based on linear elastic behavior can only indirectly predict performance. In contrast, nonlinear seismic analysis procedures aim to directly estimate the magnitude of inelastic seismic demands to improve the accuracy of performance predictions.

During the 1980s and 1990s, researchers began exploring the application of numerical methods to study the behavior of flat plate slabs under punching shear. One of the early researches on the correlation between punching shear and concrete strength and steel ratio was presented by Gardner (1990). The conclusion was that the shear capacity is proportional to the cube root of the concrete strength and the steel ratio. It was also suggested that tall columns and columns should be used to improve the shear perimeter capitals, if there is any doubt about the punching shear capacity.

Bazant and Cao (1987) investigated the size effect on punching shear strength using fracture mechanics, a theory that is based on energy and stability criteria rather than strength criteria. The size effect is the most important feature of fracture mechanics. In fracture mechanics, as the size of a structure increases, the nominal stress at failure of geometrically comparable structures decreases. The model utilized here was essentially a modified shear perimeter method. According to the theory, the post-peak decrease of the load deflection diagram gets steeper the thicker the slab, making the punching shear behavior of small slabs more similar to plasticity and that of thick slabs more similar to linear elastic fracture mechanics. The size-effect law's applicability is independently confirmed by the fact that it accurately predicts this type of behavior.

Influence of reinforcement was studied on punching shear behavior of flat slab by many. Over the last three decades, numerous tests have been conducted to extensively examine the performance of various types of shear reinforcement, including vertical and inclined stirrups, structural shear heads, bent-up bars, hooked bars, and welded-wire fabric. Song et al. (2012) investigated seismic performance of the flat plate system with shear reinforcements. In order to explore the system level seismic capacity for 45 shear-reinforced flat plate systems, non-linear pushover analysis was utilized. The

results of an experimental investigation involving three isolated internal flat slab-column connections were used to the input data of slab-column connections. The response modification factor and the over strength factor were considered as key parameters to describe the seismic capacity of the system. Except for the 5-story example, analysis results indicated that the flat plate structure reinforced with shear bands performed effectively as an RC intermediate moment resistance frame. Except for the 5-story scenario, the analysis displayed that the flat plate system reinforced with shear band demonstrated the efficiency of an RC intermediate moment resistance frame. The effective response modification factor for flat plate constructions without walls was also assessed in this work.

Mahmoud (2015) developed 16 flat-slab models using finite element method to perform nonlinear analysis both including and excluding punching shear reinforcement. The analysis showed that all models without shear reinforcement experience significant changes in thickness than the models with shear reinforcement. Parametric studies were carried out to explore the influence of applied loading and size and location of opening on the strength and rotation capabilities of flat slabs. Issa et al. (2019) examined the effect of different types of shear reinforcement using a number of distribution techniques on reinforced concrete flat slabs under concentric punching loading. The experiment was conducted using 12 test specimens with and without shear reinforcement. Non-linear finite element analyses have been carried out as well. Punching shear provisions of six building codes, namely Eurocode (2):2014, DIN 1045-1:2008, BS 8110-1:2007, ECP 203-2018, ACI 318-14 & CSA A23.3-1 were compared with the experimental results in this research. A comparison was shown between the research test results and the codes equations to improve the flat slab analysis methods. Through numerous research efforts, it has been widely accepted by the researchers that the proper utilization of shear reinforcement can improve both the ductility and punching shear resistance.

The effects of load eccentricity, opening size and location on punching strength were also investigated by many researchers. Ismail (2018) studied 27 flat plate finite element models with concentric and eccentric punching loads. This study focused on the eccentricity of the load, the opening size, the location of the opening in relation to the transfer moment, and the configuration of the reinforcement near to the opening.

The layered finite element model for reinforced concrete plates and shells was first applied in incremental-variable elasticity technique for determining the load-deflection curve by Hand et al. (1973). Loo and Guan (1997) introduced nonlinear layered finite element method for assessing the punching shear failure and cracking of reinforced concrete flat plates with spandrel beams or torsion strips. As a layered approach considers transverse shear capacities, the procedure takes into account the full interaction between cracking and failure analysis. The study focused on determining deflection and punching shear strength of reinforced concrete flat plates with or without spandrel beams at corner and edge-column connections. The model employed transverse shear deformations that come with the Mindlin hypothesis. A postprocessor was designed to display the slab's deformed shape, finite element mesh, and fracture patterns graphically. A comparative study with experimental results showed good correlation to the proposed analytical procedure validating its accuracy and reliability.

Global analysis of reinforced concrete slabs subjected to high concentrated transverse stresses was investigated by Polak (1998) using the finite element layered shell formulation. The nonlinear solution was based on an iterative, full-load, secant stiffness formulation. The procedure considered geometric nonlinearities and constitutive behavior. The sensitivity of the proposed formulation was checked using different reinforcement ratios, boundary conditions, and reinforcement orientations. According to Polak, the layered approach is a detailed, versatile and comprehensive approach to model nonlinear behavior of members subjected to bending. On the other hand, the effective stiffness method is simpler and requires less time to implement. Effective stiffness formulations for ordinary slab systems can produce results with precision comparable to the layered method.

Layered shell modeling underwent further development and refinement during the 2000s and 2010s. Wang et al. (2008) conducted nonlinear analysis on finite element model of reinforced concrete flat plate structures using the layered shell element. Analyses were conducted on a flat plate, a flat slab with drop panel, and a big flat plate with an uneven column pattern. Shell element environments were used to construct a flexible layering method that incorporates transverse shear deformation. Each layered shell element node was specified as a regular node or a shear corrected node. To simulate reinforced concrete, a three-dimensional hypo elastic material model was used. In numerical simulations, the impact of transverse shear strain distribution on the

punching shear failure mode was identified. It has been demonstrated that the suggested finite-element model can simulate the localized punched shear behavior of slab–column connections and is acceptable for global investigation of the structural performance of flat plate constructions.

Mahmud-Ul-Hasan (2019) used layered shell element to capture nonlinear behavior of slab and extract in-plane force/stress data. This study provided insight into the in-plane behavior of cast-in-place concrete diagrams near diaphragm openings next to shear walls.

The Performance Based Design (PBD) approach has recently gained popularity in the field of structural design as it provides a more comprehensive and adaptable approach to assessing the performance of buildings and their components compared to traditional building code design methods. Building code design methods aim to produce structures that can meet certain levels of performance, but they do not evaluate the actual performance of individual building designs. In contrast, PBD evaluates how a building is expected to perform given the potential hazard it may face, while accounting for uncertainties in quantifying potential hazard and assessing actual building response. This methodology analyzes the response of buildings under different levels of seismic demand, such as SLE and MCE, using advanced nonlinear analysis procedures and computer modeling tools to accurately determine the nonlinear seismic demands of the entire structure and its individual components.

Kim et al. (2008) did research on the seismic performance evaluation of flat-plate structures that were not designed to withstand earthquakes. They used both the capacity spectrum method described in ATC 40 (1996) and nonlinear dynamic analysis to determine the maximum inter-story drifts for earthquake loads. In addition, a strategy for evaluating seismic performance provided in FEMA-355F (2000) was used to assess the seismic safety of the model structures. The findings of the analysis demonstrated that the maximum inter-story drifts of the non-seismic designed flat-plate buildings were less than the limit state for the collapse prevention performance level. Nevertheless, the FEMA approach revealed that the model constructions lacked sufficient strength to guarantee seismic safety.

Nikolic-brzev and Stojadinovic (1999) assessed the seismic performance of three single-story concrete flat slab structures of varying ages located in Greater Vancouver,

which are significant in the event of a major earthquake. The primary aims were to investigate differences in seismic response estimates from different analysis procedures, compare the seismic performance of comparable structures from various periods, and evaluate the provisions of the Canadian Standard for Design of Concrete Structures concerning modeling less than nominally ductile concrete flat slab structures. The structures were evaluated using both the NBCC equivalent static analysis and the FEMA pushover analysis, and the outcomes show that the NBCC analysis provides more conservative estimates for the lateral drift ratio and force modification factor. The FEMA-defined target displacement was utilized to rate the structures' performance as Life Safety level, which meets the seismic performance objectives outlined in the National Building Code of Canada.

In summary, the history of nonlinear analysis on flat plate structures has been a constantly evolving one, with researchers making significant progress in understanding their complex behavior. The use of nonlinear analysis and layered shell elements in numerical simulations has proven to be effective in predicting the punching shear behavior of flat plates, and performance-based design has been developed to optimize their design and ensure their actual structural behavior under various loading conditions. As research in this field continues to advance, it is expected that new methods and techniques will emerge, further enhancing our understanding of the behavior of flat plate structures.

2.2.3 Provisions of Flat Plate as Per Various Design Codes

The earliest "code provisions" for slab came to existence in 1921 and was divided into two sections. The first section, which was inserted into the body of the code, provided design coefficients for the slab that were derived from solutions based on conventional theory and were only relevant to "two-way" slabs with stiff beams between all columns. The second section, which dealt with "flat" slabs, was included as an appendix to the code. Unfortunately, neither method was adequate. The University of Illinois began a thorough investigation to address the issue in the late 1950s. Thus, the Equivalent Frame Method (EFM) and Direct Design Method (DDM) were designed. These procedures were added to the code.

It is difficult to precisely analyze the structure of a flat slab because of its high uncertainty. A slab interior panel can be used as a starting point for a rough analysis.

BNBC (2020) includes Direct Design Method and Equivalent Frame Analysis for flat slab analysis. Using the Direct Design Method, the bending moment and shear force in a flat slab may be determined quickly and easily, even without the assistance of a computer. However, the results of the equivalent frame analysis are more precise.

A comparison between different methods of analysis followed by different codes is shown in Table 2.1.

Table 2.1: Methods of Analysis of Flat Plate Structure Followed by Different Codes (Khan, 2018)

Methods	BNBC 2020	BNBC 1993	ACI 318-14	Eurocode	Canadian Standards	Indian Standards
Direct Design Method (DDM)	√	√	√	√	√	√
Equivalent Frame Method (EFM)	√	√	√			√
ACI Coefficient Method		√				
Limit State Method				√		

2.3 Earthquake Trend in Bangladesh

There are millions of earthquakes that occur throughout the world each year. Many of them go unnoticed because they occur in distant places or have small magnitudes. The majority of the earthquakes that are detected are massive tectonic earthquakes. Tectonic earthquakes occur due to the movement of tectonic plates near plate boundaries. The movement of the plates relative to one another distorts the crust along the boundaries, resulting in earthquake fault systems. Tectonic plates move slowly and continuously, but occasionally friction between them causes them to lock together and become immovable. As the other plates continue to move, the stress near the faults increases, and eventually, the locked portion gives in to the stress. As a result, sections of the crust suddenly break or become displaced and the plates pass each other very quickly. This sudden slip along the faults releases energy waves that travel through the Earth's crust, causing the shaking we experience at an earthquake site.

According to BNBC (2020), the northern and eastern part of Bangladesh lie close to the Indian plate and the Eurasian plate boundaries (Figure 2.2 a). The collision of the north-east moving (around 4 cm or more annually) Indian Plate with the Eurasian plate is the primary source of earthquakes in Bangladesh.

Five tectonic blocks have been identified in Bangladesh for actively causing destructive earthquakes: i) Bogra fault zone ii) Tripura fault zone iii) Assam fault zone iv) Shillong plateau and v) Sub Dauki fault zone.

Figure 2.2.b shows the active fault zones surrounding Bangladesh. The geological configuration and plate movements make Bangladesh potentially earthquake-prone.

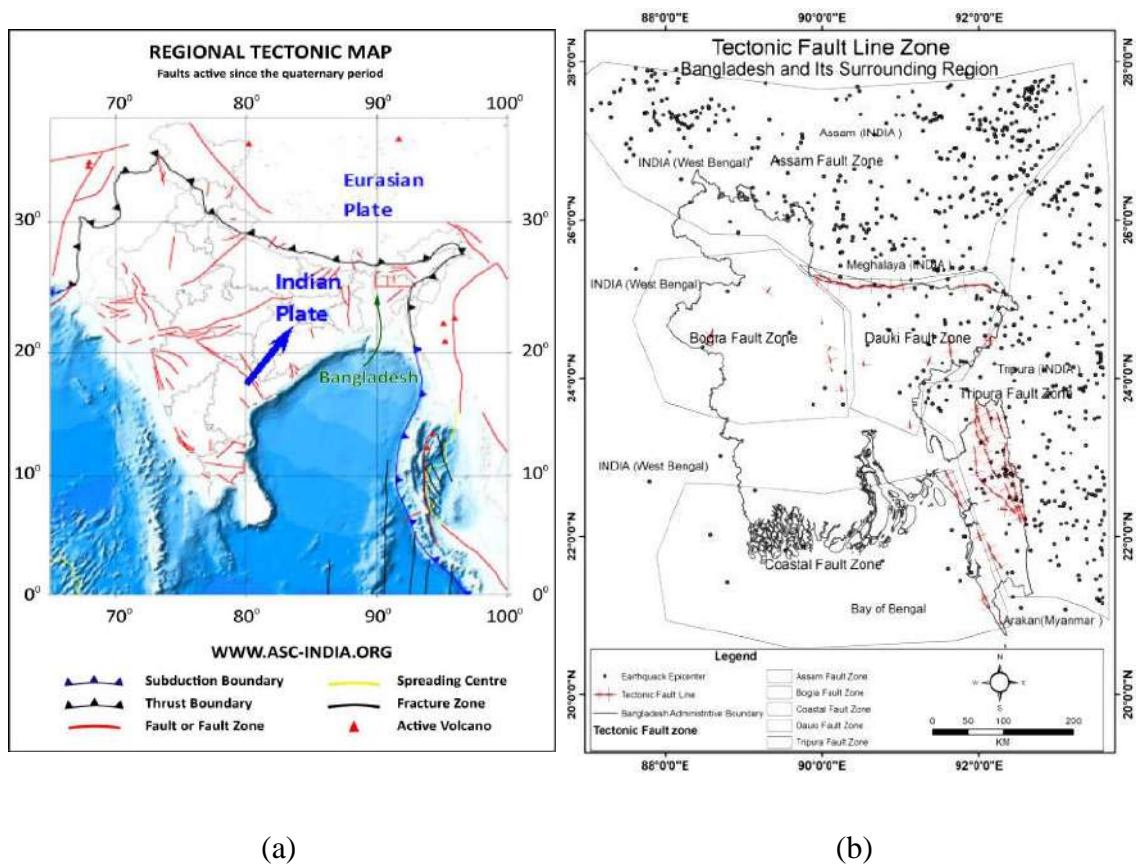


Figure 2.2: Plate Boundaries and Fault Zones Surrounding Bangladesh (BNBC, 2020)
(a) Plate Boundaries, (b) Fault Zones.

Figure 2.3 displays the location of earthquake epicenters with magnitude ($M \geq 4$) in and around Bangladesh. This is a sign of the region's strong seismic activity. Although earthquakes occur all around Bangladesh, it seems that the earthquake band in

Chittagong and Sylhet are denser. In spite of being small in number, earthquakes are also occurring in south western Bangladesh, including the sea (BNBC, 2020).

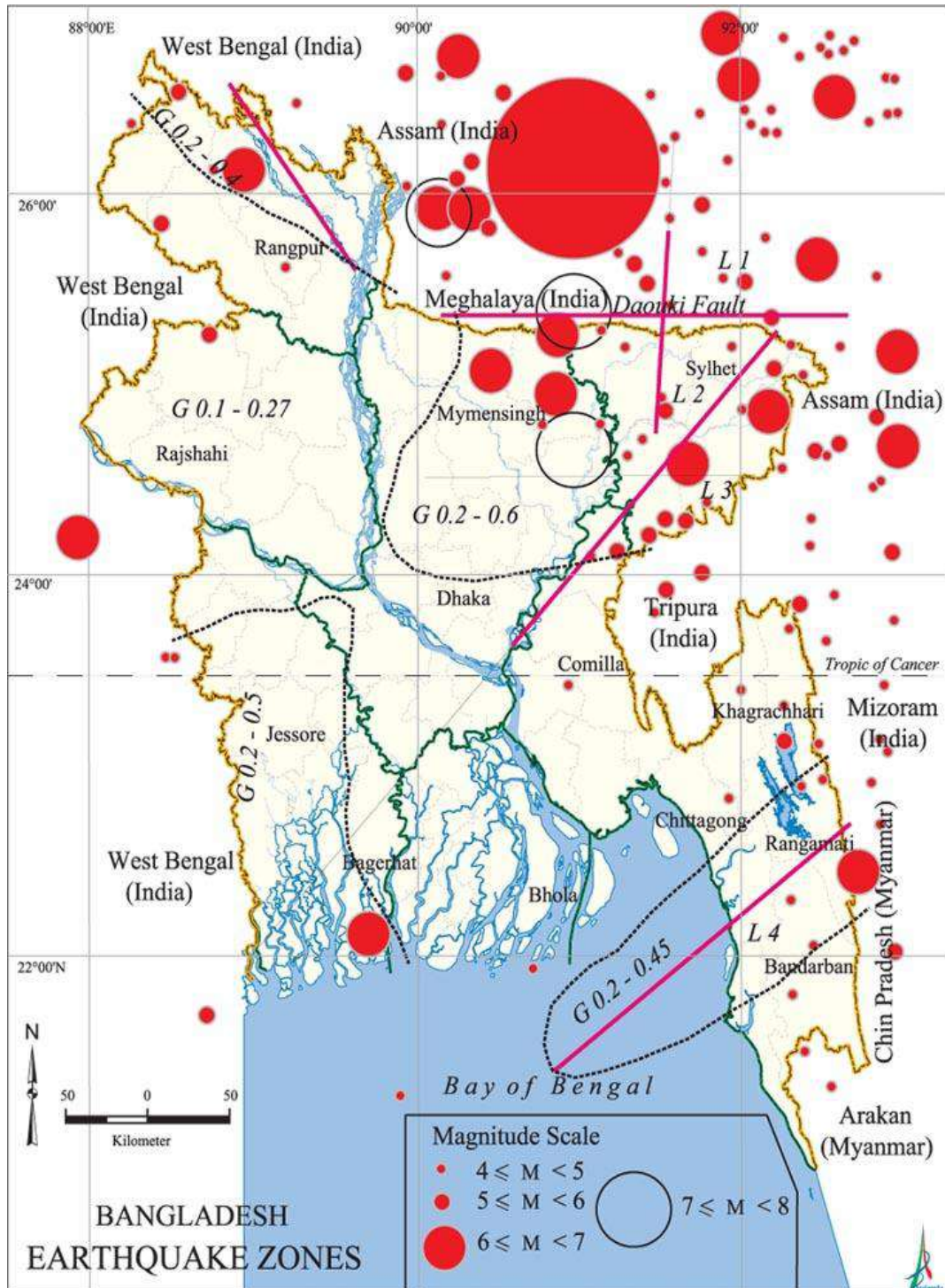


Figure 2.3: Earthquake Magnitudes in Different Areas of Bangladesh (BNBC, 2020)

Table 2.2 gives brief information about the magnitude and effects of some major earthquakes in Bangladesh.

Table 2.2: List of Major Regional Earthquakes (BNBC, 2020), (*NCEI Hazard Earthquake Search*, n.d.)

Date	Earthquake name	Epicentre	Magnitude, M	Effects
2 April, 1762	---	Near Chittagong	>7.0	Some changes in landforms in the coastal area and liquefaction.
10 January, 1869	Cachar	Cachar, Assam	7.5	Some damage occurred in Sylhet.
14 July, 1885	Bengal	Bogra	7.0	Severe damage occurred to houses in Sirajganj and Sherpur (Bogra).
12 June, 1897	Great Indian	Shillong, Assam	8.1	Greatest damage in Rangpur including railway line and buildings; intense ground fissures and vents in Mymensingh, Jamalpur, Sylhet; damages to masonry buildings covering a major portion of Bangladesh including Dhaka. The death toll in Sylhet alone was 545 due to collapse of masonry building.
8 July, 1918	Srimongal	Srimongal, Sylhet	7.6	Collapse/ severe damage of buildings in Srimongal, damage to buildings in Habiganj, Moulvibazar.
2 July, 1930	Dhubri	Garo hills	7.1	Damage to railway track in Lalmonirhat, damage to buildings in Lalmonirhat and Rangpur.

Date	Earthquake name	Epicentre	Magnitude, M	Effects
3 July, 1934	---	Dhurbi, Assam	7.1	Considerable damages in greater Rangpur district of Bangladesh.
22 November, 1997	---	Chittagong	6.0	Minor damage around Chittagong town.
22 July, 1999	---	Maheshkhali	5.1	Severely felt around Maheshkhali island and the adjoining sea. Rural mud-walled homes suffered considerable damage and collapsed.
5 August, 2006	Narail	Near Narail	4.2	Tremor was widely felt in Dhaka as well as other places in the country.
27 July, 2008	Mymensingh	Northeast of Mymensingh city	5.1	Apart from Mymensingh, tremors were felt in many parts of the Dhaka metropolitan area.
11 August, 2009	Bay of Bengal	North Andaman Islands of the Bay of Bengal and seacoast of Myanmar	7.5	Though no significant damage was reported, the tremor was felt strongly in Dhaka.
10 September, 2010	---	southwest from Dhaka	4.8	Tremor felt in Dhaka and its surrounding areas.
03 January, 2016	---	India	6.7	Tremor was felt throughout Bangladesh. At least 33 people in Bangladesh were injured, some after jumping from buildings fearing they might collapse.
03 January, 2017	---	India	5.7	The tremor killed two people in Sunamganj and left many people injured in Bangladesh

Table 2.2 shows that Sylhet, Bogra, and Chittagong in Bangladesh have all had earthquakes of a great magnitude ($M > 7.0$). Some major earthquakes ($M > 7.0$) that occurred in India were close enough to damage the Sylhet, Mymensingh, and Rangpur region.

The structural damage caused by a number of earthquakes (magnitude 4 to 6) inside the country or near the country's border has aroused concerns in recent years. The Great India Earthquake struck on 12 June, 1897 caused serious damage to masonry buildings. The collapse of the masonry buildings caused the death of 545 people in Sylhet town. Many public buildings in Mymensingh including the Justice House, were ruined and very few of the two-storied masonry buildings survived. Heavy damage was done to the bridges on the Dhaka-Mymensingh railway causing traffic interruption for about two weeks. A reinforced concrete frame building that was being built in Chittagong collapsed due to an earthquake of magnitude 6.0 on November 21, 1997, at the Bangladesh-Myanmar border. Rural mud-walled homes suffered considerable damage and collapsed as a result of the magnitude 5.1 earthquake that struck the area on July 22, 1999, and had its epicenter quite close to the island of Moheshkhali in Cox's Bazar. The earthquake also damaged a cyclone shelter column. Prisoners at the Dhaka Central Jail experienced terror and injuries as a result of the Dec. 2001 earthquake, which had an epicenter relatively close to Dhaka metropolis. Brick masonry structures and mud-walled homes both suffered significant damage in the village of Kolabunia during the magnitude 5.6 Rangamati earthquake on July 27, 2003 (BNBC, 2020).

2.4 Seismic Design Concept

Historically, the goal of seismic analysis and building design has been to lower the possibility of fatalities during the biggest anticipated earthquake. Building codes have established provisions around life safety considerations, i.e., to prevent collapse under the most violent earthquake anticipated at a site throughout the life of a structure, based on the historical performance of buildings and their deficiencies. According to Taranath (2004), these guidelines are founded on the idea that a building's performance in seismically active regions depends on a combination of strength, ductility demonstrated in construction details, and the presence of a fully integrated, balanced, and comprehensive lateral-force-resisting system.

Overall, the majority of earthquake code provisions demand that structures be able to withstand the following (Taranath, 2004):

- i. Minor earthquakes without any damage.
- ii. Moderate earthquakes that cause some nonstructural damage but little structural damage.
- iii. Major earthquakes without collapse but with some structural and nonstructural damage. It is anticipated that the structure will experience quite significant deformations due to the yielding of some structural members.

The purpose of the codes is to ensure that structures have a low likelihood of collapsing for ground motions greater than the design levels. Economical earthquake resistance is attained in most structures that are subjected to moderate-to-strong earthquakes by permitting some structural components to yield. Designing a structure to respond to maximum anticipated earthquake-induced inertia forces in the elastic range is typically both impractical and uneconomical. Thus, in seismic design, yielding is accepted in predetermined structural parts or locations, provided that the structure's vertical load-carrying capacity is maintained even after strong earthquakes. The requirement for ductility decreases significantly in low seismicity areas. Strength may even be able to compensate for a lack of ductility in some circumstances. As long as they are never stressed over their elastic limit, extremely brittle lateral-force-resisting systems can work as efficiently.

Nevertheless, for some structures, such as nuclear power plants, yielding cannot be tolerated, hence an elastic design is required. Hospitals, fire stations, power plants, and communication centers are just a few examples of buildings that must not only survive an earthquake without collapsing but also continue to function after it. Therefore, damage management is a crucial design factor for structures that are considered essential to post-earthquake functions in addition to life safety.

Taranath (2004) describes an efficient seismic design generally involves the following:

- i. Choosing an overall structural concept, including the framework of a lateral-force resisting system, that is suitable to the predicted level of ground shaking. To ensure that a building reacts as a whole to ground motion, this entails providing a redundant and continuous load path.

- ii. Identifying the forces and deformations caused by the ground motion that are prescribed by the code and transferring the forces vertically to the lateral-force-resisting system. When calculating these forces, the structural system, configuration, and site characteristics are all taken into account.
- iii. A building's analysis for the combined effects of gravity and seismic loads to ensure that sufficient vertical and lateral strength and stiffness are attained to meet the structural performance and permissible deformation levels stipulated in the governing building code.
- iv. Providing information to ensure that the structure has adequate inelastic deformability to withstand reasonably large deformations in the event of a major earthquake. Members that are detailed adequately, have the properties needed to disperse energy through inelastic deformations.

2.5 Earthquake Hazard Level

Three levels of earthquake hazard are generally used to define ground shaking: i) Serviceability Earthquake, ii) Design Earthquake, and iii) Maximum Earthquake. According to the definitions of ATC-40 (1996), these earthquake hazard levels are described below.

2.5.1 Serviceability Earthquake (SE)

The Serviceability Earthquake (SE) is defined probabilistically as the level of ground shaking that has a 50 percent chance of being exceeded in a 50- year period. This level of earthquake ground shaking is typically about 0.5 times the level of ground shaking of the Design Earthquake. The SE represents a frequent level of ground shaking that is likely to be felt during the life of the building. The SE has a mean return period of approximately 75 years.

2.5.2 Design Earthquake (DE)

The Design Based Earthquake (DE) is defined probabilistically as the level of ground shaking that has a 10 percent chance of being exceeded in a 50- year period. The DE represents an infrequent level of ground shaking that can occur during the life of the building. It has a mean return period of approximately 500 years. Minor repairable damage in the primary lateral load carrying system is expected during design earthquake. For secondary elements, the damage may be such that they require

replacement.

It has the same definition as the level of ground shaking currently used as the basis for the seismic design of new buildings by the UBC and the Capacity Based Design (CBC).

2.5.3 Maximum Earthquake (ME)

The Maximum Earthquake (ME) is defined deterministically as the maximum level of earthquake ground shaking which may ever be expected at the building site within the known geologic framework. This intensity of ground shaking may be calculated as the Level of earthquake ground motion that has a 5 percent probability of being exceeded in a 50- year time period. This level of ground shaking is typically about 1.25 to 1.5 times the level of ground shaking of the Design Earthquake. The ME has the same definition as the Maximum Capable Earthquake (MCE) required by the CBC for design of hospitals and by both the CBC and UBC for design and testing of buildings with base isolation systems. This earthquake definition is intended to represent an upper-bound on the level of ground shaking that could be reasonably expected to occur at the building site. The definition of the ME (and the MCE of the UBC and CBC) is substantially different from the definition of the Maximum Considered Earthquake proposed for both the 1997 NEHRP Provisions and the FEMA Guidelines for rehabilitation of existing buildings. In probabilistic terms, the ME has a return period of about 1,000 years, whereas the Maximum Considered Earthquake has a return period of about 2,500 years (i.e., ground shaking with a 2% probability of being exceeded in 50 years).

2.6 Seismic Design Method

According to BNBC (2020), Bangladesh is divided into four seismic zones on the seismic zoning map as shown in Figure 2.4, each of which has a distinct predicted intensity of ground motion.

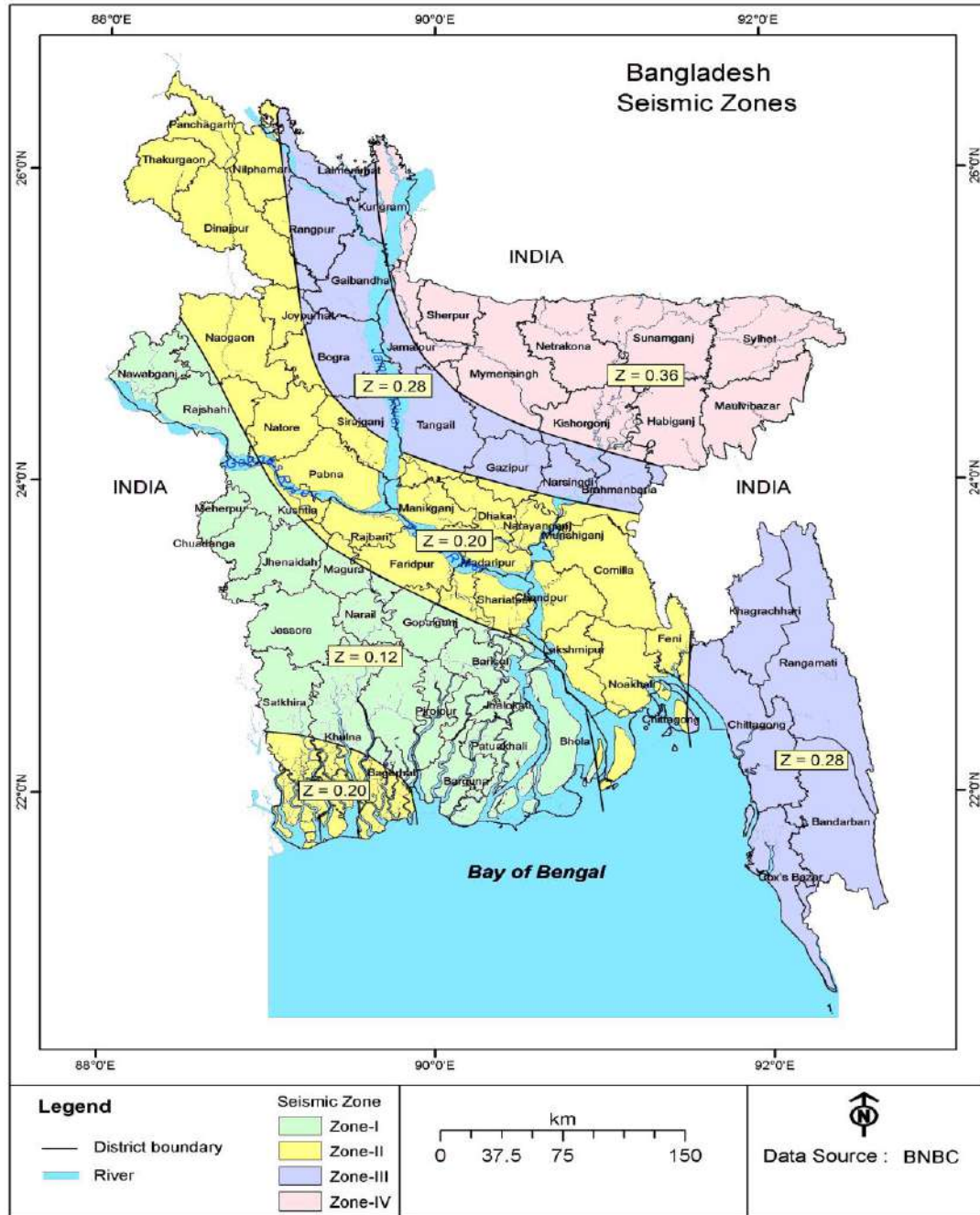


Figure 2.4: Seismic Zoning Map of Bangladesh (BNBC, 2020)

Each seismic zone has a zone coefficient that forecasts the Maximum Considered Earthquake's (MCE) peak ground acceleration values on rock or hard soil. The Design Based Earthquake (DBE) is taken as 2/3 of the Maximum Considered Earthquake.

2.6.1 Response Spectrum Analysis (RSA)

A response spectrum analysis is the analysis of a linear mathematical model of the structure to find the maximum accelerations, forces, and displacements caused by the

structure's dynamic response to ground shaking. Response spectrum analysis is sometimes referred to as a modal analysis procedure as it considers and integrates the impacts of the structure's numerous vibrational modes (BNBC, 2020).

2.6.2 Non-Linear Time History Analysis (NTHA)

Nonlinear time history analysis (NTHA) shall consist of analysis of a mathematical model of the structure which incorporates the nonlinear hysteretic behavior of the structure's components to determine its response, through methods of numerical integration, to ground acceleration time histories compatible with the design response spectrum for the site. The analysis shall be performed in accordance with the requirements of this Section. For the purposes of analysis, the structure shall be permitted to be considered to be fixed at the base or, alternatively, it shall be permitted to use realistic assumptions with regard to the stiffness of foundations. The acceleration time history (ground motion) is applied at the base of the structure. The advantage of this procedure is that actual time dependent behavior of the structural response considering inelastic deformations in the structure can be obtained (BNBC, 2020).

2.6.3 Nonlinear Static Analysis (NSA)

Nonlinear static analysis is a widely used tool for determining seismic behavior of structures, and is included in most guidelines and standards such as ATC, FEMA and ASCE. Often referred to as pushover analysis, nonlinear static analysis is a streamlined technique for assessing the nonlinear response of structures to strong earthquake ground shaking. It is a specialized method utilized in performance-based design for seismic loading. While nonlinear static analysis has been used since the 1970s, only in the recent decades has its full potential been recognized.

Nonlinear static analysis (NSA) is an alternative straightforward approach to nonlinear time history analysis (NTHA). The application of NLSA to estimate seismic demand is typically regarded as more preferable for seismic design due to its simplicity and convenience of use, despite the fact that time history analysis (THA) is more precise.

There are two methods described in BNBC (2020) to evaluate target displacement, Capacity Spectrum Method (CSM) and Displacement Coefficient Method (DCM).

i) Capacity Spectrum Method (CSM):

The capacity spectrum method is a very useful tool in the evaluation and retrofit design of both existing and new concrete structures. This method has been introduced by ATC 40 published in 1996 and enhanced in FEMA 440 published in 2005. This method provides a graphical representation of the global force-displacement capacity curve of the structure (i.e., pushover curve) and compares it to the response spectra representations of the earthquake demands. The graphical representation provides a clear depiction of how a structure responds to earthquake ground motion. The capacity curve is obtained by transforming the lateral force (V) vs. lateral displacement (d) coordinates to spectral acceleration (Sa) vs. spectral displacement (Sd) coordinates using the modal shape vectors, participation factors and modal masses obtained from a modal analysis of the structure.

A point-by-point conversion to first mode spectral coordinates is necessary in order to create the capacity spectrum from a capacity curve. Any point corresponding values of base shear, V_i and roof deflection, Δ_{roof} may be converted to the corresponding point of spectral acceleration, S_{ai} and spectral displacement, S_{di} on the capacity spectrum using relation,

$$S_{ai} = \frac{V_i / W}{\alpha_1} \quad (2.1)$$

$$S_{di} = \frac{\Delta_{roof}}{PF_1 X \Phi_{1,roof}} \quad (2.2)$$

Where:

S_{ai} = spectral acceleration

S_{di} = spectral displacement

V_i = base shear

W = building dead weight plus likely live loads

α_1 = modal mass coefficient for the first natural mode

Δ_{roof} = roof displacement

PF_1 = modal participation factor for the first natural mode.

$\Phi_{1,roof}$ = roof level amplitude of the first mode

In order to compare the structure's capacity to the earthquake demand, it is required to plot the response spectrum and the capacity spectrum on the same plot. Spectral quantities, i.e., spectral acceleration, spectral displacement and spectral velocity is interrelated to each other to a specific structural period T . Building code usually provide response spectrum in spectral acceleration vs. period format which is the conventional format. Each point on the curve is related to spectral displacement by mathematical relation,

$$S_d = \frac{T^2}{4\pi^2} S_a g \quad (2.3)$$

Converting with this relation response spectrum in ADRS format may be obtained. Any line from the origin of the ADRS format represent a constant period T_i which is related to spectral acceleration and spectral displacement by the mathematical relation,

$$T = 2\pi \sqrt{\frac{S_d}{S_a}} \quad (2.4)$$

After plotting the capacity spectrum and demand spectrum in the same plot, the intersection of the demand and capacity spectra would define the structure's performance point. To account for the hysteretic energy dissipation, or effective damping, connected with the particular point, 5% damping is applied to the demand spectrum. This is the point in the structure's operation where the capacity fits the demand or the particular earthquake. Calculation of performance point is shown in Figure 2.5 (ATC-40, 1996).

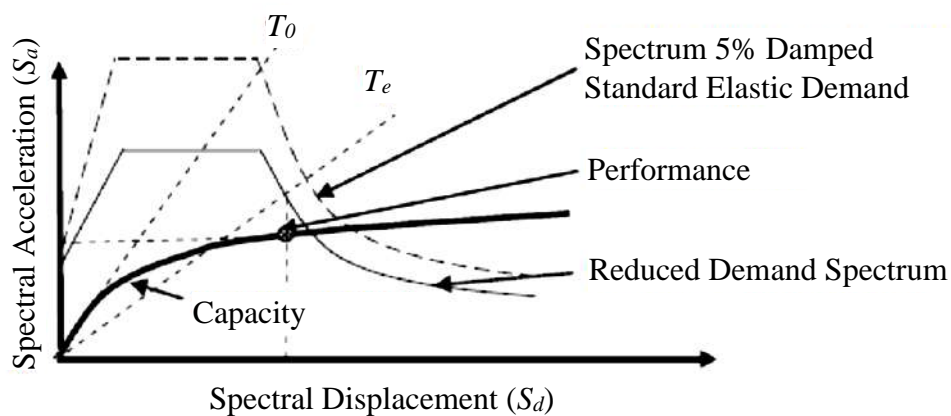


Figure 2.5: Determination of Performance Point According to Capacity Spectrum Method (Zameeruddin and Sangle, 2016)

ii) Displacement Coefficient Method (DCM):

Displacement Coefficient Method described in FEMA-356 (2000) is based on capacity curve obtained from static pushover analysis. In this method, the largest displacement demand is determined with specific coefficients. This method is enhanced in FEMA 440 published in 2005. In this method, a bilinear curve is fitted to the capacity curve so that its first segment coincides with the capacity curve at 60% of the effective yield strength, its second segment coincides with the capacity curve at the target displacement. The bilinear curve is adjusted in such a way that the area under the curve between the origin and the target displacement is equal to the area under the capacity curve. At the intersection of the two-line segments, the total lateral force applied corresponds to the effective yield strength, V_y and the control point displacement corresponds to the effective yield displacement, δ_y . The structure's effective fundamental period, T_e , in the direction under consideration is calculated using BNBC (2020) equation 6.2.51 as follows:

$$T_e = T_1 \sqrt{\frac{V_1/\delta_1}{V_y/\delta_y}} \quad (2.5)$$

Where, V_1 , δ_1 , and T_1 are determined for the first increment of lateral load.

The equation can also be written as:

$$T_e = T_i \sqrt{\frac{K_i}{K_e}} \quad (2.6)$$

Where,

T_i = Elastic fundamental period (in seconds) in the direction under consideration calculated by elastic dynamic analysis

K_i = Elastic lateral stiffness of the building in the direction under consideration

K_e = Effective lateral stiffness of the building in the direction under consideration

The target displacement of the control point, δ_t shall be determined as follows:

$$\delta_t = C_o C_1 S_a \left(\frac{T_e}{2\pi}\right)^2 g \quad (2.7)$$

Where,

C_0 = Modification factor to relate spectral displacement and likely building roof displacement

C_1 = Modification factor to relate expected maximum inelastic displacements to displacements calculated for linear elastic response

= 1.0 for $T_e \geq T_0$

= $[1.0 + (R - 1) T_0/T_e] / R$ for $T_e < T_0$

In no case may C_1 be taken as less than 1.0.

S_a = Spectral acceleration

T_e = effective fundamental period

g = Acceleration due to gravity

Calculation of target displacement is given in Figure 2.6.

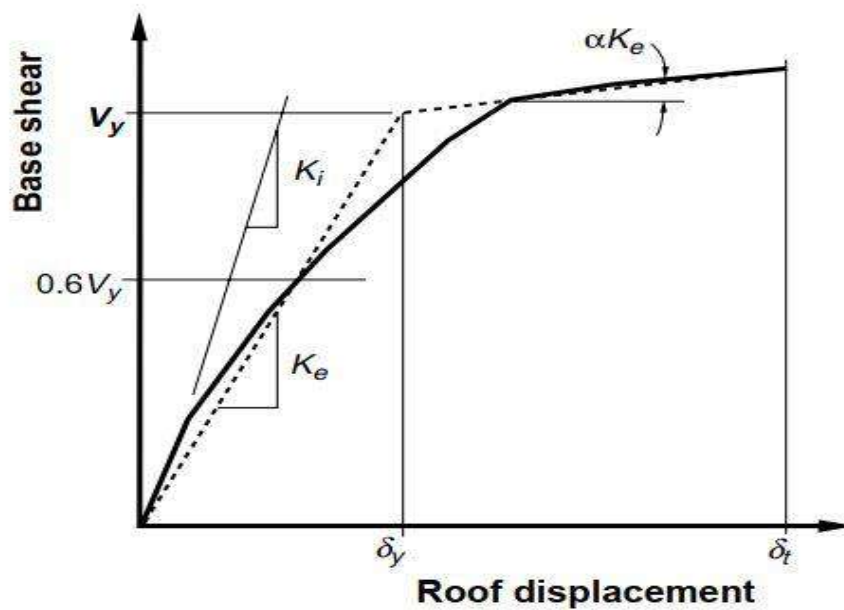


Figure 2.6: Determination of Target Displacement by Displacement Coefficient Method (FEMA 273, 1997)

A single degree of freedom at a joint or a previously established generalized displacement must be chosen as a displacement component to monitor in order to use displacement control. Additionally, the desired magnitude of the displacement to be

analyzed must be provided. To achieve that displacement, the program will try to apply the load. During the analysis, the load magnitude may increase or decrease. A control point also needs to be selected for the model. The control point for conventional buildings is usually in the center of mass of the building's topmost level, or roof.

Applying displacement loading to the structure is not the same as using displacement control. Displacement control is essentially the process of measuring the displacement caused by applied loads at a single location and modifying the magnitude of the loading to try to achieve a specific observed displacement value. Even if the displacement is regulated, the overall displaced shape of the structure will vary depending on the pattern of loading.

a) Component and Element Acceptability Limit

According to FEMA-356, All structural actions may be classified into two types:

i) Deformation controlled action and ii) Force-controlled or Load-controlled action.

FEMA 356 (2000) demonstrates all structural actions using the component force versus deformation curves shown in Figure 2.7. The Type 1 curve in Figure 2.7 illustrates ductile behavior where there is an elastic range (point 0 to point 1 on the curve) followed by a plastic range (points 1 to 3) with nonnegligible residual strength and ability to support gravity loads at point 3. The plastic range includes a strain hardening or softening range (points 1 to 2) and a strength-degraded range (points 2 to 3). Primary component actions exhibiting this behavior shall be classified as deformation-controlled if the strain-hardening or strain-softening range is such that $e > 2g$; otherwise, they shall be classified as force controlled. Secondary component actions exhibiting Type 1 behavior shall be classified as deformation-controlled for any e/g ratio. The Type 2 curve shown in Figure 2.7 is demonstrative of ductile behavior where there is an elastic range (point 0 to point 1 on the curve) and a plastic range (points 1 to 2) followed by loss of strength and loss of ability to support gravity loads beyond point 2. Primary and secondary component actions displaying such behavior shall be classified as deformation-controlled if the plastic range is such that $e > 2g$; otherwise, they shall be considered as force controlled. The Type 3 curve Figure 2.7 signifies a brittle or non-ductile behavior where there is an elastic range (point 0 to point 1 on the curve) followed by loss of strength and loss of ability to support gravity loads beyond

point 1. Primary and secondary component actions displaying Type 3 behavior shall be classified as force-controlled (FEMA 356, 2000).

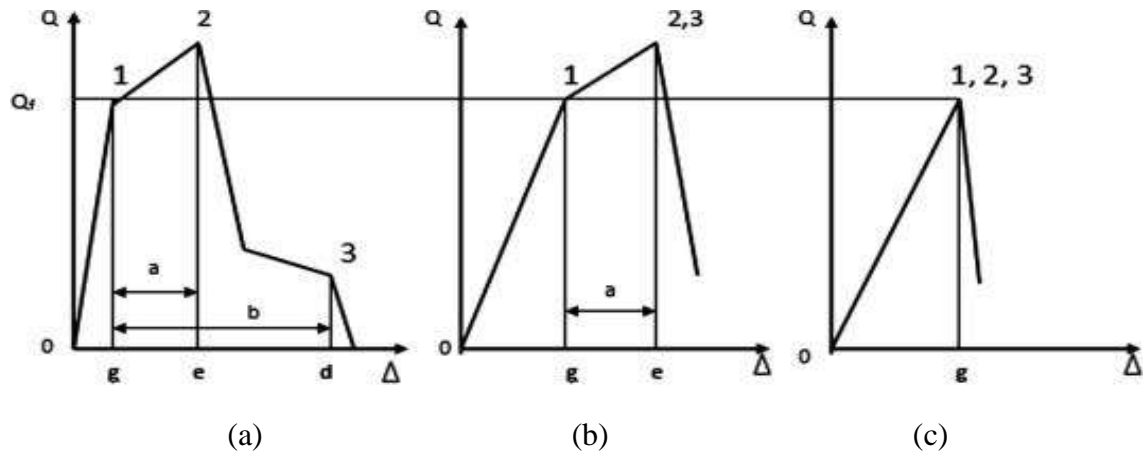


Figure 2.7: Component Force vs. Deformation Curve (a) Type 1 Curve, (b) Type 2 Curve, (c) Type 3 Curve (FEMA 356, 2000)

In pushover analysis, load-controlled action is chosen when the amount of applied load is known and the structure is expected to be able to withstand that load. A good illustration of this is the application of gravity load, which is governed by the laws of nature. All loads are applied progressively from zero to the maximum magnitude defined under load-controlled pushover analysis.

On the other hand, displacement-controlled action is used when the desired distance to move the structure is known but the required load is unknown. This is most helpful for structures that lose their ability to support loads during the analysis and become unstable.

2.7 Elements of Nonlinear Analysis

2.7.1 Shell Element

The shell element is a kind of area object that is used to simulate the behavior of membranes, plates, and shells in two- and three-dimensional systems. The material of the shell may be uniform throughout its thickness or stratified. The shell element combines membrane and plate-bending action in a three- or four-node formulation.

For specifying Material properties and loads, as well as for analyzing output, each shell element has its own unique coordinate system. Orthotropic, temperature-dependent

material characteristics are accepted. Gravity, uniform loads applied in any direction, surface pressure applied to the top, bottom, and side faces, loads resulting from strain, and temperature changes are all possible loading methods for each element.

Structures that can be modeled with this element include floor systems, wall systems, bridge decks, curved tanks and domes, detailed models of beams, columns, pipes, and other structural members.

There are two types of formulations available in a shell element. They are homogeneous (non-layered) shell and layered shell.

a) Homogeneous (Non-layered) Shell Element

The homogeneous shell element combines independent membrane and plate behavior. In the event that the element is distorted (non-planar), these behaviors become coupled. The isoparametric formulation for the membrane behavior includes translational in plane stiffness components as well as a "drilling" rotational stiffness component in the direction perpendicular to the element's plane. Displacements in planes are quadratic.

There are two thickness formulations available, depending on inclusion of transverse shearing deformations in the plate-bending behavior of a plate or shell element: i) The thick-plate (Mindlin/Reissner) formulation, which includes the effects of transverse shear deformation and ii) The thin-plate (Kirchhoff) formulation, which neglects transverse shearing deformation.

Shearing deformations are typically significant when the thickness is higher than one-tenth to one-fifth of the span. They can also be very important when there are bending-stress concentrations nearby, such as close to abrupt changes in thickness or support conditions, next to holes, or close to re-entrant corners. Despite being a little stiffer, the thick-plate formulation tends to be more accurate than the thin-plate formulation, even for thin-plate bending problems where shearing deformations are in fact insignificant. However, compared to the thin-plate formulation, the precision of the thick-plate formulation is more susceptible to large aspect ratios and mesh distortion.

Thick-plate formulation is recommended expect when working with a deformed mesh and minimum shearing deformations, or it is required to match a theoretical thin-plate solution. Only the plate-bending behavior is affected by the thickness formulation, not membrane behavior.

Although pure-membrane, pure-plate, or full-shell behavior for each homogeneous shell component in the structure can be modelled, it is typically advised to model the full shell behavior unless the entire structure is planar and properly restrained.

b) Layered Shell Element

The layered shell element allows for the specification of any number of layers, each with its own position, thickness, behavior, and material. Materials might exhibit nonlinear behavior.

In most cases, the layered Shell is a representation of full-shell behavior, but this can be adjusted on individual level, if desired. The behavior of the membrane and the plate are coupled in a layered shell unless the layering is totally symmetrical in the thickness direction.

Each layer's membrane deformation employs the strain-projection technique (Hughes, 2000). Displacements in planes are quadratic. The "drilling" degrees of freedom are not used, and they shouldn't be loaded, unlike for the homogenous shell. To avoid instability, these rotations perpendicular to the element's plane are only loosely coupled to the rigid-body rotation of the element.

The thick-plate (Mindlin/Reissner) formulation is always utilized for bending in the layered shell, which takes into account transverse shear deformations. In consistence with the in-plane displacements, the out-of-plane displacements are quadratic.

- **Modified Darwin-Pecknold Concrete Model**

A two-dimensional nonlinear concrete material model is available for use in the layered shell. This model is based on the Darwin-Pecknold model, with consideration of Vecchio-Collins behavior. This model represents the concrete compression, cracking, and shear behavior under both monotonic and cyclic loading, and considers the stress-strain components $\sigma_{11}-\varepsilon_{11}$, $\sigma_{22}-\varepsilon_{22}$, and $\sigma_{33}-\varepsilon_{33}$. A state of plane stress is assumed.

The direction of cracking can change during the loading history, and the shear strength is affected by the tension strain in the material. The axial stress-strain curve specified for the material is simplified to account for initial stiffness, yielding, ultimate plateau, and strength loss due to crushing. Zero tensile strength is assumed.

The layered shell allows this material to be used for membrane and/or flexural behavior and to be combined with steel reinforcement placed in arbitrary directions and locations.

Transverse (out-of-plane) shear is assumed to be elastic and isotropic using the shear stiffness G_{13} for both $\sigma_{13}-\gamma_{13}$ and $\sigma_{23}-\gamma_{23}$ behavior.

- **Layer Properties**

There is no limit on the number of layers that can be defined in a layered shell, even a single layer is acceptable. The location of layers is relative to a reference surface. This reference surface can be specified in any location, including the top, bottom, neutral surface, middle surface, and more. Though the element nodes are located on the reference surface by default, this can be modified via joint offsets.

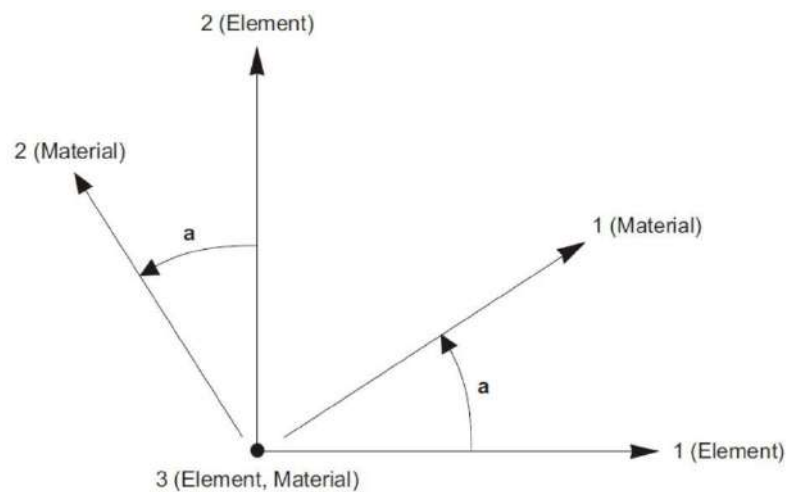


Figure 2.8: Shell Section Material Angle (CSI, 2016)

According to CSI (2016), the following parameters are used to define each layer:

- Layer Name**

Despite being arbitrary, the layer name must be distinct within a single section. However, using the same layer name in different sections can be helpful because the results for a given layer name can be plotted at the same time for different Sections of elements.

- Layer Distance**

The location of each layer is determined by stating the distance, measured in the element's positive local-3 direction, from the reference surface to the layer's center. Figure 2.9 shows an example of layer distance from reference surface.

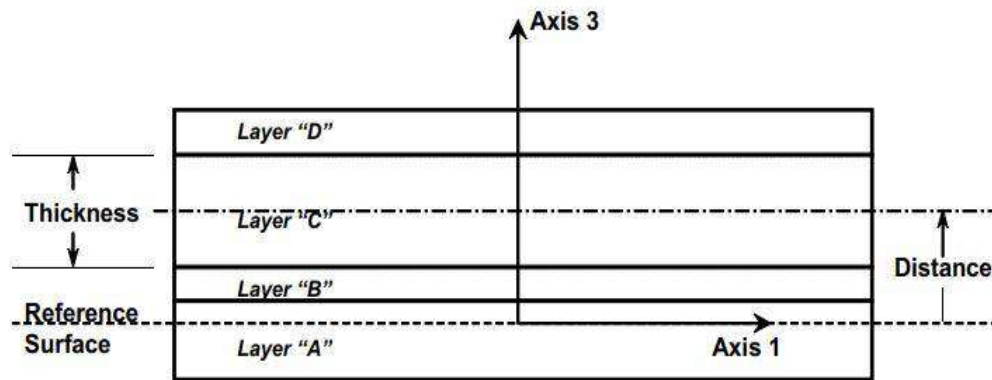


Figure 2.9: Four-Layer Shell, Showing The Reference Surface, The Names Of The Layers, And The Distance And Thickness For Layer “C” (CSI, 2016)

iii. Layer Thickness

Each layer has a single thickness that is determined by measuring it in the element's local-3 direction. A very thin "smeared" layer can be specified with an equivalent cross-sectional area to model rebar or material fibers.

iv. Layer Type

Layers can be defined in three ways as follows:

- **Membrane:** In membrane type layer, strains ($\epsilon_{11}, \epsilon_{22}, \gamma_{12}$) are computed solely from in-plane membrane displacements, and stresses in the layer ($\sigma_{11}, \sigma_{22}, \sigma_{12}$) exclusively contribute to in-plane membrane forces (F_{11}, F_{22}, F_{12}).
- **Plate:** Strains in plate type layer ($\epsilon_{11}, \epsilon_{22}, \gamma_{12}, \gamma_{13}, \gamma_{23}$) are evaluated from plate-bending rotations and transverse displacements, and stresses in the layer ($\sigma_{11}, \sigma_{22}, \sigma_{12}, \sigma_{13}, \sigma_{23}$) contribute exclusively to plate-bending moments and transverse shearing forces ($M_{11}, M_{22}, M_{12}, V_{13}, V_{23}$).
- **Shell:** A shell combines both membrane and plate behavior. Strains in shell layer ($\epsilon_{11}, \epsilon_{22}, \gamma_{12}, \gamma_{13}, \gamma_{23}$) are computed combinedly from all displacements and plate-bending rotations, and stresses in the layer ($\sigma_{11}, \sigma_{22}, \sigma_{12}, \sigma_{13}, \sigma_{23}$) contribute to all forces and plate-bending moments ($F_{11}, F_{22}, F_{12}, M_{11}, M_{22}, M_{12}, V_{13}, V_{23}$).

In most applications, layers should use shell behavior. However, in special cases, membrane and plate behavior may require to be separated. According to CSI (2016),

mass and weight are computed only for membrane and shell layers, not for plate layers. This prevents double-counting when independent membrane and plate layers are used for the same material.

v. Thickness Integration Points

Along thickness direction of each layer, a finite number of points are used to integrate (or sample) the material behavior. For each layer, up to five points can be selected which are placed according to accepted Gauss integration techniques.

For a single layer of linear material, one thickness integration point can sufficiently represent membrane behavior, and two points are capable of capturing both membrane and plate behavior. Again, a single point for can be used for thinner layers if the number of layers is numerous.

More integration points or more layers may be required to capture nonlinear yielding near the top and bottom surfaces. However, having an excessive number of integration points could lengthen the analysis process. A balance between accuracy and processing effectiveness should be determined using trial and error.

vi. Layer Material

Each layer's material attributes are defined in relation to a previously defined Material. An orthotropic, uniaxial, or isotropic material may exist. If an anisotropic substance is selected, orthotropic characteristics will be applied. The selection of material component behavior determines the material's behavior.

vii. Material Angle

The material axes for orthotropic and uniaxial materials may be rotated with respect to the element axes. The material angle in each layer could be different. For instance, two layers of uniaxial material with material angles spaced 90° apart can be used to model rebar in two orthogonal directions.

viii. Material Behavior

There are two types of material behavior specified by CSI (2016) - "Directional" and "Coupled". All materials exhibit "Directional" behavior. Only concrete materials are capable of "Coupled" behavior, which incorporates the modified Darwin-Pecknold behavior.

ix. Layer Material Components

Only "Directional" material behavior is affected by the material component selection. For each of the three membrane stress components ($\sigma_{11}, \sigma_{22}, \sigma_{12}$), linear, nonlinear, or inactive behavior can be selected. In case of a uniaxial material, the value of σ_{22} is always zero (0), so only the components (σ_{11}, σ_{12}) are significant. Material components are defined in the material local coordinate system, which relies on the material angle and may vary from layer-to-layer.

In the event when all three components are linear (two for the uniaxial material), the linear material matrix is used for the layer. All linear components utilize an uncoupled isotropic linear stress-strain law, all nonlinear components use the nonlinear stress strain relationship, and all inactive components assume zero stress if one or more of the three components are nonlinear or inactive. The elements become uncoupled and act as though Poisson's ratio is zero (CSI, 2016).

x. Interaction Between Layers

Since each layer has a distinct identity, gaps or overlaps between layers are also acceptable. We should determine what is appropriate.

For instance, when simulating a concrete slab, a single layer can be selected to represent the entire thickness of concrete and four layers to represent the rebar (two layers towards the top at a 90° angle to one another and two levels similar to these at the bottom). Since the cross-sectional area of the steel is represented by an equivalent thickness, these rebar layers would be extremely thin. The fact that the rebar layers overlap the concrete is not a concern because the layers are so thin. In the overlapping area, there is only a very minor amount of extra concrete.

All layers are kinematically linked according to the Mindlin/ Reissner formulation which assumes that normal to the reference surface remain straight after deformation (CSI, 2016). This is the shell equivalent to the beam assumption which states that plane sections remain plane after bending.

xi. Integration in the Plane

Force-deflection relationship in a layered shell is computed by integrating the stress-strain behavior through the thickness and over the 1-2 plane of the element. According to CSI (2016), for each of these thickness locations, integration in the plane is done at

the standard 2 x 2 Gauss points (coordinates ± 0.577 on a square of size ± 1.0). Only at these points nonlinear behaviors are captured. This is similar to having two fibers in each of the local directions 1 and 2, roughly at the 1/4 and 3/4 points. Other than the four Gauss points, plotted or tabulated stresses are extrapolated or interpolated and may not accurately reflect the measured nonlinear stresses. As a result, stresses at the joints may occasionally seem to be greater than failure stresses.

c) Shell Element Internal Forces

The internal shell element forces are forces per unit length that act along the mid-surface of the shell element. Figure 2.10 illustrates the six faces of a shell element: positive face 1, negative face 1, positive face 2, negative face 2, positive face 3, and negative face 3.

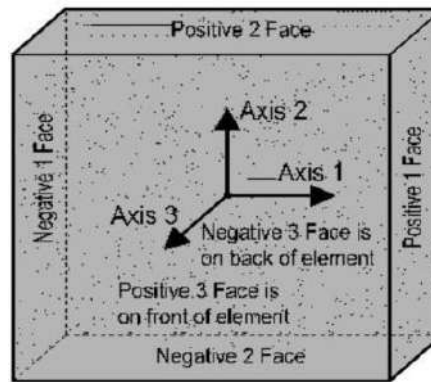


Figure 2.10: Positive and Negative Faces of Shell Element in ETABS (CSI, 2023).

In general, shell forces are represented in the form F_{ij} , where i can be equal to 1 or 2 and j can be equal to 1, 2 or 3. F_{ij} denotes that the force occur on face i of an element in direction j . Direction j refers to the local axis direction of the shell element. The basic in- plane shell element forces are identified as F_{11} , F_{22} , and F_{12} . F_{11} denotes the direct forces that occur on face 1 of the element (perpendicular to the local 1 axis) and act in the direction parallel to the local 1 axis (that is, the stresses act normal to face 1). Likewise, F_{22} signifies the direct forces that occur on face 2 of the element (perpendicular to the local 2 axis) and act in the direction parallel to the local 2 axis (that is, the stresses act normal to face 2). F_{12} denotes shearing forces that occur on face 1 of the element (perpendicular to the local 1 axis) and act in the direction parallel to the local 2 axis (that is, the stresses act parallel to face 1). F_{21} is always equal to F_{12} so

it is not necessary to report F_{21} . ETABS 2016 reports values for the shell internal forces at the element nodes. Figure 2.11 shows internal F_{11} forces acting on the mid surface of a shell element. In the figure, the force distribution labeled (a) represents an actual F_{11} force distribution. The force distribution labeled (b) shows how the software calculates only the internal forces at the corner points of the shell element. The force distribution labeled (c) in the figure shows how the F_{11} forces are assumed to vary linearly along the length of the shell element between the calculated F_{11} force values at the element nodes for graphical plotting purposes only (CSI 2023).

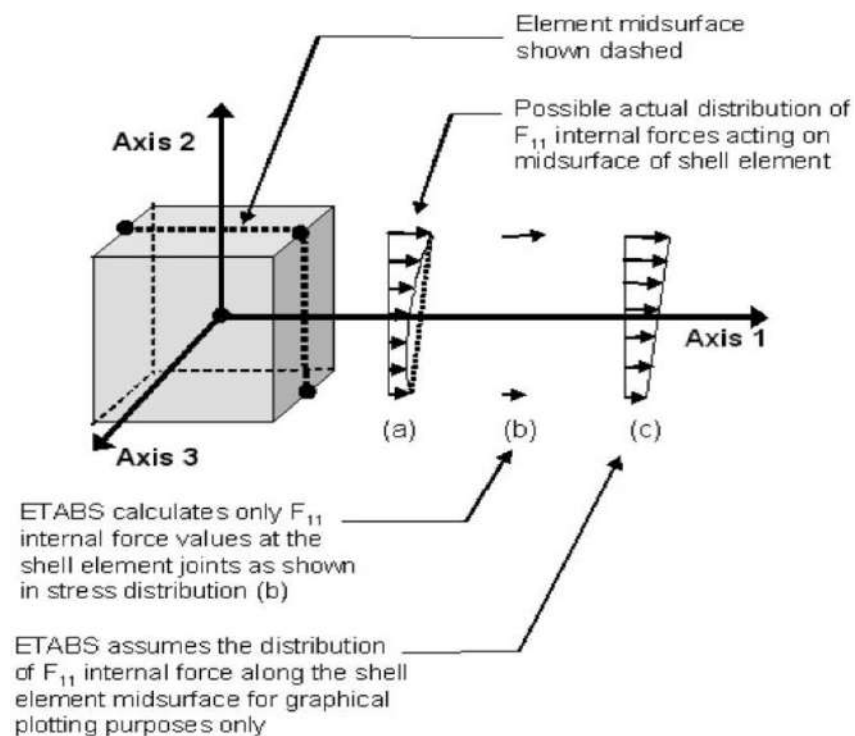


Figure 2.11: Distribution of Internal F_{11} Force (CSI, 2023).

Figure 2.12 below illustrates the positive directions for shell element internal forces F_{11} , F_{22} , F_{12} , V_{13} and V_{23} .

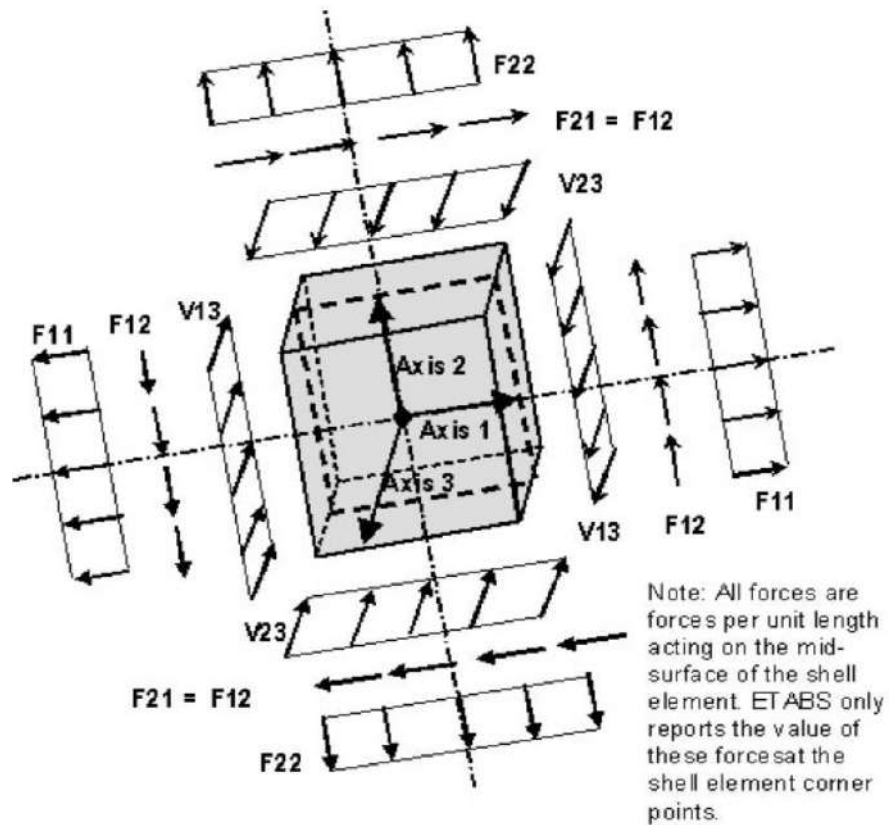


Figure 2.12: The Positive Directions for Shell Element Internal Forces F_{11} , F_{22} , F_{12} , V_{13} and V_{23} (CSI, 2023).

The internal shell element stresses are stresses effective on the edges (not the positive and negative three-axis faces) of the shell element (area object). Comparable to shell forces, shell stresses are represented in the form S_{ij} , where i can be equal to 1 or 2 and j can be equal to 1, 2 or 3. S_{ij} denotes that the force occur on face i of an element in direction j . Direction j refers to the local axis direction of the shell element. S_{11} stresses are the direct stresses that occur on face 1 of the element (perpendicular to the local 1 axis) and act in the direction parallel to the local 1 axis (that is, the stresses act normal to face 1). Similarly, S_{22} stresses are the direct stresses that occur on face 2 of the element (perpendicular to the local 2 axis) and act in the direction parallel to the local 2 axis (that is, the stresses act normal to face 2). S_{12} denotes shearing stresses that occur on face 1 of the element (perpendicular to the local 1 axis) and act in the direction parallel to the local 2 axis (that is, the stresses act parallel to face 1) (CSI, 2023).

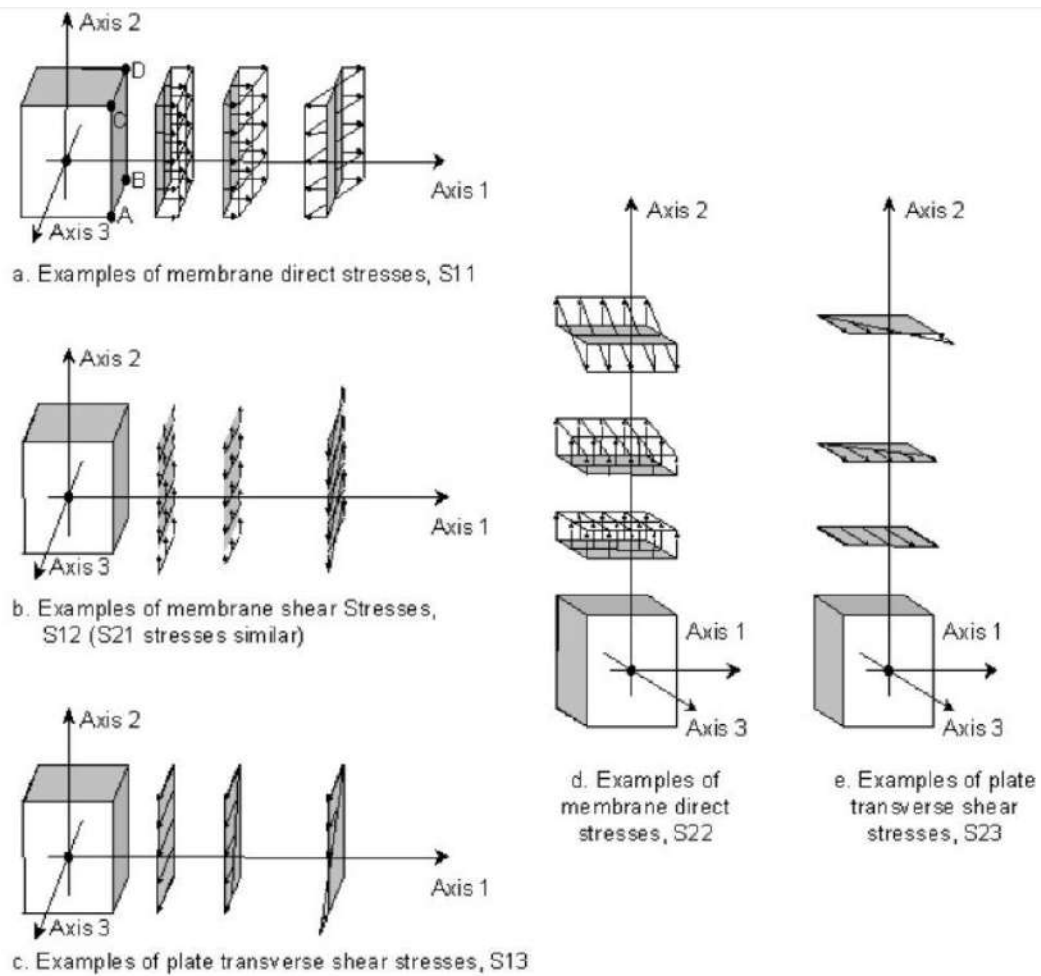


Figure 2.13: Direct and Shearing Stress Components of Shell Elements in ETABS (CSI, 2023).

The shell element internal stresses act throughout the element. Although it is possible to calculate these stresses at any location on the shell element, they are calculated only at the corner points as it is a suitable location and it keeps the amount of output within a reasonable limit.

Figure 2.13 shows direct and shearing stress components of shell elements. The points where ETABS 2016 (2017) reports the shell element internal stress values for the positive 1 face internal stresses is shown in Figure 2.14 and the positive directions for shell element internal stresses are illustrated in Figure 2.15.

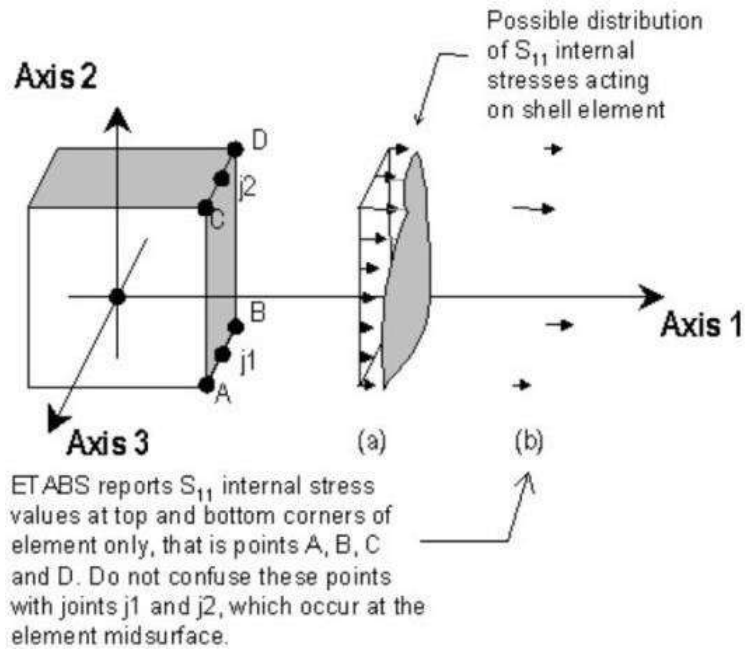


Figure 2.14: The Points Where ETABS Reports the Shell Element Internal Stress Values for the Positive 1 Face Internal Stresses (CSI, 2023).

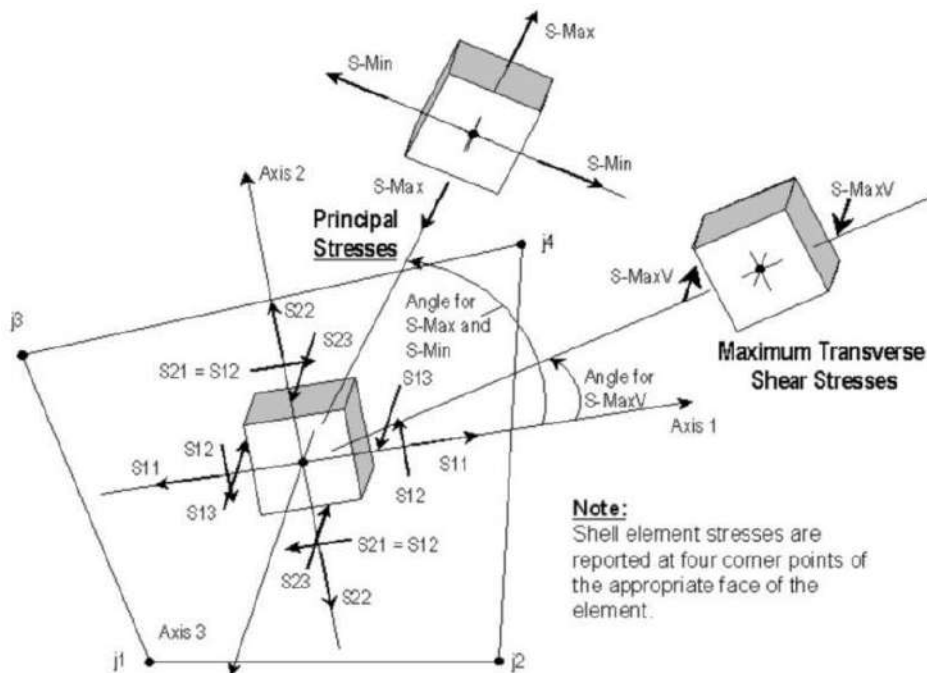


Figure 2.15: The Positive Directions for Shell Element Internal Stresses S_{11} , S_{22} , S_{12} , S_{13} , S_{23} , the Principal Stresses (S_{Max} And S_{Min}) and the Positive Directions for the Maximum Transverse Shear Stresses, $S_{\text{Max-V}}$ (CSI, 2023).

2.7.2 Nodes

The shell element can consist of three or four nodes. It is important to note that the four-joint element does not necessarily have to be planar. To determine the stiffness of the shell element, a four-point numerical integration formulation is employed. Stresses, internal forces, and moments within the element, in the local coordinate system, are evaluated at specific Gauss integration points and then extrapolated to the joints of the element (CSI, 2016).

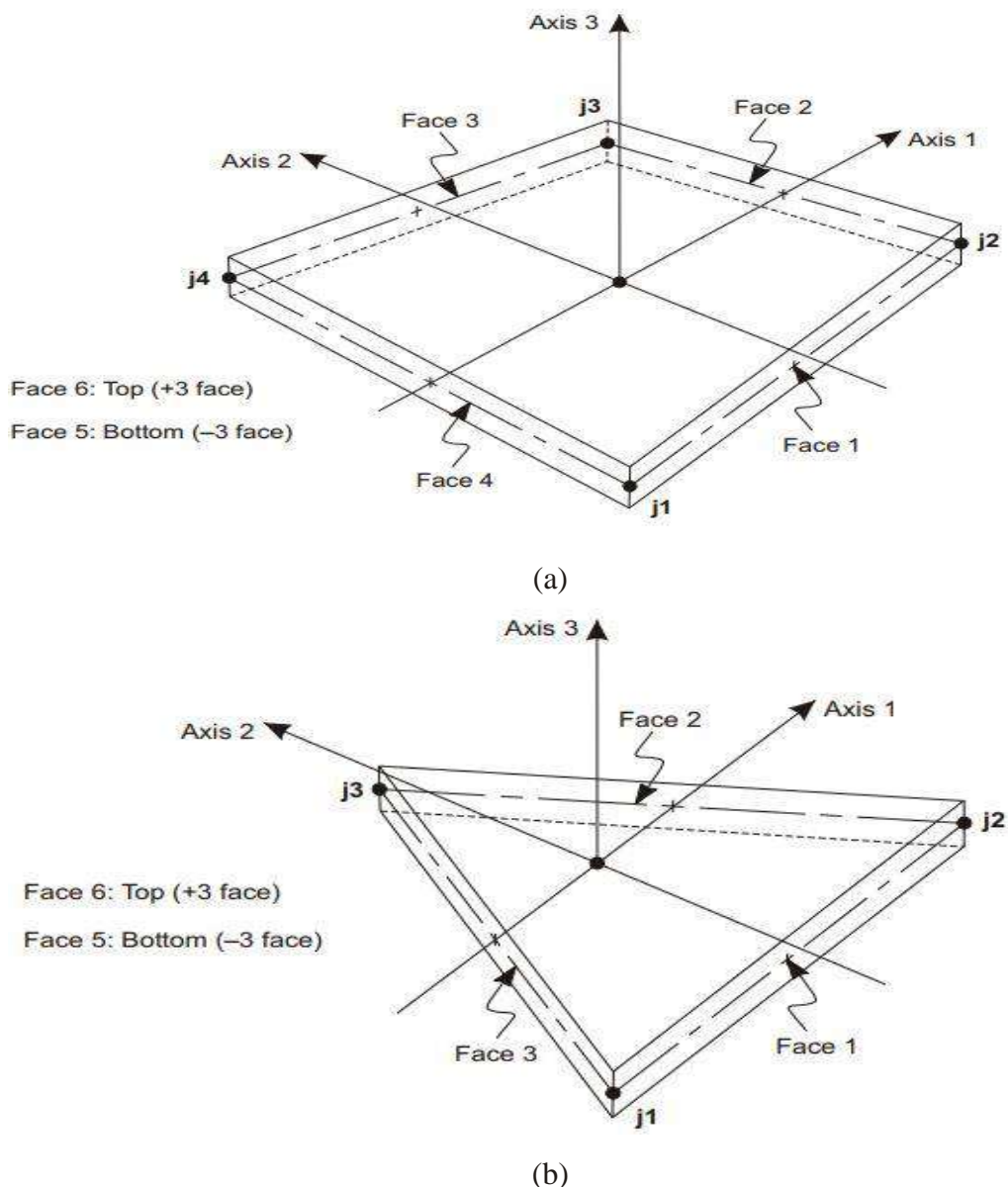


Figure 2.16: Nodes in Shell Element (a) Four-Node Quadrilateral Shell Element (b) Three-Node Triangular Shell Element (CSI, 2016)

Figure 2.16 illustrates the various shapes that can be associated with shell elements and other types of area objects/elements. These shapes can be classified into two categories:

- a) Quadrilaterals: These shapes are defined by four joints, namely j_1 , j_2 , j_3 , and j_4 .
- b) Triangles: These shapes are defined by three joints, namely j_1 , j_2 , and j_3 .

In the case of shell elements, the corners of the reference surface are defined by joints j_1 to j_4 . For homogeneous shells, this reference surface corresponds to the mid-surface of the element (CSI, 2016). However, in layered shells, there is flexibility to choose the position of this surface relative to the material layers.

2.7.3 Hinges

A hinge property is a set of nonlinear properties that can be assigned to an element. Non-linear behavior of a Frame or Shell (shear wall) element can be observed by adding hinges to the element. A frame element may have any number of hinges assigned to it anywhere along the element's clear length. There are four types of hinges available - shear, torsion, uncoupled moment, and axial force hinges. Additionally, coupled P-M2-M3 hinges can yield as a result of the interaction of an axial force and bi-axial bending moments at the hinge position. Subsets of these hinges can exhibit P-M2, P-M3, and M2-M3 behavior.

Hinges affect the behavior of the structure in nonlinear static and nonlinear time-history analyses. Nonlinear modal time-history (FNA) analyses are affected by hinge behavior only when hinges are modeled as links.

Hinges can be categorized into two types- i) Force and moment type hinges and ii) Fiber hinges. Fiber hinges are often more realistic than force-moment hinges, but requires more computational effort.

a) Force and Moment Type Hinges

Force and moment type hinges have rigid-plastic properties. Plastic force-displacement behavior can be specified for each force degree of freedom (axial and shear), and plastic moment-rotation behavior can be chosen for each moment degree of freedom (bending and torsion). According to CSI (2016), each hinge property may have plastic properties specified for any number of the six degrees of freedom. The axial force and the two bending moments may be coupled through an interaction surface. Degrees of freedom that are not specified remain elastic. For force/moment-type hinges, elastic deformation

occurs along the entire length of the Frame element and is not affected by the presence of the hinges.

b) Fiber Hinges

Fiber hinges are used to characterize the combined axial force and bi-axial bending behavior at places along the length of a frame member. They are elastic-plastic in nature and consist of a series of material points, each of which represents a portion of the frame's cross-section composed of the same material. Force-deflection and moment-rotation curves are not specified in fiber hinge, instead are computed from the stress-strain curves of the material points during the analysis. These hinges can be defined manually, or created automatically for certain types of frame sections, such as Section-Designer sections.

In ETABS, fiber P-M3 hinges can be assigned to vertical shear walls which act at the center of the shell element. When hinges are included in a shear wall shell element, the vertical membrane stress behavior is controlled by the hinge, whereas the horizontal and shear membrane stress, as well as out-of-plane bending behavior, are controlled by the shell element's characteristics.

The Fiber P-M2-M3 (Fiber PMM) hinge models the axial behavior of a number of representative axial “fibers” distributed across the cross section of the frame element. Each fiber has a location, a tributary area, and a stress-strain curve. The axial stresses are integrated over the section to compute the values of P, M2 and M3. Likewise, the axial deformation U1 and the rotations R2 and R3 are used to compute the axial strains in each fiber. Plane sections are assumed to remain planar.

The material direct nonlinear stress-strain curve is utilized for individual fiber in the cross section to evaluate the axial $\sigma_{11} - \epsilon_{11}$ relationships at a fiber hinge. The $\sigma_{11} - \epsilon_{11}$ remains the same for any material type, i.e., Uniaxial, Isotropic, Orthotropic, or Anisotropic. Shear behavior is not considered in the fibers, instead is computed for the frame section using the linear shear modulus g12. Combining the behavior of all the fibers at a cross section and multiplying by the hinge length gives the axial force-deformation and biaxial moment-rotation relationships (CSI, 2016).

2.8 Available Lateral-Force-Resisting Systems

Seismic or earthquake loads are influenced by the mass, stiffness, and ability of a structure to absorb energy, such as through damping and ductility. To ensure optimal seismic performance, it is crucial to have a complete lateral force resisting system that establishes a continuous load path between the foundation, all levels of diaphragms, and all components of the building. This system will help distribute the seismic forces and ensure that the structure can withstand the effects of an earthquake. Connections to horizontal diaphragms transmit seismic forces that originate throughout the building, mostly in the heavier mass components like diaphragms, and the diaphragms distribute these forces to vertical members. The vertical components transfer the forces into the foundation, which then transmits the forces to the soil's supporting structure. The following vertical components are commonly utilized to transmit lateral forces to the ground (Taranath, 2004): 1) moment-resisting frames; 2) shear walls and 3) braced frames.

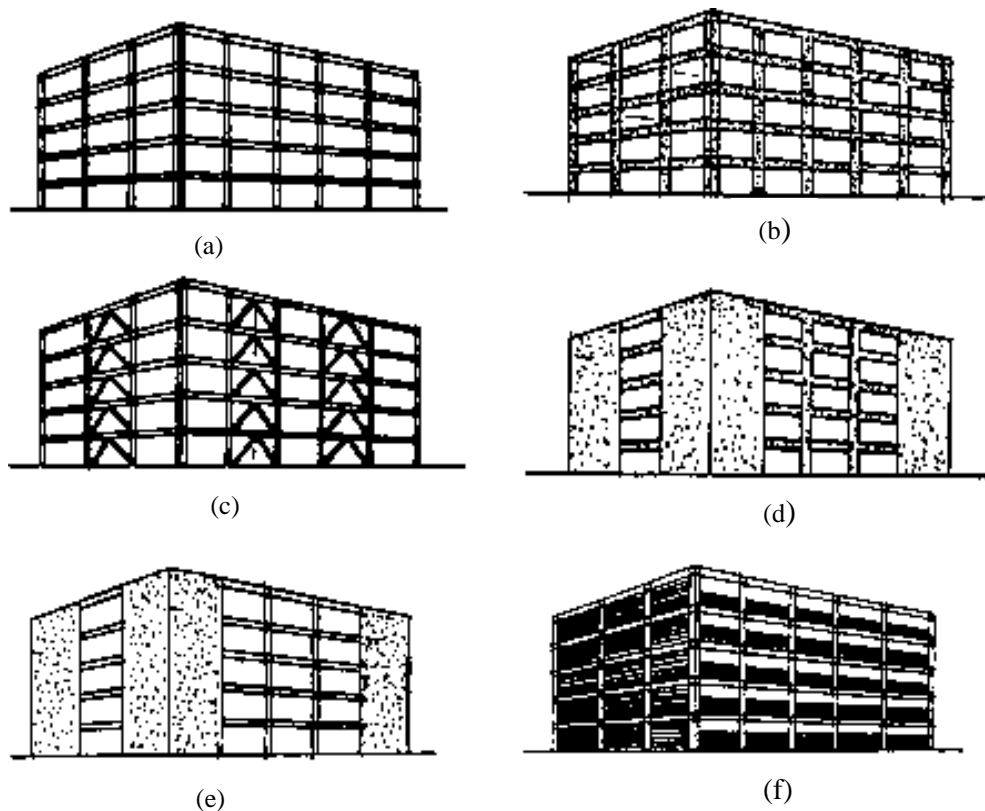


Figure 2.17: Lateral-Force-Resisting Systems: (a) Steel Moment-Resisting Frame; (b) Reinforced Concrete Moment-Resisting Frame; (c) Braced Steel Frame; (d) Reinforced Concrete Shear Walls; (e) Steel Frame Building with Cast-In-Place Concrete Shear Walls; (f) Steel Frame Building with In-Filled Walls of Nonreinforced Masonry. (Taranath, 2004)

As described by Taranath (2004), some common systems that can be used effectively for providing resistance to seismic lateral forces are shown in Figure 2.17. A complete, three-dimensional space frame, a coordinated system of moment frames, shear walls, or braced frames with horizontal diaphragms, or a mix of the systems, are prerequisites for all of the systems.

2.8.1 Bearing Wall System

The space frame supporting gravity loads is not complete in buildings with bearing wall system. Shear walls (or braced frames) provide support for all or most gravity loads as well as lateral loads. Generally, a shear wall (or braced frame) building is more rigid than a framed one. Shear walls' deflection is considerably small as the design stress limits are low. Shear wall construction is an inexpensive way to brace structures to prevent damage, and typically up to roughly 15 floors, it is economically viable. Shear walls often operate exceptionally well, with two notable exceptions - when their height-to-width ratio exceeds a certain point making it susceptible to overturning and when they have an excessive number of openings. Additionally, if the ground beneath a shear wall's footings is soft, the entire shear wall may rotate, resulting in localized damage to the area around the wall.

2.8.2 Building Frame System

It is a structural system with an essentially complete space frame where support for gravity loads are given by the frame system and resistance to lateral loads are given by shear walls or braced frames individually. This system utilizes shear walls or braced frames to resist 100% of the lateral forces. A building frame system's seismic safety is based on meeting the standards for deformation compatibility. When a structure's designated lateral-force-resisting system deforms, the subsystems that had been arbitrarily chosen as gravity systems, will inevitably deform together since they are connected at every floor level. If the gravity-based subsystems fail to sustain their gravity load-carrying capacity as a result of lateral displacement brought on by earthquake, then life-safety is compromised. Therefore, it is a specific requirement of all seismic codes, including BNBC, that structural elements or subsystems not designed to be part of the lateral-force-resisting system must be able to sustain their gravity load-

carrying capacity at an amplified elastic lateral displacement under code-prescribed design seismic forces.

2.8.3 Moment-Resisting Frame

Moment-resisting frames have an essentially complete space frame where the members are connected by rigid joints that transfer moment. The columns and beams act in bending in buildings when a space frame resists the earthquake stresses. Story-to-story deflection (story drift) during a strong earthquake might be supported by the structural system without risking the integrity of the columns or beams. However, the drift might be enough to harm components that are rigidly tied to the structural system including brittle partition walls, stairways, pipes, outside walls, and other parts that span multiple stories. Buildings can therefore sustain significant interior and exterior nonstructural damage while remaining structurally sound. Although repelling seismic forces by frame action has great theoretical and financial justifications, for specific buildings, this technique may not be worth the financial risk unless extra damage-control procedures are applied.

2.8.4 Dual System

If the moment-resisting frame is independently capable of withstanding at least 25% of the applicable total seismic lateral force, the system is referred to as a dual system. Moment frames and shear walls (or braced frames) are designed according to their relative rigidities to resist the design base shear (Taranath, 2004).

2.9 Structural Performance Levels

The Performance of a building under any particular event depends on a wide range of parameters. In guidelines such as ATC-40 and FEMA 356, these parameters are qualitatively defined in terms of the safety the building provides to the occupants both during and after the event; the cost and feasibility of restoring the building to its pre-earthquake condition; the amount of time the building is out of service while repairs are being made; and the economic, architectural, or historic effects on the larger community. The extent of damage the building would sustain is closely correlated with these performance parameters. A performance level describes a limiting damage condition which may be considered satisfactory for a given building and a given ground motion. The seismic performance of a building structure is measured by the state of

damage under certain seismic hazard which is quantified by roof displacement and corresponding deformation of the structural members.

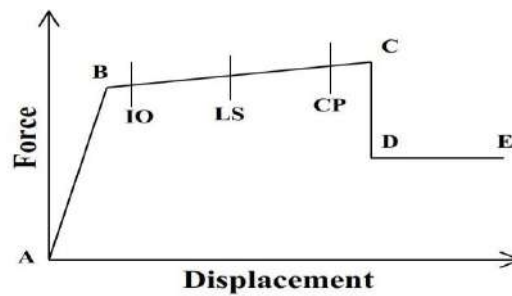


Figure 2.18: The A-B-C-D-E Curve for Force vs. Displacement and Moment vs. Rotation

Figure 2.18 shows force- displacement relation for plastic hinge in pushover analysis. A similar curve is used for showing moment-rotation relationship as well. A force-displacement (moment-rotation) curve can be defined for each force or moment degree of freedom that illustrates the yield value and the plastic deformation following yield. There are five points labelled A, B, C, D, and E used to define the force-deformation behavior of the plastic hinge. The state specified by each point is described below:

- Point A defines the origin.
- Point B represents yielding. No deformation occurs in the hinge up to point B, regardless of the deformation value specified for point B. The displacement (rotation) at point B will be subtracted from the deformations at points C, D, and E. Only the plastic deformation beyond point B will be exhibited by the hinge.
- Point C represents the ultimate capacity for pushover analysis. However, a positive slope from C to D can be specified for other purposes.
- Point D represents a residual strength for pushover analysis. Nevertheless, a positive slope from C to D or D to E may be specified for other purposes.
- Point E represent total failure. Beyond point E the hinge will drop load down to point F (not shown) directly below point E on the horizontal axis.

Three points labelled IO (immediate occupancy), LS (life safety), and CP (collapse prevention) are used to define acceptance criteria for the hinge. There are six levels of structural performance defined in FEMA 356, 2000, i.e., Immediate occupancy (S-1), Damage control range (S-2), Life safety (S-3), Limited safety range (S-4), Collapse

prevention (S-5), and Not considered (S-6). These performance levels are described as in the standard below:

2.9.1 Immediate Occupancy Structural Performance Level (S-1)

Immediate occupancy structural performance level S-1 may be defined as the post-earthquake damage state of a structure that remains safe to occupy, essentially retains the pre-earthquake design strength and stiffness of the structure, and is in compliance with the acceptance criteria specified in FEMA 356. This damage state considers very limited structural damage has occurred. The basic vertical and lateral-force-resisting systems of the building retain nearly all of their pre-earthquake strength and stiffness. The risk of life-threatening injury as a result of structural damage is very low, and although some minor structural repairs may be appropriate, these would generally not be required prior to re-occupancy.

2.9.2 Damage Control Structural Performance Range (S-2)

Damage control structural performance range S-2, may be defined as the continuous range of damage states between the life safety structural performance level (S-3) and the immediate occupancy structural performance level (S-1). Design for the damage control structural performance range may be desirable to minimize repair time and operation interruption, as a partial means of protecting valuable equipment and contents, or to preserve important historic features when the cost of design for immediate occupancy is excessive.

2.9.3 Life Safety Structural Performance Level (S-3)

Structural performance level S-3, life safety, may be defined as the post-earthquake damage state that includes damage to structural components but retains a margin against onset of partial or total collapse in compliance with the acceptance criteria specified in FEMA 356 for this structural performance level. Structural performance level S-3, life safety, means the post-earthquake damage state in which significant damage to the structure has occurred, but some margin against either partial or total structural collapse remains. Some structural elements and components are severely damaged, but this has not resulted in large falling debris hazards, either within or outside the building. Injuries may occur during the earthquake; however, the overall risk of life-threatening injury as a result of structural damage is expected to be low. It should be possible to repair the structure; however, for economic reasons this may not be practical. While the damaged

structure is not an imminent collapse risk, it would be prudent to implement structural repairs or install temporary bracing prior to re-occupancy.

2.9.4 Limited Safety Structural Performance Range (S-4)

Limited safety structural performance range S-4 may be defined as the continuous range of damage states between the life safety structural performance level (S-3) and the collapse prevention structural performance level (S-5).

2.9.5 Collapse Prevention Structural Performance Level (S-5)

Structural performance level S-5, collapse prevention, may be defined as the post-earthquake damage state that includes damage to structural components such that the structure continues to support gravity loads but retains no margin against collapse in compliance with the acceptance criteria specified in FEMA 356 for this structural performance level. Structural performance level S-5, collapse prevention, means the post-earthquake damage state in which the building is on the verge of partial or total collapse. Substantial damage to the structure has occurred, potentially including significant degradation in the stiffness and strength of the lateral-force resisting system, large permanent lateral deformation of the structure, and to more limited extent degradation in vertical load carrying capacity. However, all significant components of the gravity load resisting system must continue to carry their gravity load demands. Significant risk of injury due to falling hazards from structural debris may exist. The structure may not be technically practical to repair and is not safe for re-occupancy, as aftershock activity could induce collapse.

2.10 Global Building Acceptability Limits

Nonlinear modeling parameters and acceptance criteria for slab-column connections are provided in ASCE 41-17. Diverse relations shall be permitted where verified by experimentally obtained cyclic response relations of slab-column subassemblies. The values provided in Table 2.3 are used to assess punching failures at slab-column connections. Elwood et al. (2007) provides a comparison of the modeling parameters in Table 10-15 and test data summarized by Kang and Wallace (2006). Lateral drift ratio is typically reported for test data; therefore, plastic rotations were derived from the test data assuming column deformations were negligible and yield rotations of 0.01 and 0.015 radians for reinforced concrete and posttensioned slabs, respectively. The

larger rotation value for posttensioned connections reflects the larger span-to-slab thickness ratios common for this type of construction.

Table 2.3: Modeling Parameters and Numerical Acceptance Criteria for Nonlinear Procedures—Two-Way Slabs and Slab–Column Connections (ASCE 41-17, 2017)

Conditions		Modeling Parameters ^a			Acceptance Criteria ^a		
		Plastic Rotation Angle (Radians)		Residual Strength Ratio	Performance Level		
		a	b		IO	LS	CP
Condition i. Reinforced concrete slab–column connections ^b							
(V _g /V _o) ^c	Continuity Reinforcement ^d						
0	Yes	0.035	0.05	0.2	0.01	0.035	0.05
0.2	Yes	0.03	0.04	0.2	0.01	0.03	0.04
0.4	Yes	0.02	0.03	0.2	0	0.02	0.03
≥ 0.6	Yes	0	0.02	0	0	0	0.02
0	No	0.025	0.025	0	0.01	0.02	0.025
0.2	No	0.02	0.02	0	0.01	0.015	0.02
0.4	No	0.01	0.01	0	0	0.008	0.01
0.6	No	0	0	0	0	0	0
≥ 0.6	No	0	0	0	__e	__e	__e
Condition ii. Posttensioned slab–column connections ^b							
(V _g /V _o) ^c	Continuity Reinforcement ^d						
0	Yes	0.035	0.05	0.4	0.01	0.035	0.05
0.6	Yes	0.005	0.03	0.2	0	0.025	0.03
≥ 0.6	Yes	0	0.02	0.2	0	0.015	0.02
0	No	0.025	0.025	0	0.01	0.02	0.025
0.6	No	0	0	0	0	0	0
≥ 0.6	No	0	0	0	__e	__e	__e
Condition iii. Slabs controlled by inadequate development or splicing along the span ^b							
		0	0.02	0	0	0.01	0.02
Condition iv. Slabs controlled by inadequate embedment into slab–column joint ^b							
		0.015	0.03	0.2	0.01	0.02	0.03
^a Values between those listed in the table should be determined by linear interpolation.							
^b Where more than one of conditions i, ii, iii, and iv occur for a given component, use the minimum appropriate numerical value from the table.							
^c V _g is the gravity shear acting on the slab critical section as defined by ACI 318, and V _o is the direct punching shear strength as defined by ACI 318.							

^d“Yes” should be used where the area of effectively continuous main bottom bars passing through the column cage in each direction is greater than or equal to $0.5 V_g / (\phi f_y)$. Where the slab is posttensioned, “Yes” should be used where at least one of the posttensioning tendons in each direction passes through the column cage. Otherwise, “No” should be used.

^eAction should be treated as force controlled. Action should be treated as force controlled

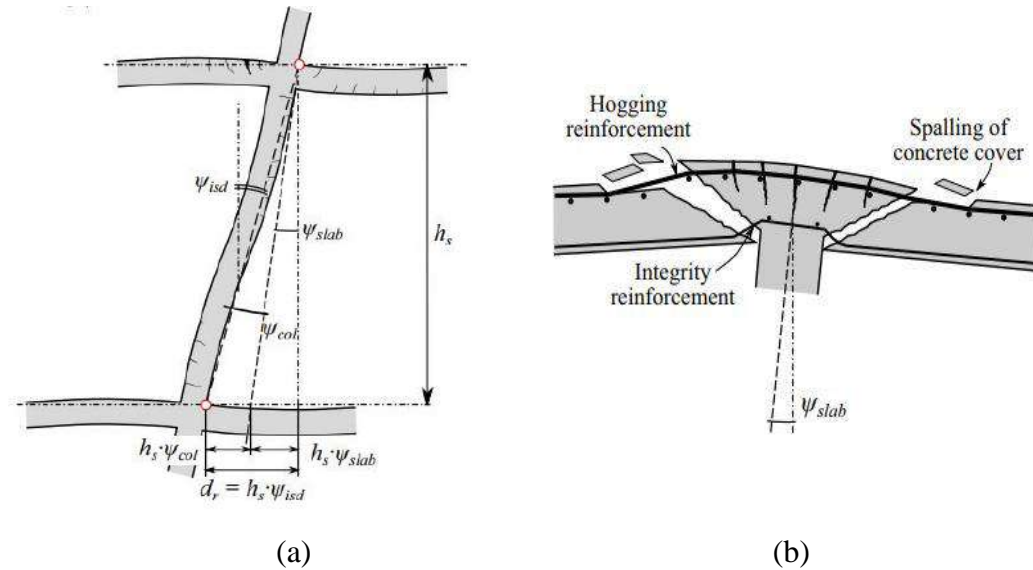


Figure 2.19: Slab Rotation (a) Relationship between Interstorey Drift D_r , Column Rotation Ψ_{col} and Contribution of the Slab Ψ_{slab} to the Interstorey Drift Ratio Ψ_{isd} ; (b) Situation after Punching (Coronelli et al., 2022)

Figure 2.19 illustrates the plastic rotation angle for global limit check. As shown in Figure 2.19, the interstorey drift d_r typically comprises the deformation of the slab (rotation ψ_{slab}) and of the column (rotation ψ_{col}) (Drakatos et al., 2018). The relation can be expressed as:

$$d_r = (\psi_{slab} + \psi_{col}) h_s \quad (2.8)$$

Here, h_s is the story height. Since, for non-slender columns, the column rotation ψ_{col} is often small compared to the slab rotation ψ_{slab} , the latter is often approximated with the interstorey drift ratio $\psi_{isd} = d_r / h_s$ ($\psi_{slab} \approx \psi_{isd}$).

2.11 Remarks

In this chapter, notable experimental studies and analytical methods used by different researchers to investigate the failure mechanisms of flat plate structures have been

explored. A specific focus is placed on the examination of the punching shear failure mechanism in flat plate structures. Additionally, it covers the essential requirements outlined in different building codes for this analysis. The chapter also presents seismic design concepts and provisions adopted by various codes. The study reveals that BNBC (2020) incorporates the ACI Code with slight adjustments.

Chapter 3

NUMERICAL MODELLING

3.1 Introduction

This section introduces the numerical modeling used for pushover analysis of the shear wall-flat plate (SW-FP) structural system. This study utilized a ready-made garments (RMG) manufacturing facility located in Narayanganj, Bangladesh. Case study structures have been modeled in three dimensions using ETABS 2016. For structural analysis, all elements are designed and detailed in accordance with ACI 318-08, ASCE 7-05, and BNBC 2020 forces and load combinations. Nonlinear static (NLSA) or pushover analysis has been carried out in compliance with ASCE 41-13 after all elements have been designed. This chapter has covered the fundamental design aspects for linear static analysis and nonlinear static or pushover analysis (NLSA).

3.2 Linear Static Analysis

3.2.1 Design Codes

Structural analysis and design of all models have been performed according to the load requirements in Bangladesh National Building Code (BNBC) 2020 and ASCE 7-05. The design of structural components was carried out according to the provisions of the ACI 318-08.

3.2.2 Material Specifications

For concrete, 20 MPa (3 ksi) and for steel reinforcement, 420 MPa (60 ksi) material strength have been considered in this research. All structural components have been designed with this specification.

3.2.3 Loading Criteria

The building has been analyzed for two types of possible load actions, Gravity and Lateral Loads (seismic and wind loads).

a) Gravity Loads

Gravity Loads, such as dead and live loads applied at the floors or roofs of the building according to the provision of Chapter 2, Part 6 of BNBC 2020 are shown in Table 3.1.

Table 3.1: Considered Loads

Load type	Typical floor		Roof	
	Load name	Value (KN/m ²)	Load name	Value (KN/m ²)
Dead load	Floor finish	1.2(25 psf)	Floor finish	1.9(40 psf)
	Partition Wall on floors	1.2(25 psf)	Parapet Wall on beams	1.75 (120 plf)
	Fixed Partition Wall on beams	13.15kN/m (900 plf)		
Live load	Floor Live Load	3.01(63 psf)	Roof Live Load	2.01(42 psf)
	Stair case	4.78(100 psf)		

b) Lateral Loads

Lateral Loads, such as Wind Load and Seismic Load applied at the building in accordance with the provisions of Chapter 2, Part 6 of BNBC 2020 is as follows:

i) Wind Load Consideration Parameters

Basic Wind Speed, V_b	: 61.1 m/s (Narayanganj, Bangladesh)
Occupancy category	: II
Structural Importance Coefficient, I	: 1.00
Exposure Category	: A
Topographic Factor, K_{zt}	:1
Wind Directionality Factor, K_d	:0.85

ii) Seismic Load Consideration Parameters

Seismic load parameters have been taken from BNBC (2020). According to BNBC (2020), the spectral acceleration for the design earthquake is given by the following equation:

$$S_a = \frac{2}{3} \frac{ZIC}{R} C_s \quad (3.1)$$

Where,

S_a = Design spectral acceleration (in units of g) which shall not be less than $0.67\beta ZIS$

β = Coefficient used to calculate lower bound for S_a . Recommended value for β is 0.11

Z= Seismic zone coefficient

I = Structure importance factor

R = Response reduction factor which depends on the type of structural system given in

Table 6.2.19. The ratio I/R cannot be greater than one.

C_s = Normalized acceleration response spectrum

The fundamental building period T (in sec) may be approximated by the following formula:

$$T = C_t (h_n)^m \quad (3.2)$$

Where,

h_n = Height of building in meters from foundation or from top of rigid basement. This excludes the basement stories, where basement walls are connected with the ground floor deck or fitted between the building columns. But it includes the basement stories, when they are not so connected.

C_t and m = Constants that are obtained from Table 6.2.20 of BNBC (2020).

Building period T shall not exceed the approximate fundamental period determined by Eq. 6.2.38 of BNBC (2020) by more than 40 percent.

The seismic design base shear force in a given direction shall be determined from the following relation:

$$V = S_a \times W \quad (3.3)$$

Where,

S_a = Lateral seismic force coefficient. It is the design spectral acceleration (in units of g) corresponding to the building period T .

W = Total seismic weight of the building defined.

All the models are designed as dual system flat plate slabs. They are special moment frames capable of resisting at least 25% of prescribed seismic forces (with bracing or shear wall). The type Special Reinforced Concrete Shear Walls has been considered as the structural system. The soil profile has been taken as deposits of loose-to-medium cohesion less soil or of predominantly soft-to-firm cohesive soil. The parameters considered for seismic design are listed below:

Seismic Zone Coefficient, Z : 0.2 [BNBC Table 6.2.15]

Zone II (Narayanganj, Bangladesh)

Structural Importance Factor, I	: 1 [BNBC Table 6.2.9]
Response Reduction Factor, R	: 7 [BNBC Table 6.2.19]
System Overstrength Factor, Ω_o	: 2.5 [BNBC Table 6.2.19]
Deflection Amplification Factor, C_d	: 5.5 [BNBC Table 6.2.19]
Spectral response acceleration parameters:	
S_s	: 0.5 [BNBC Table 6.C.1]
S_1	: 0.2 [BNBC Table 6.C.1]
Site Coefficient:	
F_a	: 1.35 [Table 6.C.2]
F_v	: 2.7 [Table 6.C.3]
Spectral Response Acceleration Parameter:	
SD_s	: 0.45 [Table 6.C.4]
SD_1	: 0.36 [Table 6.C.5]

3.2.4 Load Combinations

Ultimate Strength Design (USD) method and various loads have been applied to the structures in combination with factors listed below in reviewing the quantity of reinforcement of all structural members.

Factored load combinations that have been used in the design according to BNBC (2020) are as follows:

1. 1.4D
2. 1.2D + 1.6L
3. 1.2D + L
4. 1.2D + 0.8W_x
5. 1.2D - 0.8W_x
6. 1.2D + 0.8W_y
7. 1.2D - 0.8W_y
8. 1.2D + L + 1.6W_x
9. 1.2D + L - 1.6W_x

10. $1.2D + L + 1.6W_y$
11. $1.2D + L - 1.6W_y$
12. $1.2D + L + E_x + 0.3E_y + E_v$
13. $1.2D + L + E_x - 0.3E_y + E_v$
14. $1.2D + L - E_x + 0.3E_y + E_v$
15. $1.2D + L - E_x - 0.3E_y + E_v$
16. $1.2D + L + E_y + 0.3E_x + E_v$
17. $1.2D + L + E_y - 0.3E_x + E_v$
18. $1.2D + L - E_y + 0.3E_x + E_v$
19. $1.2D + L - E_y - 0.3E_x + E_v$
20. $0.9D + 1.6W_x$
21. $0.9D - 1.6W_x$
22. $0.9D + 1.6W_y$
23. $0.9D - 1.6W_y$
24. $0.9D + E_x + 0.3E_y - E_v$
25. $0.9D + E_x - 0.3E_y - E_v$
26. $0.9D - E_x + 0.3E_y - E_v$
27. $0.9D - E_x - 0.3E_y - E_v$
28. $0.9D + E_y + 0.3E_x - E_v$
29. $0.9D + E_y - 0.3E_x - E_v$
30. $0.9D - E_y + 0.3E_x - E_v$
31. $0.9D - E_y - 0.3E_x - E_v$

Here, E_v = effect of vertical seismic forces

The vertical seismic load effect E_v may be determined as:

$$E_v = 0.5a_h D \quad (3.4)$$

Where,

a_h = expected horizontal peak ground acceleration (in g) for design = $(2/3)ZS$

D = effect of dead load,

S = site dependent soil factor (Table 6.2.16 of BNBC 2020).

3.2.5 Boundary Conditions

In order to replicate structural behavior, column base supports were represented as fixed supports in the 3D model of the superstructure.

3.2.6 Model Element Details

The modeling considerations taken into account for column, beam, shear wall, and slab elements in buildings are described in this section. A summary of each structural member's dimensions, position, and reinforcement is provided in Appendix-A.

a) Column

The columns are modeled as frame element in ETABS 2016. The moment of inertia for columns in models are taken as $0.7I_g$ for elastic analysis at factored load level as per Table 6.6.3.1.1(a) of ACI 318-19 (2019).

b) Beam

The Beams are modeled in ETABS 2016 as a frame component. According to Table 6.6.3.1.1(a) of ACI 318-19 (2019), the moment of inertia for beams in models is taken to be $0.35I_g$ for elastic analysis at the factored load level.

c) Shear Wall

The shear walls are modeled as shell element in ETABS 2016. The moment of inertia for shear walls in models is taken as $0.7I_g$ for elastic analysis at factored load level as per Table 6.6.3.1.1(a) of ACI 318-19 (2019). The shear walls in models are considered to be uncracked in factored load level for elastic analysis.

d) Slab

The slabs in the buildings are modeled in two ways. 18 models are designed with slab having nonlinear layered shell element property and the remaining 18 models are designed with slab having thick shell property.

The shell elements consist of four nodes, each with six degrees of freedom: translation in the x, y, and z directions and rotation in x, y, z direction. This element is designed to handle plastic deformation, cracking in three orthogonal directions, and crushing. The treatment of material properties is a crucial aspect of this element. In the case of thick

shell slabs, nonlinear material properties are not considered. However, the layered shell slab element takes into account the nonlinear behavior of materials. The element's geometry, node locations, and coordinate system are depicted in Figure 3.1.

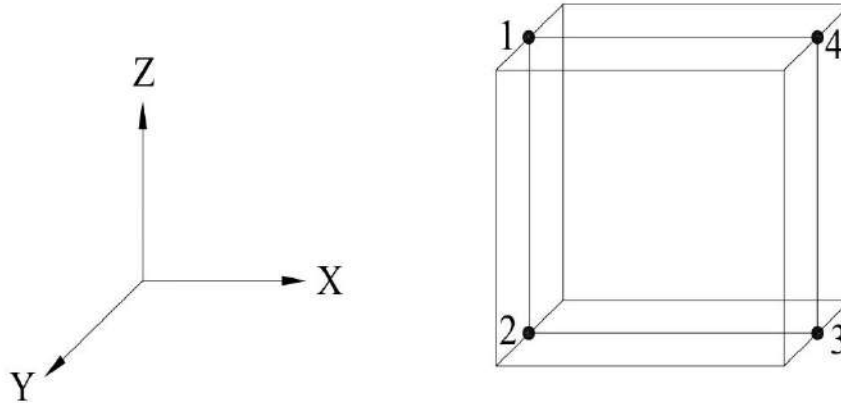


Figure 3.1: Four-Node Shell Element

In case of nonlinear layered shell slabs, the slab material behavior is selected having “coupled” property. This material behavior makes all of its in-plane stress components (S_{11} , S_{22} , and S_{33}) nonlinear. The modified Darwin-Pecknold behavior, which simulates concrete compression, cracking, and shear behavior under both monotonic and cyclic loading and takes crack rotation into consideration, is used to describe the coupled behavior of concrete.

For reinforcing in the slab, the directional material behavior is taken into account. Three stress components can be individually controlled using the directional material behavior. The S_{11} and S_{12} reinforcement components are assumed to perform in nonlinear manner. The S_{22} component of reinforcement is chosen to be inactive. It is taken into account that once concrete cracks, the slab's reinforcement will be subjected to shear. Consequently, the S_{12} component of reinforcement is chosen to be nonlinear instead of inactive. For the layer, the number of integration points needs to be specified in the direction of layer thickness. In order to capture yielding near the top and bottom of surfaces, nonlinear behavior may require additional integration points or more layers. Two integration points are selected for concrete along thickness of concrete and one integration point is selected for reinforcement along equivalent layer thickness of reinforcement. Figure 3.2 shows nonlinear layered shell property which are assigned in nonlinear layer shell.

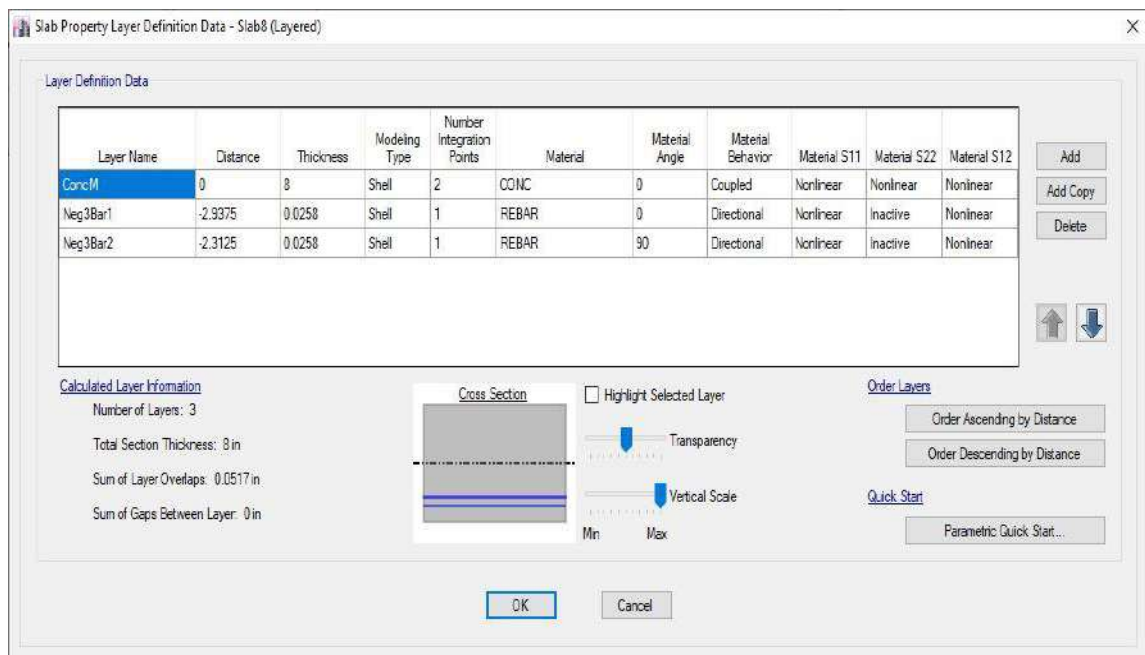


Figure 3.2: Slab Layer Properties

e) Diaphragm and Mesh

The diaphragm of slab is taken as rigid. The Finite element mesh size should preferably be 1/5 to 1/3 of the bay length or wall length to model the diaphragm flexibility. The mesh size is taken 1m×1m (40in.×40in). for diaphragm of the models to be analyzed.

3.2.7 Base Model

The case study building is a ten (10) story reinforced concrete shear wall-flat plate structural system (SW-FP) with an overall height of 35.97 m. (118 ft). The plinth level is 2.44 m (8 ft) high and the height of each of the remaining stories including roof is 3 m (10 ft). The building is essentially rectangular, symmetric in shape and is 53 m (174 ft) long by 29.26 m (96 ft) wide and floor area per floor is 1552.65 m² (16704ft²).

The plan and 3D view of the case study building are shown in Figure 3.3 and Figure 3.4 respectively.

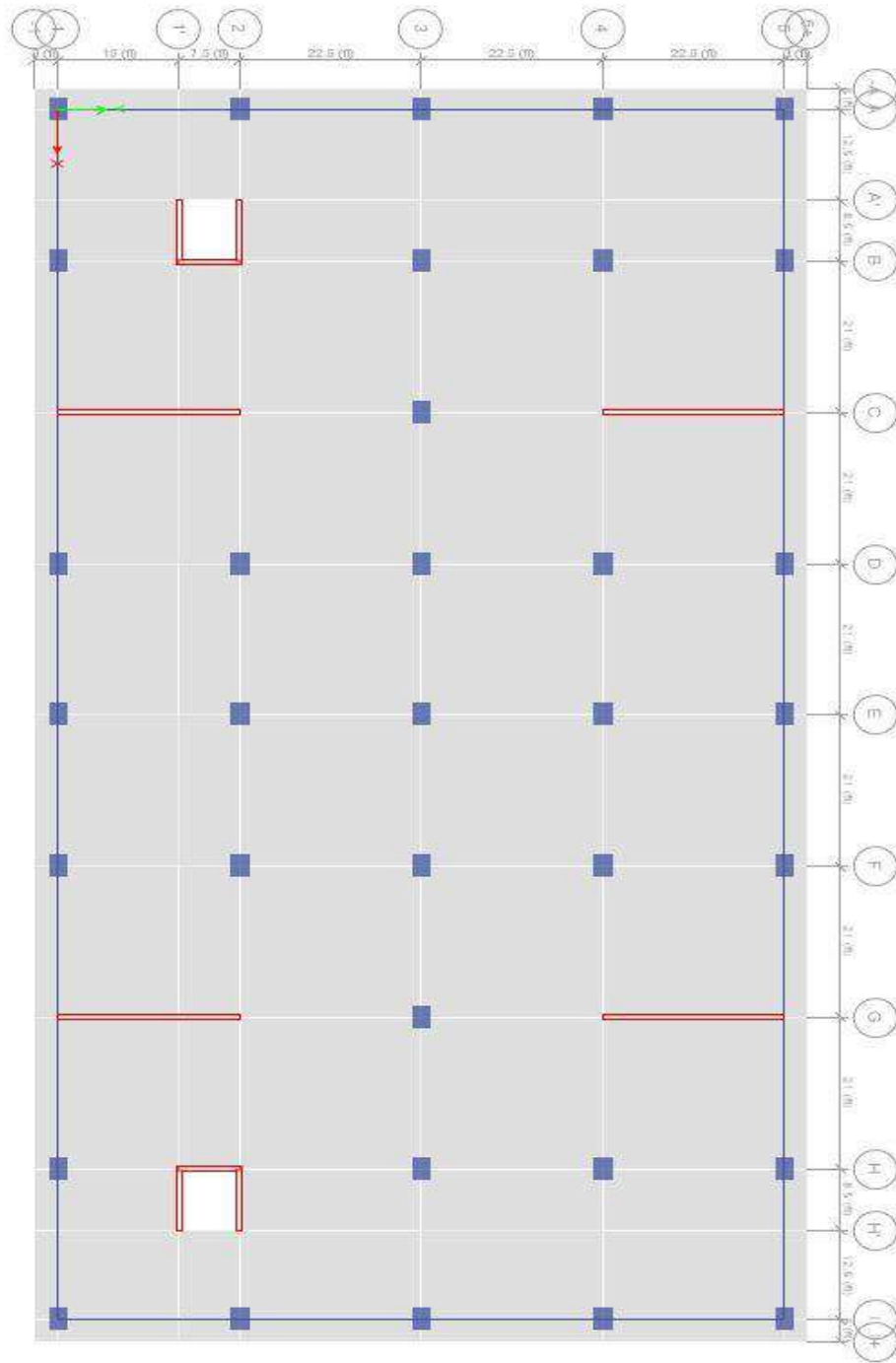


Figure 3.3: Plan of Base Building Model Type-A

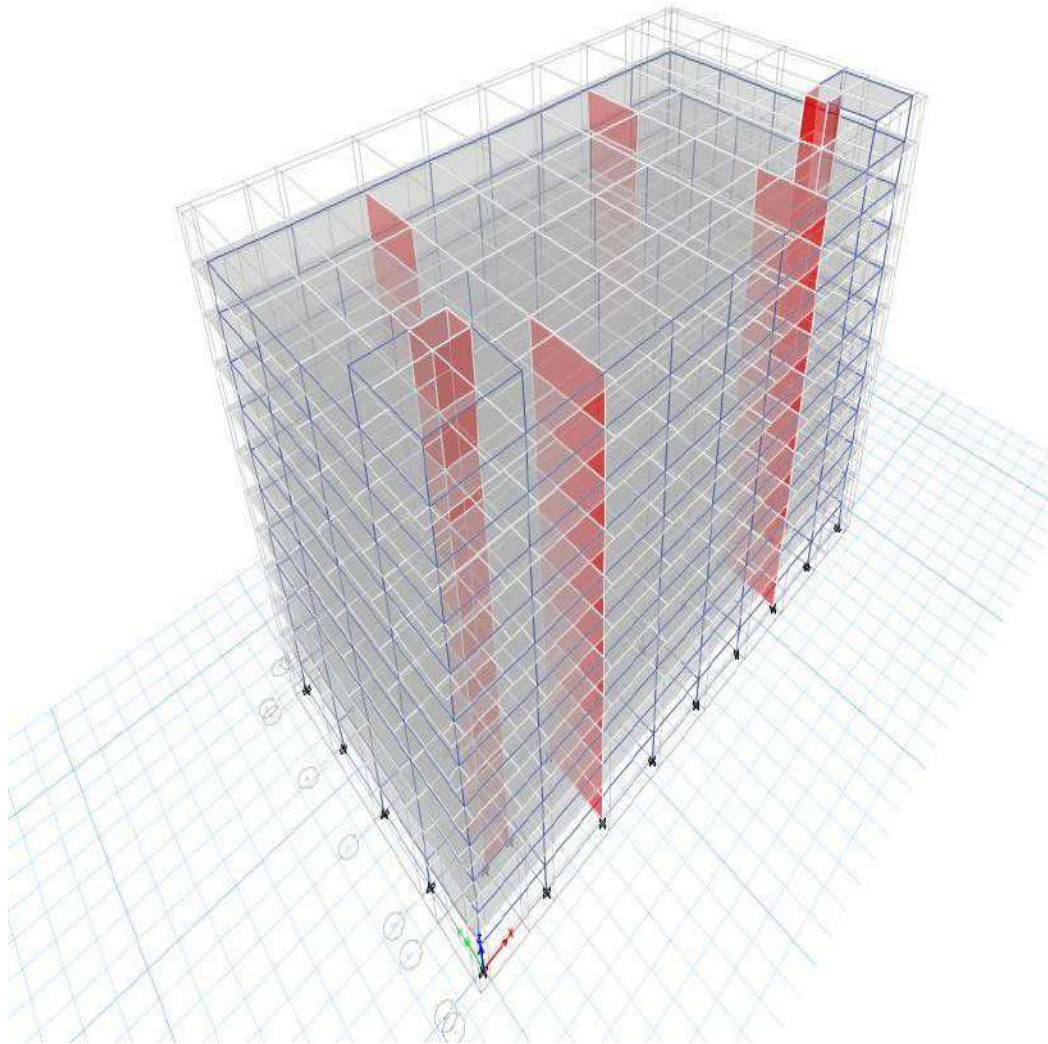


Figure 3.4: 3d View of Base Building Model Type A

3.2.8 Model Variations

Three types of aspect ratios have been used in this research. The first type is the case study building configuration (type A) and the other two aspect ratios have been generated reducing number of bays in y-direction (type B) and in x-direction (type C). The size of each panel is taken as $6.858\text{m} \times 7\text{m}$ ($22.5' \times 21'$). Number of stories, material properties and slab thickness have been varied to generate total 36 model types. All models have been designed twice using layered shell slab and thick shell slab to perform parametric study using NLSA procedure. Figure 3.5 and Figure 3.6 represent typical layout of model type B and model type C respectively.

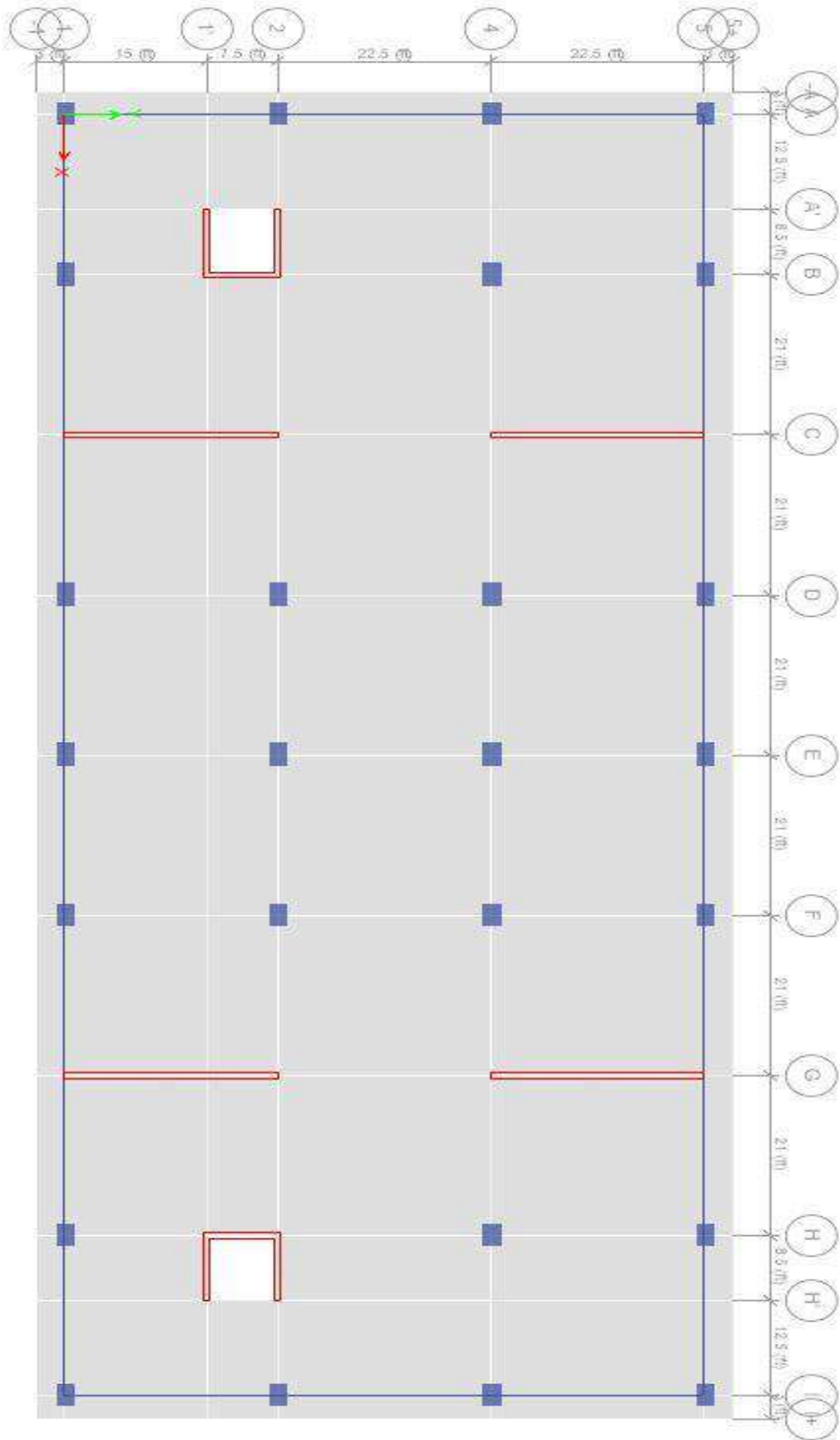


Figure 3.5: Building Type-B

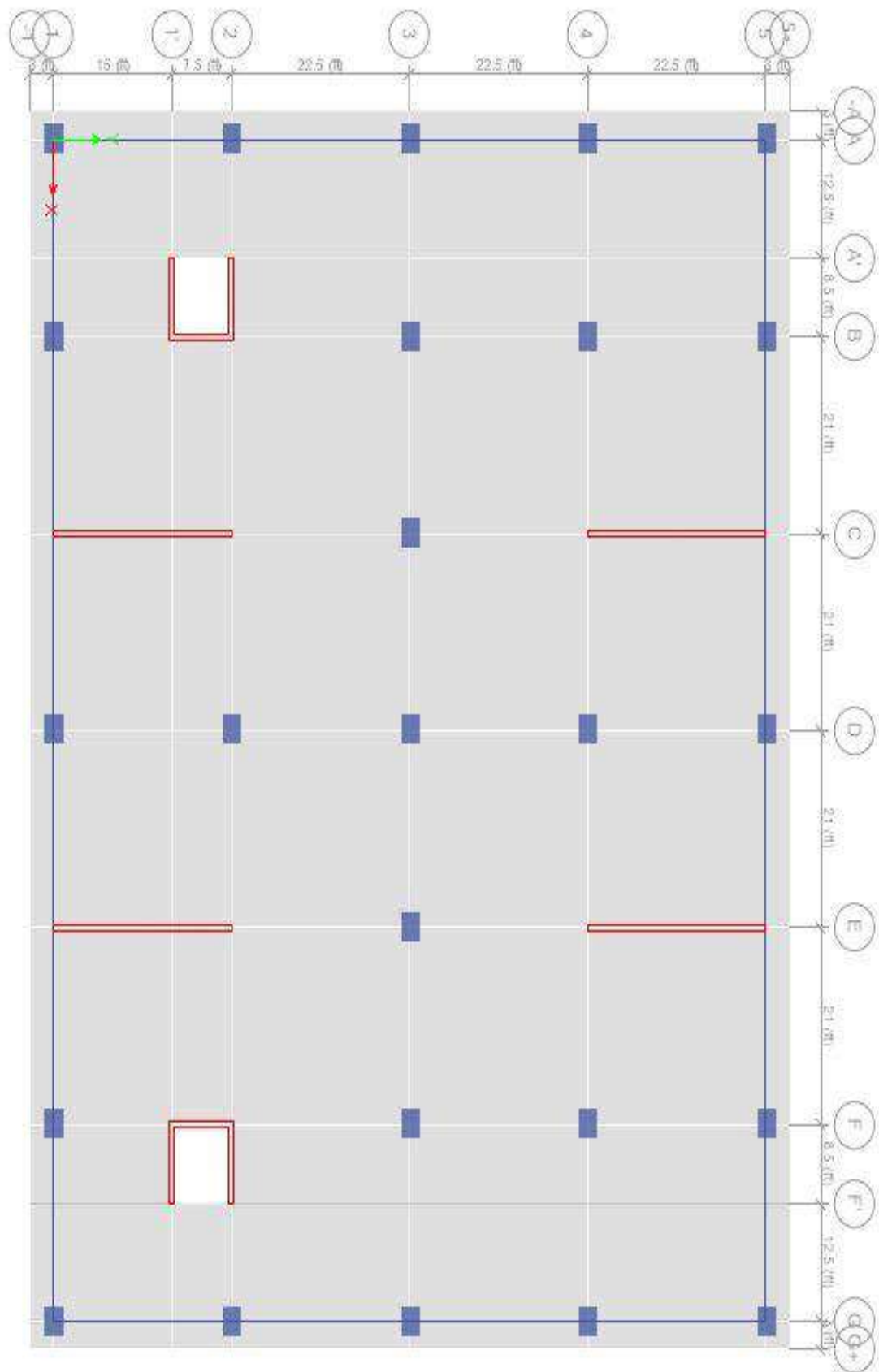


Figure 3.6: Building Type-C

Structural configurations of analyzed building models are listed in Table 3.2.

Table 3.2: Structural Configurations of Building Models

Aspect ratio (LXB)	No of story	Model ID					
		Layered Shell			Thick Shell		
		Slab thickness =200mm (8 in)	Slab thickness =225mm (9 in)	Slab thickness =250mm (10 in)	Slab thickness =200mm (8 in)	Slab thickness =225mm (9 in)	Slab thickness =250mm (10 in)
53m×29.26m (174'×96')	7	A.L.8.7	A.L.9.7	A.L.10.7	A.T.8.7	A.T.9.7	A.T.10.7
	10	A.L.8.10	A.L.9.10	A.L.10.10	A.T.8.10	A.T.9.10	A.T.10.10
53m×22.4m (174'×73.5')	7	B.L.8.7	B.L.9.7	B.L.10.7	B.T.8.7	B.T.9.7	B.T.10.7
	10	B.L.8.10	B.L.9.10	B.L.10.10	B.T.8.10	B.T.9.10	B.T.10.10
38.41m×29.26m (126'×96')	7	C.L.8.7	C.L.9.7	C.L.10.7	C.T.8.7	C.T.9.7	C.T.10.7
	10	C.L.8.10	C.L.9.10	C.L.10.10	C.T.8.10	C.T.9.10	C.T.10.10

3.3 Nonlinear Static or Pushover Analysis (NLSA)

Nonlinear static analysis is performed in this research as per BNBC (2020) and ASCE 41-13 (2013).

3.3.1 Hinge Assignment

The mathematical models define nonlinear load deformation relationships for various reinforced components. To represent the nonlinear flexural response of the beam in pushover analysis, nonlinear hinges are assigned in beams, columns and shear walls. Nonlinear flexural Auto M3 hinges are provided at both ends of beams using Table 10-7 (concrete beam-flexure) of ASCE 41-13 (2013). Similarly, nonlinear Auto P-M2-M3 hinges are placed at the ends of columns to reflect the nonlinear response of columns. The automatic P-M2-M3 hinges produced in columns correspond to Table 10-8 (Concrete Columns) of ASCE 41-13 (2013). Shear walls are given auto fiber P-M3 hinges as they can capture the nonlinear behavior of shear walls more efficiently. These hinges always act at the center of the shell element. When hinges are incorporated into a shear wall shell element, the vertical membrane stress behavior is controlled by the hinge, whilst the properties of the shell element control the horizontal and shear membrane stress, as well as out-of-plane bending behavior (CSI, 2016).

Since frame sections have an impact on auto hinges, the concrete frame design must be performed after the ETABS assignment of the auto hinges so that the auto hinges can benefit from the concrete frame design's section features. Reinforcements must

otherwise be assigned based on design. The reinforcements have been assigned to the beams and columns using concrete frame designs in order to generate auto hinges in accordance with ACI 318-14 (2014) depending on the properties of the proposed section. Shear wall auto P-M3 hinges are also section dependent. In ETABS 2016, the section properties of shear walls can be assigned using a variety of methods. There are various techniques to assign shear walls' section characteristics in ETABS 2016. To create section properties for auto P-M3 hinges, the reinforcement size and layout in shear walls based on design can be defined. Concrete shear wall design in can also be used to establish the designed section properties for shear walls. Another method of defining section parameters for auto P-M3 hinges of shear walls is by assigning vertical and horizontal reinforcement ratio. Shear walls are given vertical and horizontal reinforcement ratios based on shear wall design in accordance with ACI 318-14 (2014) for pushover analysis. According to CSI (2016), these reinforcing ratios provide the section properties for the auto P-M3 hinges.

3.3.2 Gravity Load

For gravity load analysis, nonlinear static load case is generated using load combination defined in Eq.7-3 of ASCE 41-17 (ASCE, 2017). According to ASCE 41-17, gravity load Q_G for nonlinear action can be found from the following equation:

$$Q_G = Q_D + Q_L + Q_S \quad (3.5)$$

Here,

Q_D = Action caused by dead loads;

Q_L = Action caused by live load, equal to 25% of the unreduced live load obtained in accordance with ASCE 7 but not less than the actual live load; and

Q_S = Action caused by effective snow load.

Since Bangladesh experiences no snow loads, action caused by effective snow load (Q_S) is ignored in this study. For this load case, ETABS 2016 uses a full load control application. P- Δ effects are also taken into account in this load case.

3.3.3 Pushover Load

A new load case called "Pushover" is created for nonlinear static lateral load analysis. The nonlinear gravity load case serves as the condition's initial condition. The nonlinear static analysis load application control is chosen as displacement control, and the load

pattern is selected as modal. The vertical distribution of lateral loads for NSP is determined by the form of the fundamental mode in the considered direction. The most widely used load pattern is mode 1, which assumes the building will primarily deform in 1st mode shape pattern. It is generally accepted with building time period ≤ 1 s. All models analyzed here have building time period ≤ 1 s. Representative fundamental lateral displacement patterns for the X-direction and the Y-direction are modes 1 and 3, respectively. As the control node, one corner on a building's roof is chosen. The initial target displacement assumption is set at 4% of building height. P-effects are also considered in this instance of load.

3.3.4 Response Spectrum

In order to determine the target displacement in pushover analysis, demand spectrum must be generated. This demand spectrum is derived from the design response spectrum. The design response spectrum depicts the seismic ground motion for which the building must be designed. This spectrum displays the spectral acceleration for which the building has to be designed as a function of the building period, taking into account the ground motion intensity.

The spectrum is based on elastic analysis; however, the spectral accelerations are decreased by the response modification factor R to account for energy loss caused by inelastic deformation and the advantages of structural redundancy. The spectral accelerations are increased by the importance factor I in case of important structures. The normalized acceleration response spectrum C_s incorporates the influence of local soil conditions on the response spectrum. The following equation provides the spectral acceleration for the design earthquake:

$$S_a = \frac{2}{3} \frac{ZI}{R} C_s \quad (3.6)$$

Where,

S_a = Design spectral acceleration (in units of Q) which shall not be less than $0.67\beta ZI S$

β = Coefficient used to calculate lower bound for S_a . Recommended value for β is 0.11.

Z = Seismic zone coefficient

I = Structure importance factor

R = Response reduction factor which depends on the type of structural system. The ratio cannot be greater than one.

C_s =Normalized acceleration response spectrum, which is a function of structure (building) period and soil type (site class) as defined by the following equations:

$$C_s = S(1 + \frac{T}{T_B} (2.5\eta - 1)) \text{ for } 0 \leq T \leq T_B \quad (3.7)$$

$$C_s = 2.5S\eta \text{ for } T_B \leq T \leq T_C \quad (3.8)$$

$$C_s = 2.5S\eta(\frac{T}{T_C}) \text{ for } T_C \leq T \leq T_D \quad (3.9)$$

$$C_s = 2.5S\eta(\frac{T_C T_D}{T^2}) \text{ for } T_D \leq T \leq 4 \text{ sec} \quad (3.10)$$

C_s depends on S and values of T_B , T_C and T_D , which are all functions of the site class. Constant C_s value between periods T_B and T_C represents constant spectral acceleration.

S = Soil factor which depends on site class

T = Structure (building) period

T_B =Lower limit of the period of the constant spectral acceleration branch

T_C =Upper limit of the period of the constant spectral acceleration branch

T_D =Lower limit of the period of the constant spectral displacement branch

η =Damping correction factor as a function of damping with a reference value of $\eta=1$ for 5% viscous damping. It is given by the following expression:

$$\eta = 10 / (5 + \xi) \geq 0.55 \quad (3.11)$$

In this research, the design response spectrum is generated for Narayanganj city, zone-2, soil type SD as per BNBC 2020 to define seismic demand for nonlinear static procedures.

3.3.5 Analysis Procedure

In this research, the pushover load case has been defined for both X and Y direction. The start point of the analysis has been set from nonlinear gravity load case. Loads are applied for 1st mode shape. Deformation control load application has been assumed.

Displacement Coefficient Method (DCM) has been used to determine the target displacement following ASCE 41-13NSP. BNBC 2020 response spectrum has been used as the spectrum source. The scale factor has been adjusted by the equation Ig/R , where I is the importance factor, g is gravitational acceleration and R is the response reduction factor.

3.4 Remarks

In this study, the structural analysis and design of all models has been conducted in accordance with the load requirements specified in the Bangladesh National Building Code (BNBC) 2020 and ASCE 7-05. The design of structural components followed the provisions outlined in the ACI 318-08.

Linear analysis considered gravity loads and lateral loads such as wind and earthquake loads. For nonlinear analysis, separate gravity load cases and pushover load cases were created. Nonlinear hinges were assigned to columns, beams, and shear walls, and nonlinear material properties were incorporated into slabs. After designing all elements, a nonlinear static analysis (NLSA) or pushover analysis was carried out, adhering to ASCE 41-13 guidelines. The target displacement was determined using the Displacement Coefficient Method (DCM) as per ASCE 41-13NSP.

Taking into account the factors discussed above, the reinforced concrete flat plate slabs were effectively modeled for nonlinear finite element analysis to accurately predict their seismic behavior.

Chapter 4

RESULTS AND DISCUSSIONS

4.1 Introduction

The objective of this chapter is to provide an in-depth understanding of the structural performance of the models under consideration. In this chapter, the structural performance of the selected models has been analyzed through both linear static analysis (LSA) and nonlinear static analysis (NLSA). The results obtained from linear static analysis of model type A have been presented and discussed here. Furthermore, a comparison of the nonlinear behavior of model type B, and model type C has been provided, taking into account different parameters such as number of stories, slab thickness, and slab shell type.

4.2 Model Validation

To ensure the accuracy of the developed finite element models in predicting the behavior of RC slabs, it is essential to validate them by comparing against well-established theoretical solutions, experimental results or other finite element (FE) models. This study selected two RC slabs from reputable literature and journals to create models, perform analyses, and validate the results using available experimental data and previously done FE model. Two RC slabs (A-1a and A-7b) tested by Elstner and Hognestad (1956) have been chosen here for numerical modelling. These slabs were previously validated by Islam (2014) in FE modelling software ABAQUS. The material properties and dimensions for these models are given in Table 4.1 and the reinforcement details are given in Table 4.2. Figure 4.2 shows a typical section of test slab used by Elstner and Hognestad (1956).

In order to simulate the test condition in the finite element (FE) models, the boundary condition is set to $U_2=0$ (vertical direction) along the supports. The mesh is selected as $50\text{mm} \times 50\text{mm}$ through mesh sensitivity analysis. The graph in Figure 4.3 illustrates the maximum load capacity of a square slab (A-1a plate) at different mesh sizes in layered shell model, ranging from $5\text{mm} \times 5\text{mm}$ to $75\text{mm} \times 75\text{mm}$. The results indicate that numerical solutions are sensitive during the analysis of mesh size, and it is

important to find a balance. If the mesh is too fine, it can lead to numerical instability, while a mesh that is too coarse may result in insufficient accuracy. Hence, for this study, a mesh size of $50\text{mm} \times 50\text{mm}$ is considered reasonable as it provides acceptable results for finite element analysis while also saving analysis time. Figure 4.1 illustrates maximum slab deflection obtained by varying mesh size in plate A-1a.

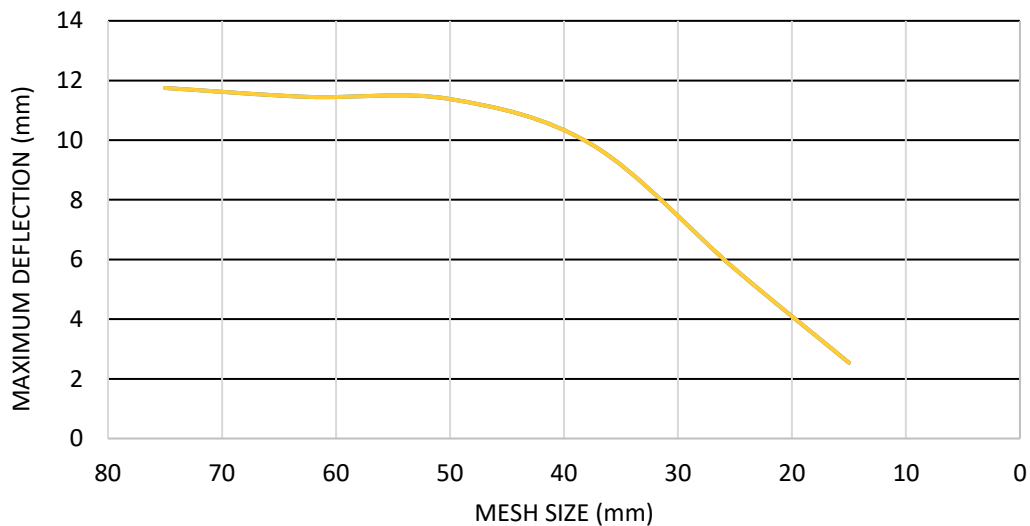


Figure 4.1: Maximum Deflection of Slab A-1a for Varying Mesh Size

Instead of modelling the column stub, the slab is meshed into $250\text{mm} \times 250\text{mm}$ portion at center of slab and load is applied uniformly through that portion. Subsequently, the slab central deflection obtained from the numerical models were compared with the experimental results. Figure 4.3 and Figure 4.4 illustrate maximum deflection in FE models for plate A-1a and A-7b respectively.

Table 4.1: Material Property and Dimensions of Slabs Tested by Elstner and Hognestad (1956)

Model No.	f'_c (MPa)	f_y (MPa)	E_c (GPa)	E_s (GPa)	Slab Dimension (m×m×m)	Column Stub Dimension (m×m)	d (m)	Support Condition
A-1a	13.79	332.33	17.58	200	1.8×1.8×0.15	0.25×0.25	0.12	Symmetrical Support on four edges
A-7b	24.13	321.30	25.23	200	1.8×1.8×0.15	0.25×0.25	0.10	Symmetrical Support on two opposite edges

Table 4.2: Reinforcement Details of Slabs Tested by Elstner and Hognestad (1956)

Model No.	Slab Reinforcement							Column Reinforcement	
	Tension			Compression					
	Bar size (mm)	Spacing		ρ percent	Bar size (mm)	Spacing			ρ percent
Bottom (mm)		Top (mm)	Bottom (mm)			Top (in)			
A-1a	19	228	190	1.15	12	178	203	0.56	4- Φ 16
A-7b	25	203	159	2.47	19	190	228	1.15	4- Φ 16

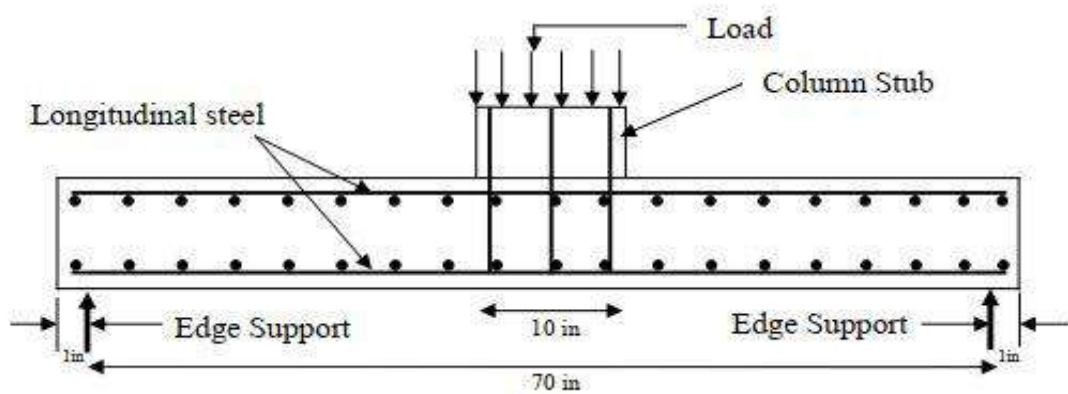


Figure 4.2: Test Slab Used by Elstner and Hognestad (1956)

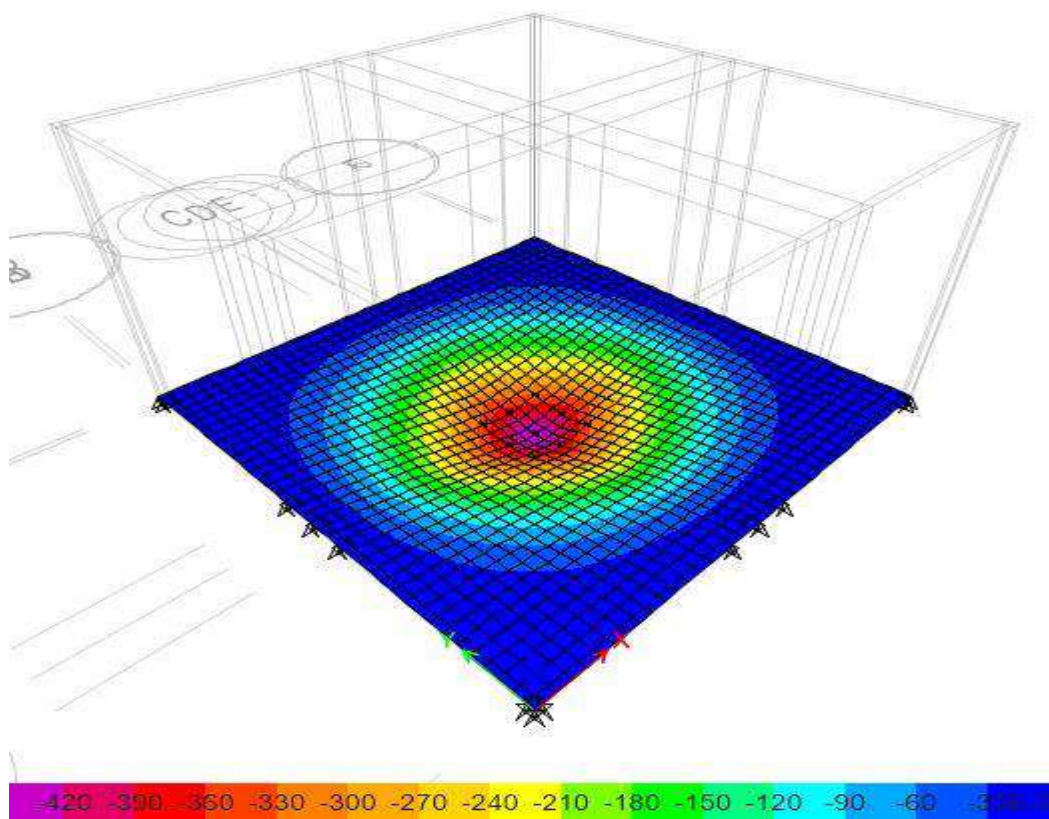


Figure 4.3: Maximum Deflection Observed in Plate A-1a

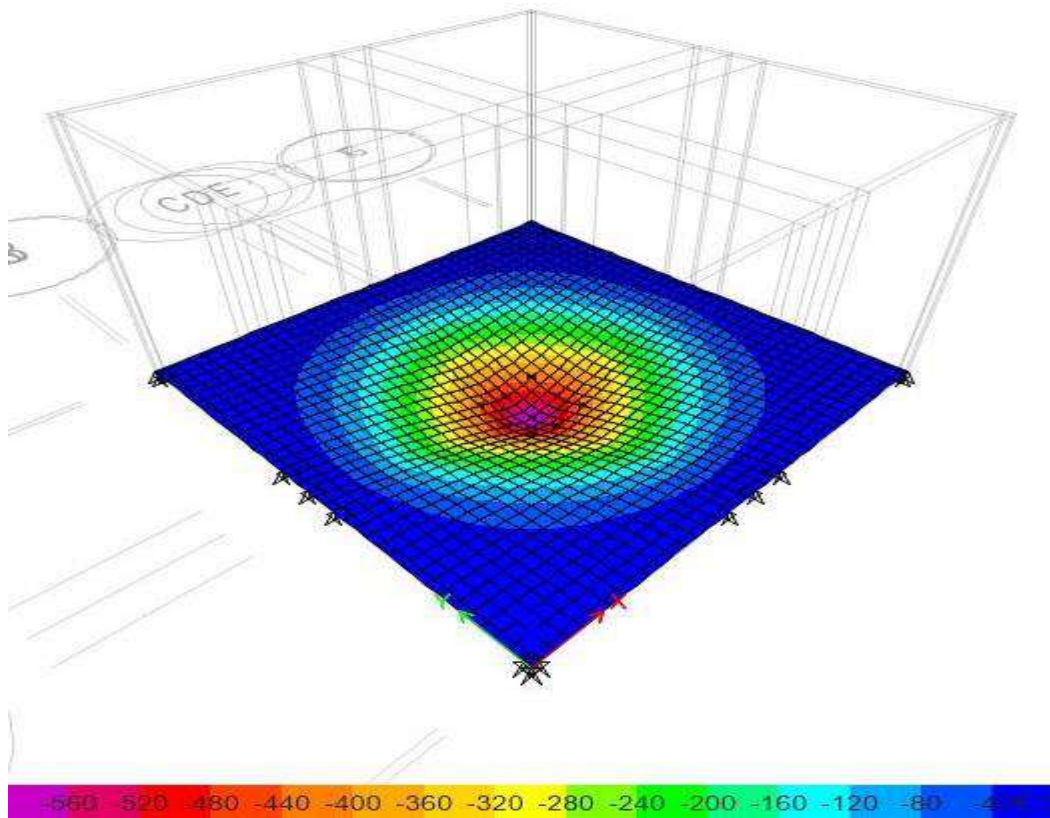


Figure 4.4: Maximum Deflection Observed in Plate A-7b

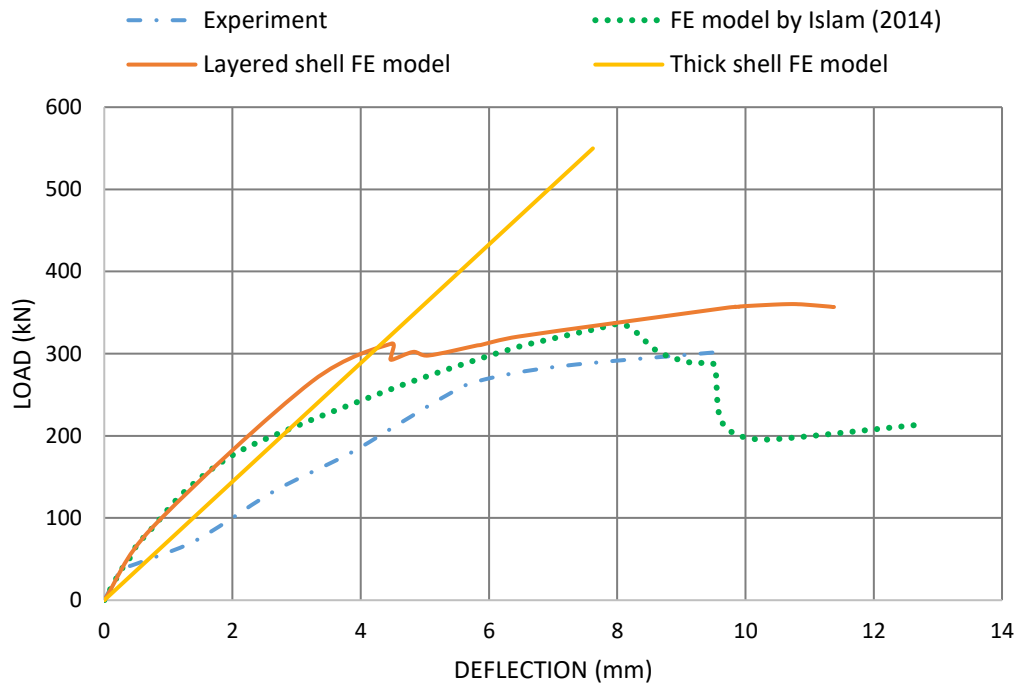


Figure 4.5: Load vs. Deflection for Plate A-1a

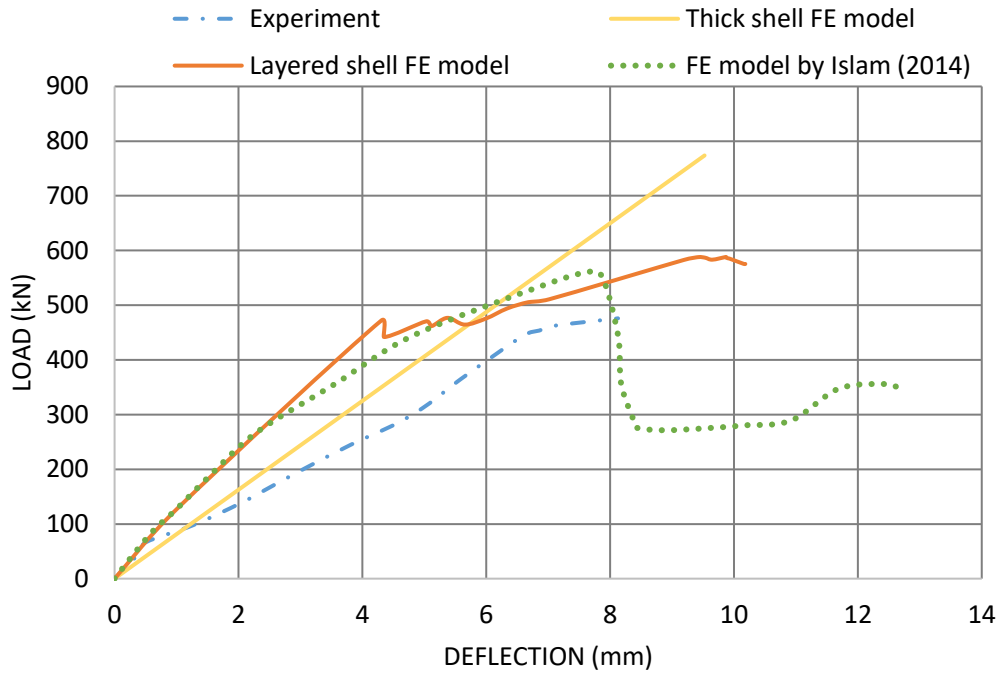
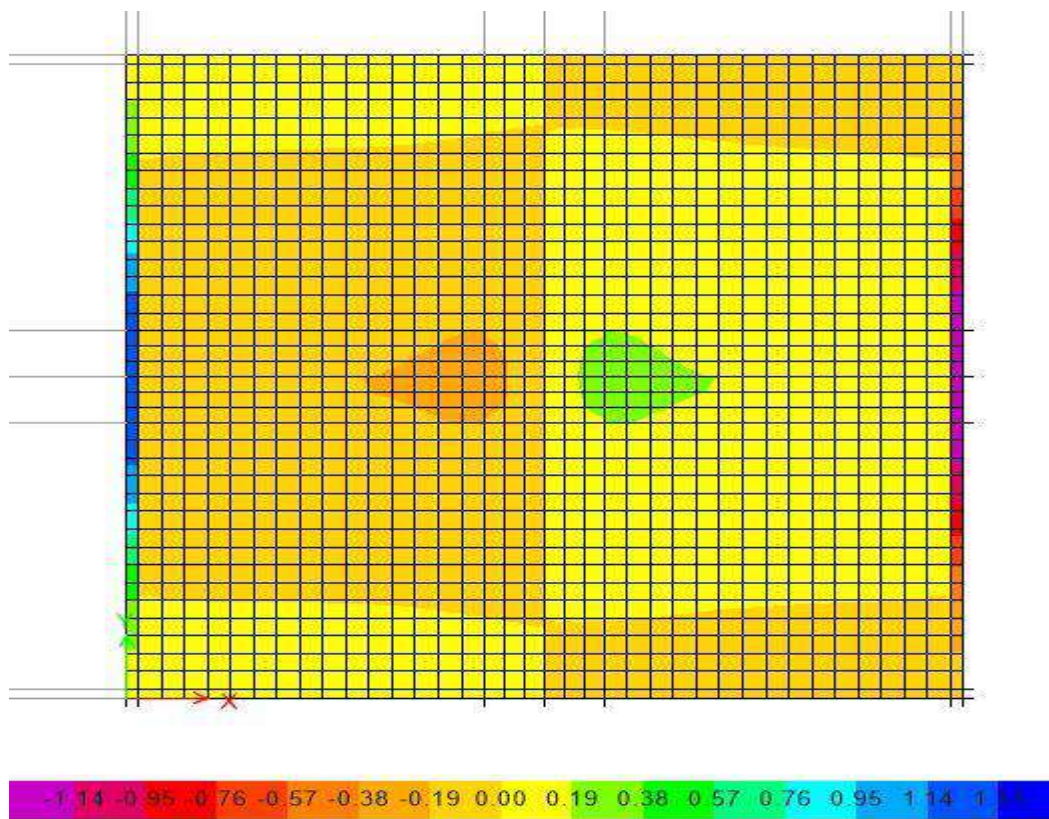


Figure 4.6: Load vs. Deflection for Plate A-7b

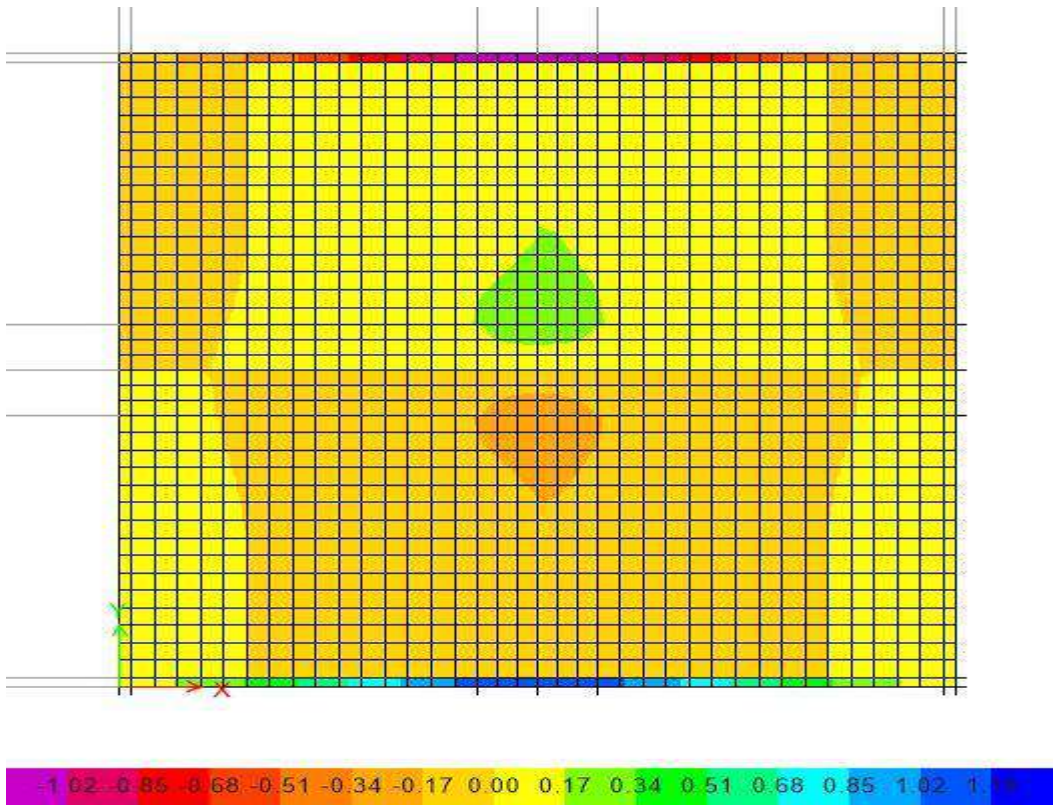
The deflection results of plate A-1a and A-7b obtained from the FE analysis and test results are presented in the load versus deflection curves in Figure 4.5 and Figure 4.6 respectively. Nonlinear load-deflection response can be observed in the experimental result, layered shell FE model and FE model by Islam (2014). At the initial stage of the loading process, the experimental and the two (layered shell FE model and FE model by Islam (2014)) FE models exhibit similar linear and elastic behavior without any signs of cracking or yielding. However, nonlinear response seen in FE analysis and experimental results are slightly different. In terms of quantitative analysis, for slab A-1a, the numerically obtained punching load (368.7 kN) exceed the experimental and previous FE model failure load (Islam, 2014) (302.48 kN and 334.5 kN) by 21.89% and 10.22% respectively. Additionally, at the maximum load for slab A-1a, the numerical vertical displacements measure 11.37 mm, which corresponds to approximately 17.82% and 39.91% greater than the experimental and previous FE model (Islam, 2014) values respectively. Again, for slab A-7b, the numerically obtained punching load (582.83 kN) exceed the experimental and previous FE model failure load (Islam, 2014) (475.96 kN and 560.48 kN) by 22.45% and 3.99% respectively. Additionally, at the maximum load for slab A-7b, the numerical vertical displacements measure 9.19 mm, which corresponds to approximately 13.09% and 20.63% greater than the experimental and previous FE model (Islam, 2014) values (8.12 mm and 12.7 mm) respectively.

However, since the thick shell formulation do not take into account nonlinear material behavior, in both slab A-1a and A-7b, the thick shell FE models exhibit linear relationship between load and deflection. Nonetheless, the pattern of cracking and the observed failure phenomenon in the finite element (FE) model closely resemble the experimental results, indicating a strong agreement between the two.

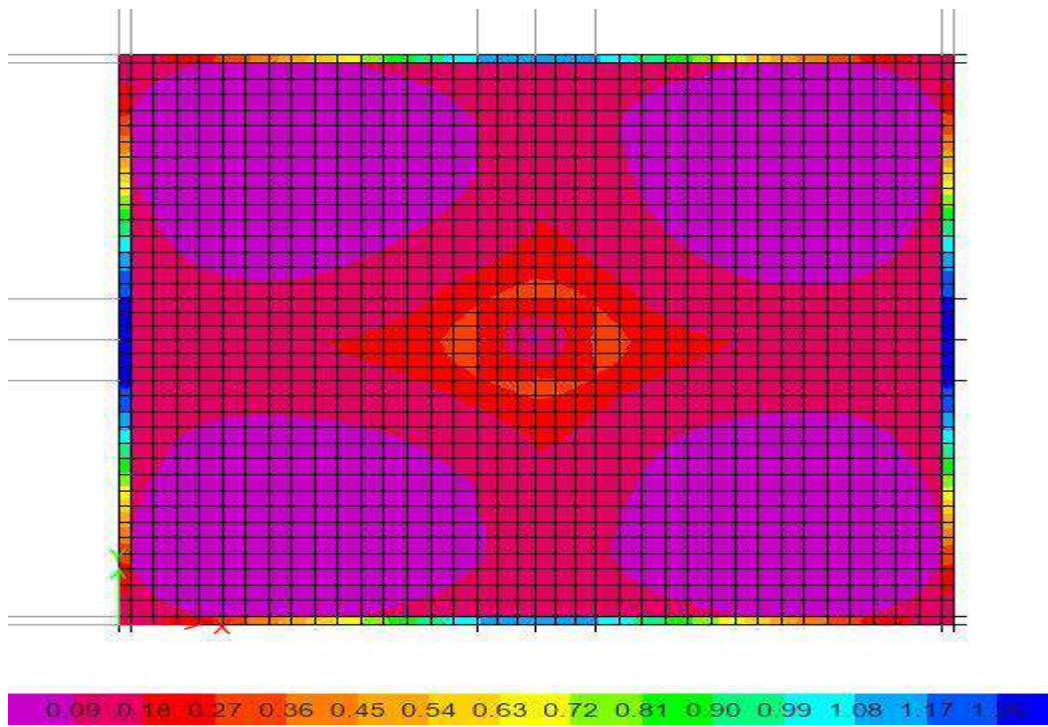
The punching shear stress results of plate A-1a and A-7b obtained from the layered shell FE analysis are shown in Figure 4.5 and Figure 4.6 respectively. The maximum observed stresses are compared with punching shear stress capacity calculated following ACI 318-19 (2019). Table 4.3 demonstrates that the maximum observed stress in both slab A-1a and A-7b exceeds the capacity of punching shear stress of the respective slabs. This indicates that this method can be utilized in determining punching shear failure phenomenon in flat plate slabs.



(a)

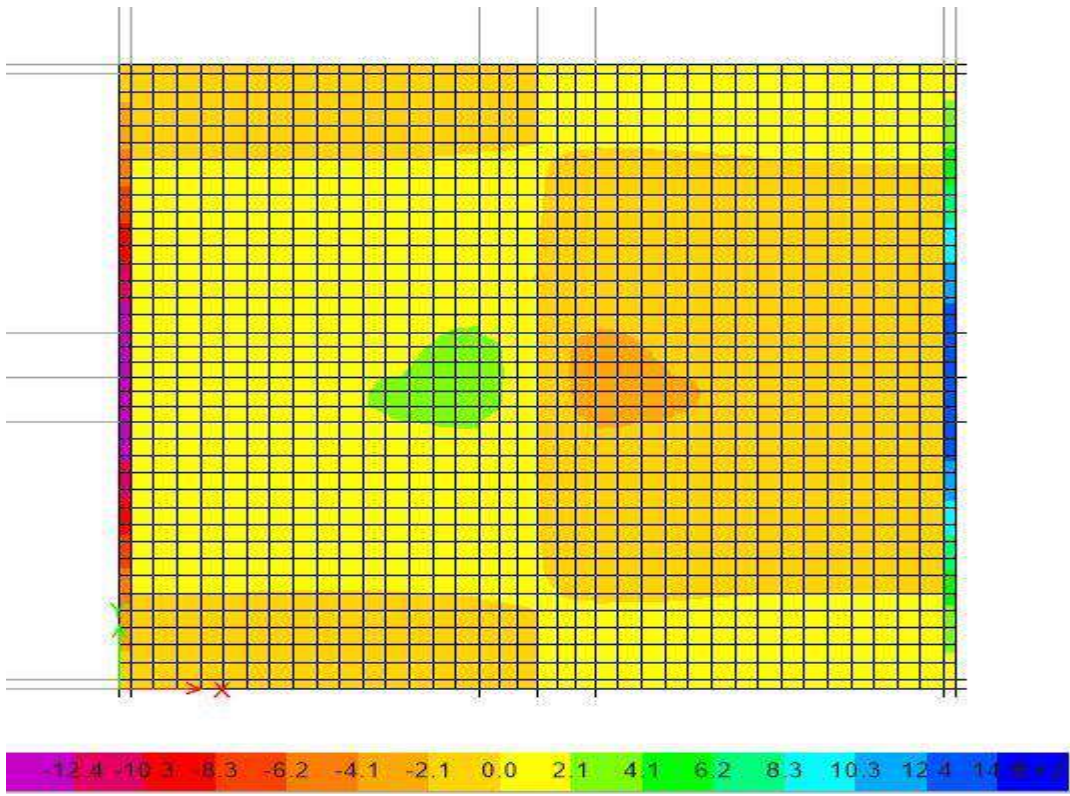


(b)

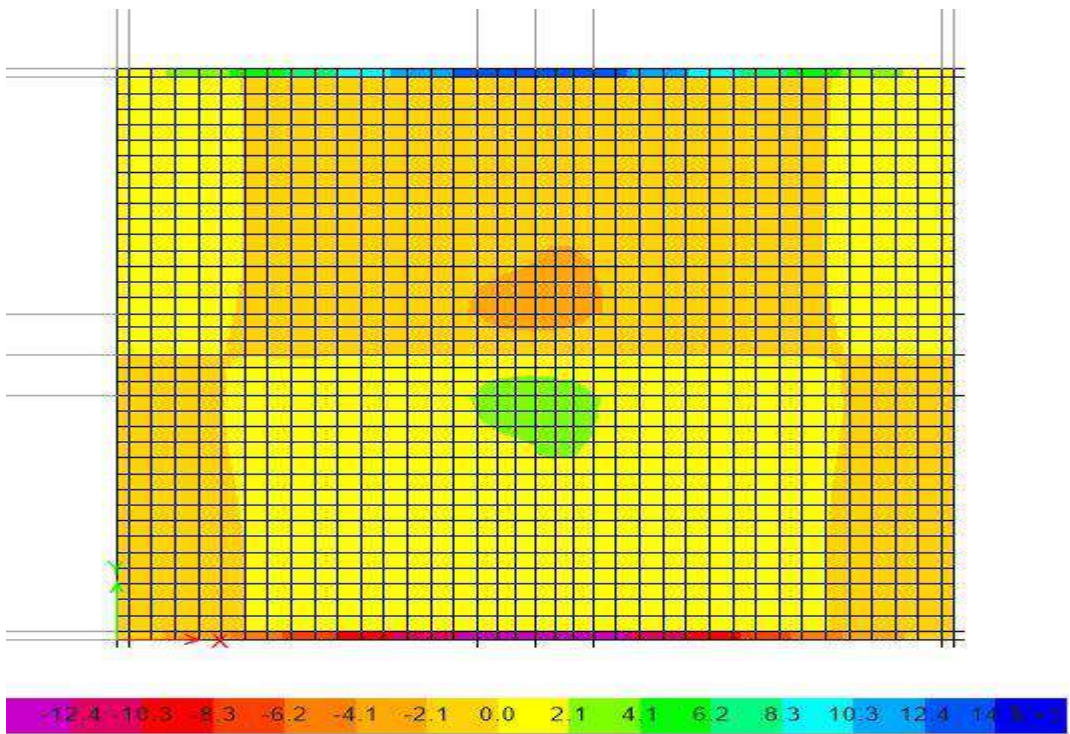


(c)

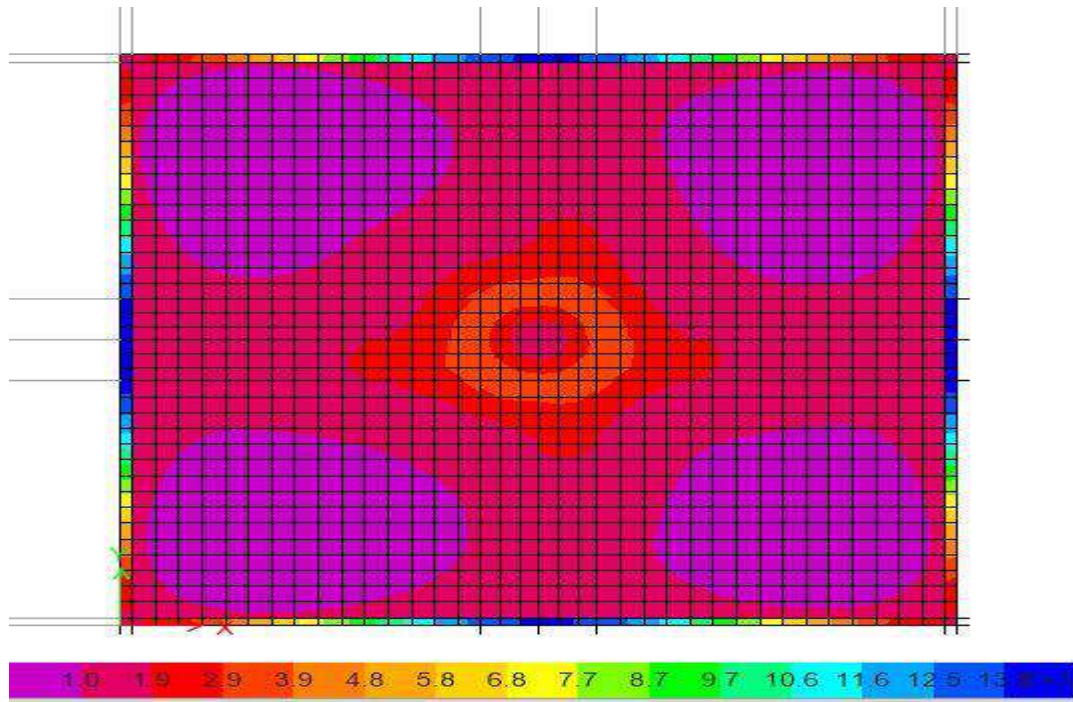
Figure 4.7: Observed Stress in Layered Shell FE Model A-1a (a) V13 (b) V23 (c) SmaxV



(a)



(b)



(c)

Figure 4.8: Observed Stress in Layered Shell FE Model A-7b (a) V13 (b) V23 (c) SmaxV

Table 4.3: Punching Shear Stress Comparison

Model ID	Effective depth, d (mm)	Column size (mmxmm)		bo (mm)	Punching shear stress capacity at d/2 distance, vc (MPa)	Observed stress at d/2 distance (MPa)	Remarks
A-1a	117.6	254	254	1486.41	0.93	2.06	Fails in punching shear
A-7b	114.3	254	254	1473.20	1.22	3.08	Fails in punching shear

In summary, it can be stated that the FE models show slightly higher stiffness than the experimental result and the previous FE model done by Islam (2014). This can be attributed to the absence of certain data used in the FE models and the failure to replicate some real-life phenomena such as bond slip between concrete and reinforcement, dowel action, and aggregate interlock by FE models and different computational method followed by individual FE modelling software. However, the result variation is within acceptable limit. In addition, the punching shear stress observed in the layered shell FE models exceed the capacity of punching shear stress, which proves strong agreement

between the experiment and numerical model. Therefore, it can be concluded that, the numerical models employed in this research provide reliable results and can be confidently used to study and understand the structural response of RC flat plate structures.

4.3 Structural Performance from Linear Static Analysis

As per the parameters discussed in chapter 3, linear static analysis and design have been conducted for all 36 models. The analysis takes into account various parameters such as the building dimensions, number of stories, and slab thickness. BNBC 2020 has been followed for design and comparison of results of linear static analysis.

All the models in the study have been designed as dual systems, providing the frame with the necessary capacity to resist seismic forces equivalent to or greater than 25% of the prescribed seismic forces. Appendix B summarizes the seismic force resistance capacity (in percentage) of frames in model type A, B and C.

4.3.1 Base Model Analysis

A summary of the maximum story displacement, drift, shear, and stiffness from the linear static analysis for Model A.L.8.10 for layered shell and Model A.T.8.10 thick shell slab is presented and discussed here.

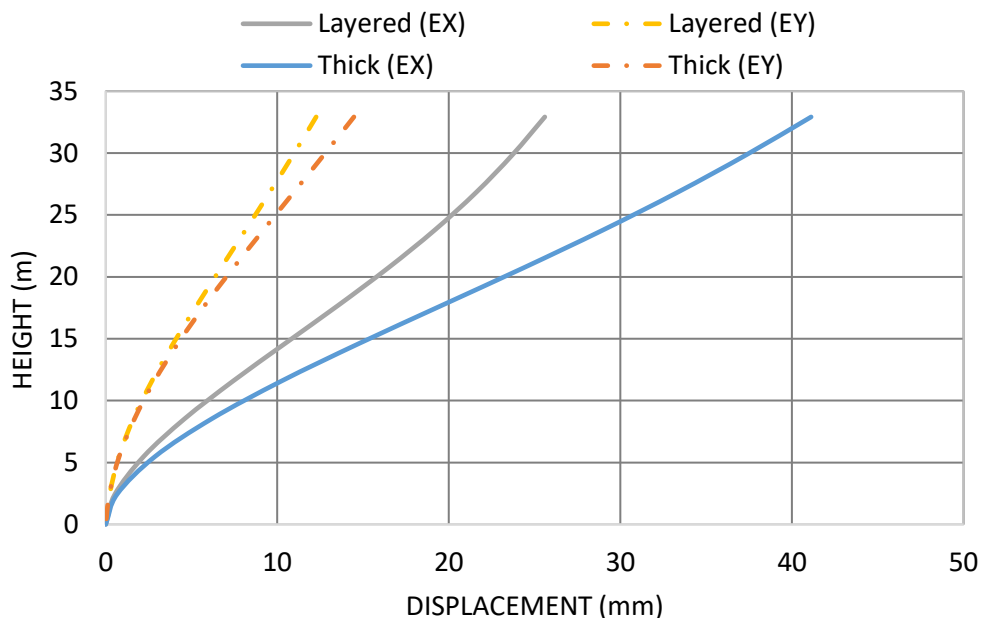


Figure 4.9: Story Height vs. Lateral Displacement (Base Model)

It is apparent from the story height vs. lateral displacement plot (Figure 4.9) that for earthquake forces displacement along the x-direction is larger than that of the y-direction, understandably because of the orientation of the shear walls along the y-direction imparting much more stiffness along that direction. Difference in earthquake forces is seen in the layered shell model and the thick shell model. The thick shell model shows more displacement than layered shell. This can be attributed to the varying stiffness properties of the concrete and reinforcement layers considered in the layered shell slab.

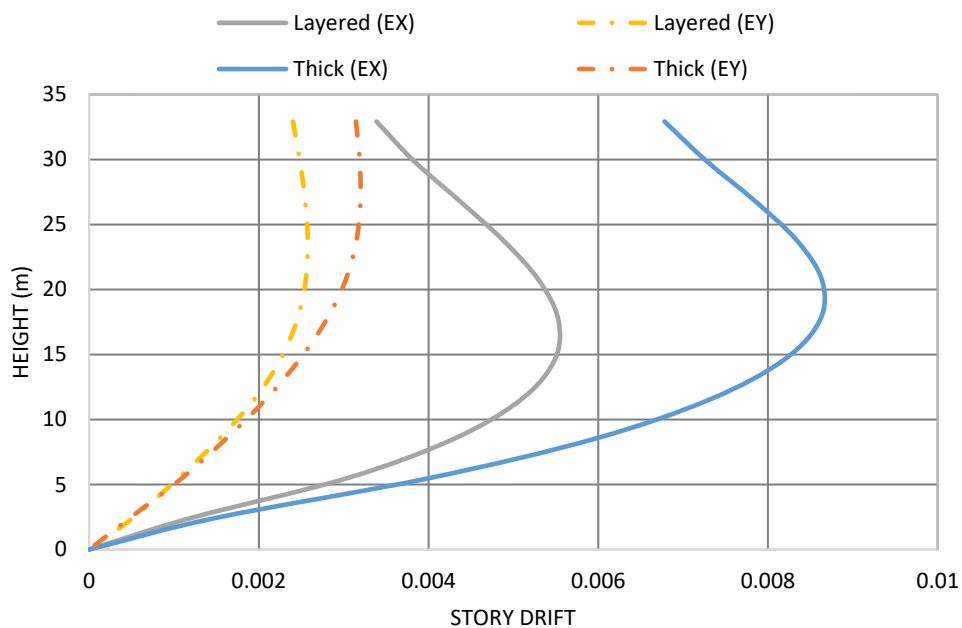


Figure 4.10: Story Height vs. Story Drift (Base Model)

Story drifts (Figure 4.10) are also smaller in y-direction of the structure, than the x-direction. The presence of shear walls along the y-direction limits the story drift in the y-direction. Since change in displacement between two successive stories are larger in the lower floors compared to the upper floors, story drift gradually decreases along the height of a building. The layered shell models showed lower drift than the thick shell models. This is possibly due to the layered shell models considering distinct stiffness properties of each layer. The story drift is checked according to BNBC 2020 in Table 4.4, Table 4.5, Table 4.6 and Table 4.7. For both layered shell and thick shell models, the drift value observed is considerably lower than the allowable limit, indicating the structure is safe.

Table 4.4: Drift Check for Earthquake (Layered Shell in X-Direction)

Story	Height, h_{sx} (m)	δ_{xe} (m)	$\delta_x = \frac{C_d \delta_{xe}}{I}$ (m)	Drift, $D = \delta_x - \delta_{x-1}$ (m)	Allowable Drift, D_a (m)	Comment
OHWT	35.97	0.025	0.140	-0.001	0.719	Within Allowable Limit
Roof	32.92	0.026	0.141	0.010	0.658	Within Allowable Limit
LEVEL9	29.87	0.024	0.130	0.012	0.597	Within Allowable Limit
LEVEL8	26.82	0.022	0.119	0.013	0.536	Within Allowable Limit
LEVEL7	23.77	0.019	0.105	0.015	0.475	Within Allowable Limit
LEVEL6	20.73	0.016	0.091	0.016	0.415	Within Allowable Limit
LEVEL5	17.68	0.014	0.074	0.017	0.354	Within Allowable Limit
LEVEL4	14.63	0.010	0.058	0.017	0.293	Within Allowable Limit
LEVEL3	11.58	0.007	0.041	0.016	0.232	Within Allowable Limit
LEVEL2	8.534	0.005	0.025	0.013	0.171	Within Allowable Limit
LEVEL1	5.486	0.002	0.012	0.009	0.110	Within Allowable Limit
BGB	2.438	0.001	0.003	0.003	0.049	Within Allowable Limit
Base	0	0.000	0.000	0.000	0.000	Within Allowable Limit

Table 4.5: Drift Check for Earthquake (Layered Shell in Y-Direction)

Story	Height, h_{sx} (m)	δ_{ye} (m)	$\delta_y = \frac{C_d \delta_{ye}}{I}$ (m)	Drift, $D = \delta_y - \delta_{y-1}$ (m)	Allowable Drift, D_a (m)	Comment
OHWT	35.97	0.014	0.074	0.007	0.719	Within Allowable Limit
Roof	32.92	0.012	0.067	0.007	0.658	Within Allowable Limit
LEVEL9	29.87	0.011	0.060	0.008	0.597	Within Allowable Limit
LEVEL8	26.82	0.010	0.053	0.008	0.536	Within Allowable Limit
LEVEL7	23.77	0.008	0.045	0.008	0.475	Within Allowable Limit
LEVEL6	20.73	0.007	0.037	0.008	0.415	Within Allowable Limit
LEVEL5	17.68	0.005	0.029	0.007	0.354	Within Allowable Limit
LEVEL4	14.63	0.004	0.022	0.007	0.293	Within Allowable Limit
LEVEL3	11.58	0.003	0.015	0.006	0.232	Within Allowable Limit
LEVEL2	8.534	0.002	0.009	0.005	0.171	Within Allowable Limit
LEVEL1	5.486	0.001	0.004	0.003	0.110	Within Allowable Limit
BGB	2.438	0.000	0.001	0.001	0.049	Within Allowable Limit
Base	0	0.000	0.000	0.000	0	Within Allowable Limit

Table 4.6: Drift Check for Earthquake (Thick Shell in X-Direction)

Story	Height, h_{sx} (m)	δ_{xe} (m)	$\delta_x = \frac{C_d \delta_{xe}}{I}$ (m)	Drift, $D = \delta_x - \delta_{x-1}$ (m)	Allowable Drift, D_a (m)	Comment
OHWT	35.97	0.042	0.230	0.004	0.719	Within Allowable Limit
Roof	32.92	0.041	0.226	0.021	0.658	Within Allowable Limit
LEVEL9	29.87	0.037	0.205	0.022	0.597	Within Allowable Limit
LEVEL8	26.82	0.033	0.183	0.024	0.536	Within Allowable Limit
LEVEL7	23.77	0.029	0.159	0.025	0.475	Within Allowable Limit
LEVEL6	20.73	0.024	0.134	0.026	0.415	Within Allowable Limit
LEVEL5	17.68	0.020	0.108	0.026	0.354	Within Allowable Limit
LEVEL4	14.63	0.015	0.081	0.025	0.293	Within Allowable Limit
LEVEL3	11.58	0.010	0.056	0.022	0.232	Within Allowable Limit
LEVEL2	8.534	0.006	0.034	0.018	0.171	Within Allowable Limit
LEVEL1	5.486	0.003	0.016	0.012	0.110	Within Allowable Limit
BGB	2.438	0.001	0.004	0.004	0.049	Within Allowable Limit
Base	0	0	0	0	0	Within Allowable Limit

Table 4.7: Drift Check for Earthquake (Thick Shell in Y-Direction)

Story	h_{sx} (m)	δ_{xe} (m)	$\delta_x = \frac{C_d \delta_{xe}}{I}$ (m)	$D = \delta_x - \delta_{x-1}$ (m)	Allowable Drift, D_a (m)	Comment
OHWT	35.97	0.016	0.089	0.009	0.719	Within Allowable Limit
Roof	32.92	0.014	0.080	0.010	0.658	Within Allowable Limit
LEVEL9	29.87	0.013	0.070	0.010	0.597	Within Allowable Limit
LEVEL8	26.82	0.011	0.060	0.010	0.536	Within Allowable Limit
LEVEL7	23.77	0.009	0.051	0.010	0.475	Within Allowable Limit
LEVEL6	20.73	0.007	0.041	0.009	0.415	Within Allowable Limit
LEVEL5	17.68	0.006	0.032	0.009	0.354	Within Allowable Limit
LEVEL4	14.63	0.004	0.023	0.008	0.293	Within Allowable Limit
LEVEL3	11.58	0.003	0.016	0.006	0.232	Within Allowable Limit
LEVEL2	8.534	0.002	0.009	0.005	0.171	Within Allowable Limit
LEVEL1	5.486	0.001	0.004	0.003	0.110	Within Allowable Limit
BGB	2.438	0.000	0.001	0.001	0.049	Within Allowable Limit
Base	0	0	0	0	0	Within Allowable Limit

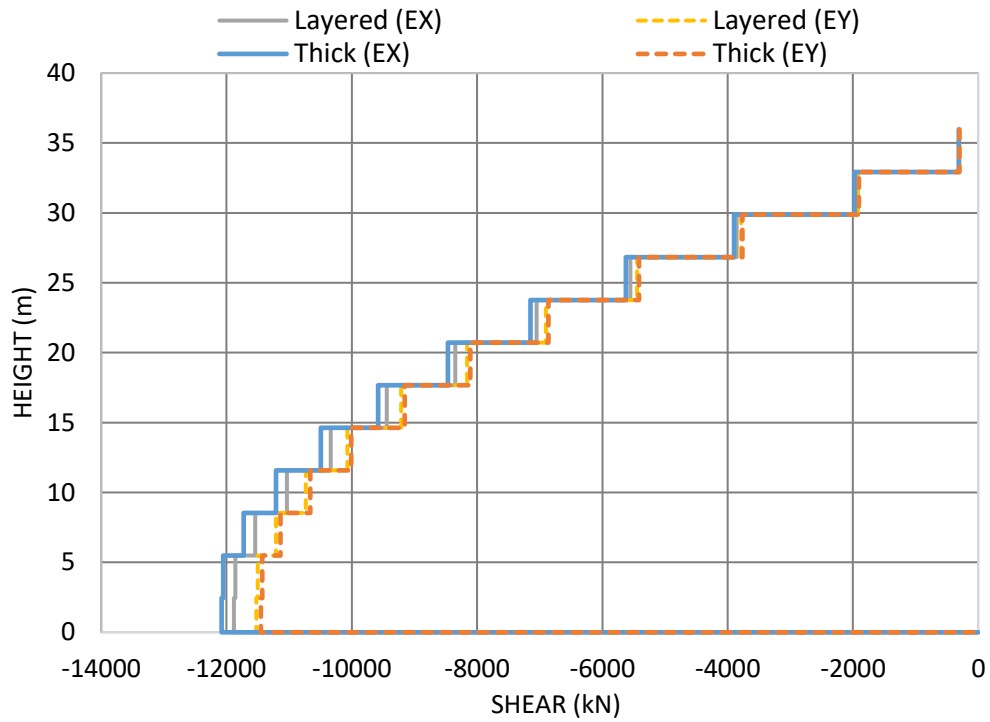


Figure 4.11: Story Height vs. Story Shear (Base Model)

Since seismic base shear isn't directional, story shears (Figure 4.11) along the x and y-directions are same at the top of the building, slight difference is seen at the bottom in x-direction.

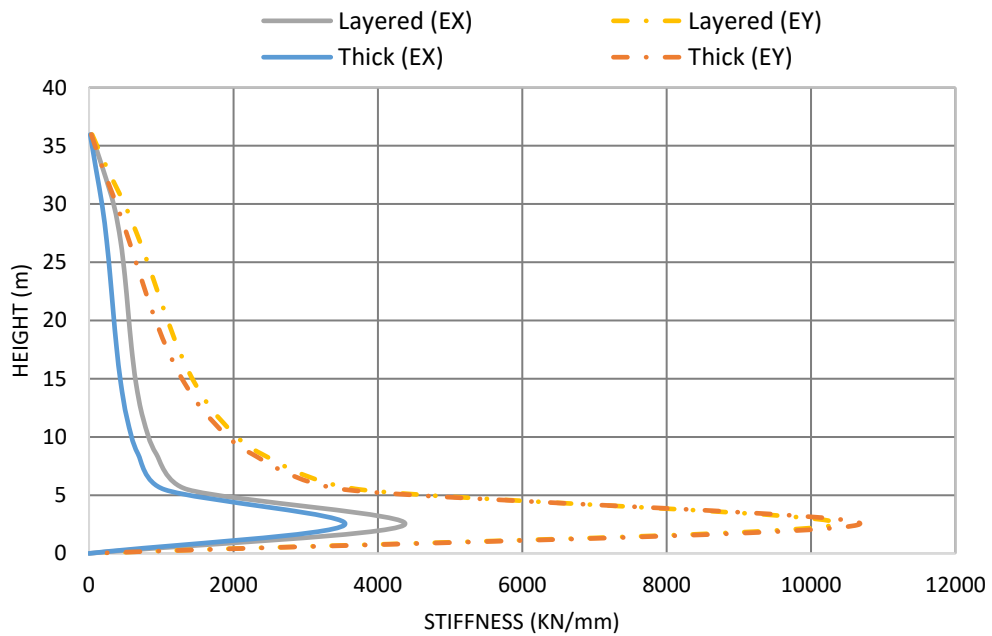
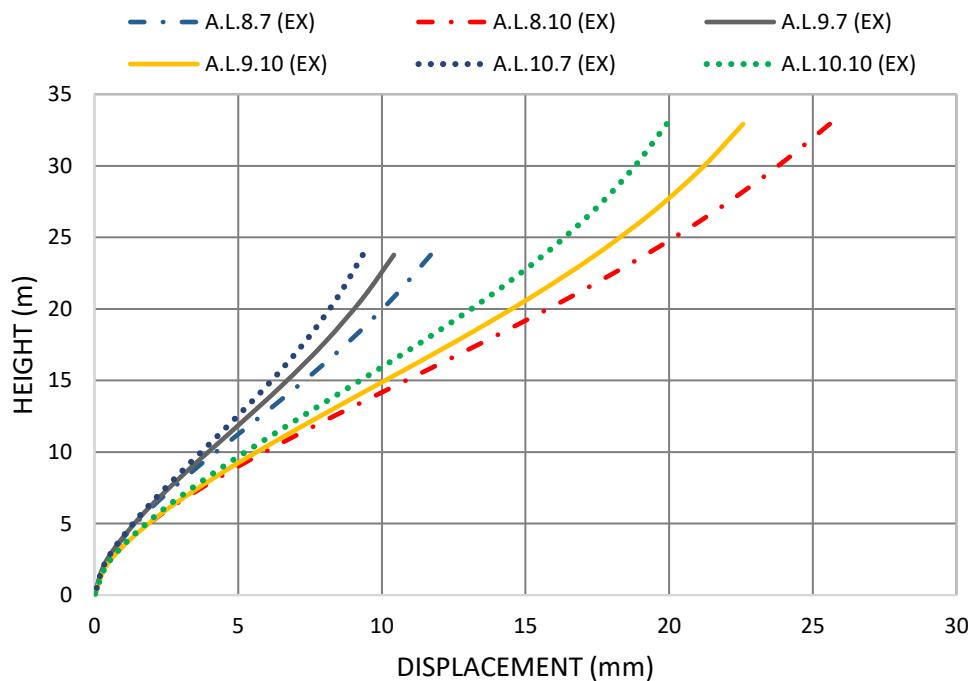


Figure 4.12: Story Height vs. Stiffness (Base Model)

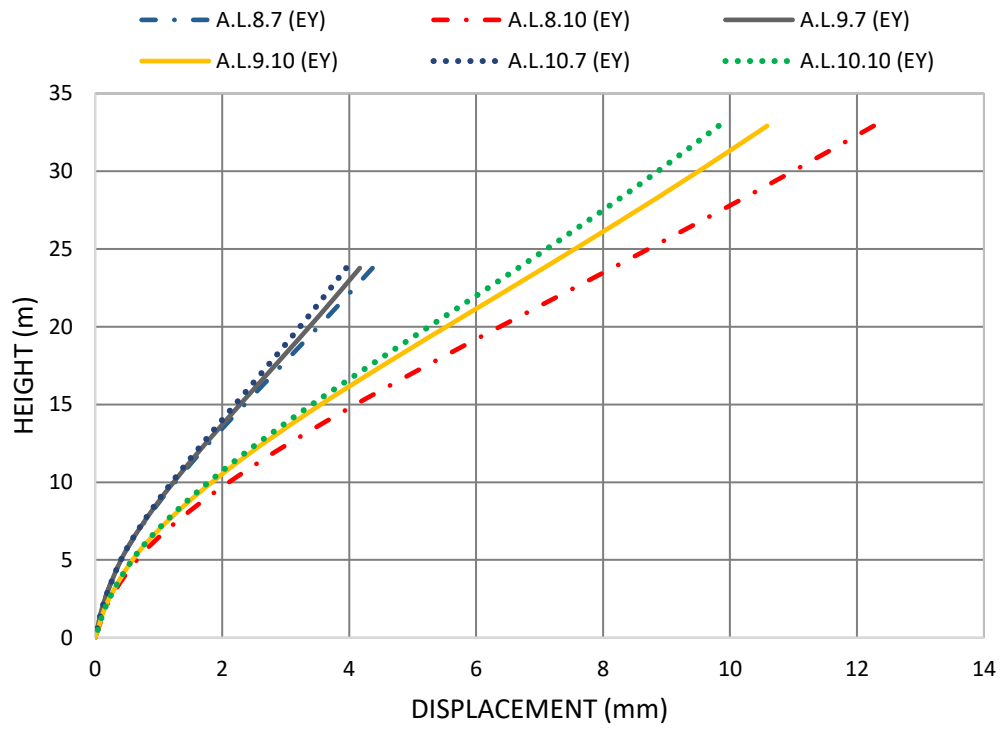
It can be seen from the graphs (Figure 4.12) that the story stiffness along x-direction is lower than in y-direction. Since the orientation of the shear walls are parallel to y-direction, the stiffness value is higher. The stiffness value in layered shell model is slightly higher than thick shell. Layered shell models take into account the distinct stiffness properties of each layer, such as concrete and reinforcement, thus demonstrating higher stiffness.

4.3.2 Comparison Between Model Variations

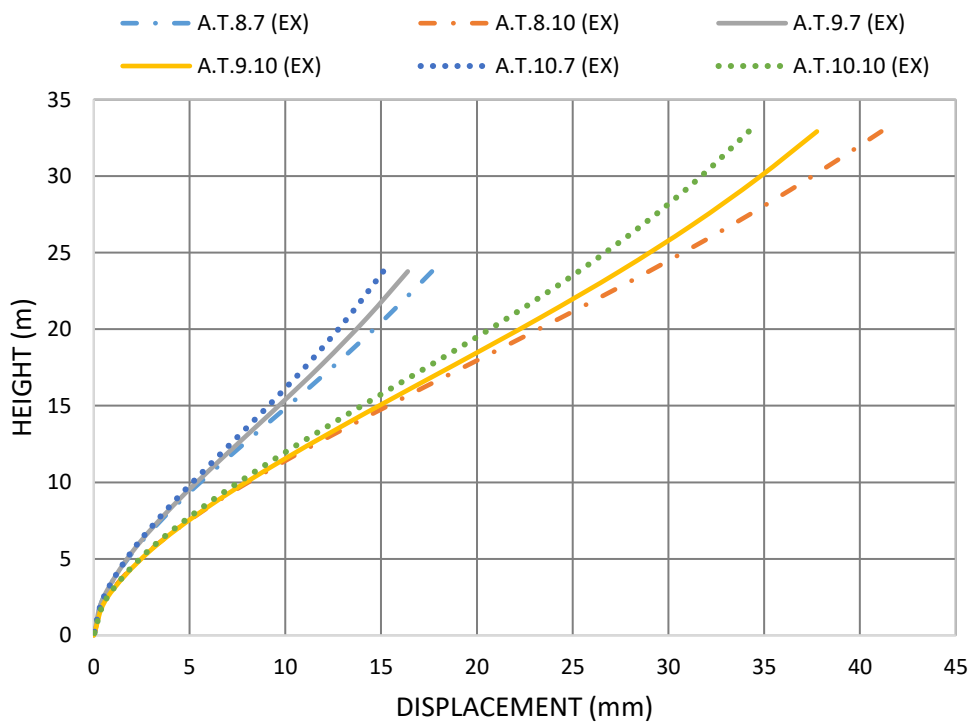
Comparison of maximum story displacement, drift, shear, and stiffness among different model types are shown here in order to understand the effect of different parameters, such as, building dimensions, number of stories, and slab thickness on structure.



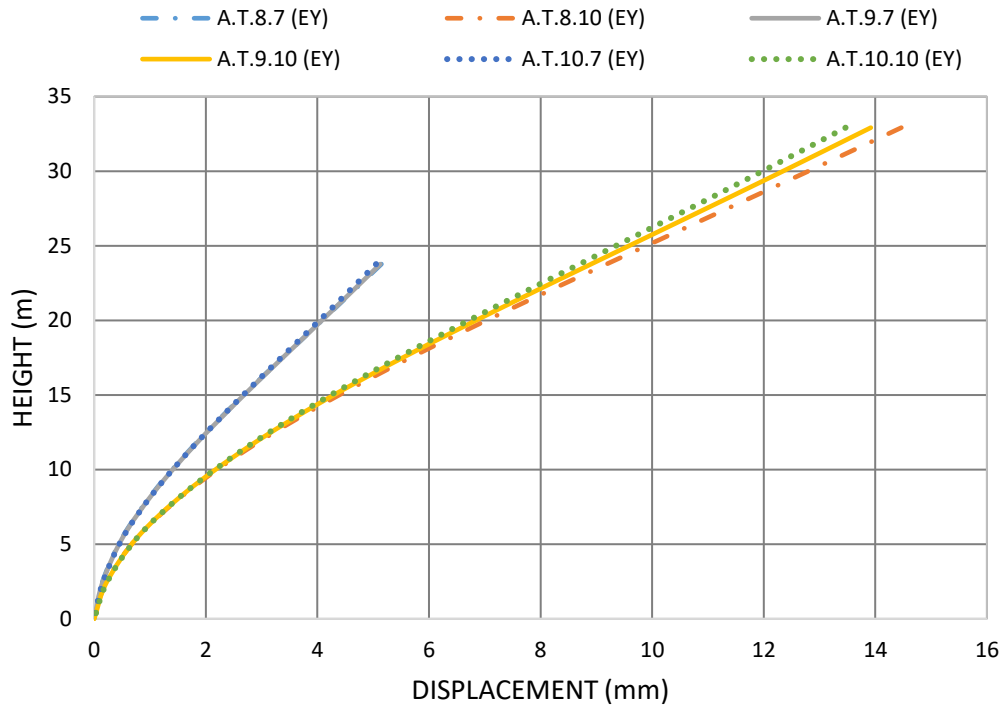
(a)



(b)



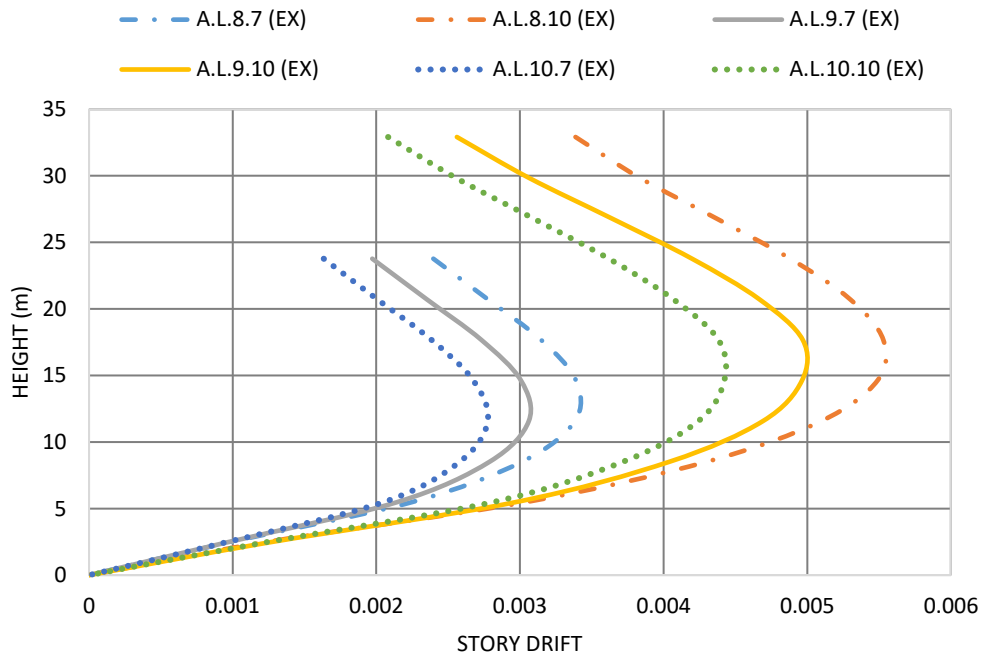
(c)



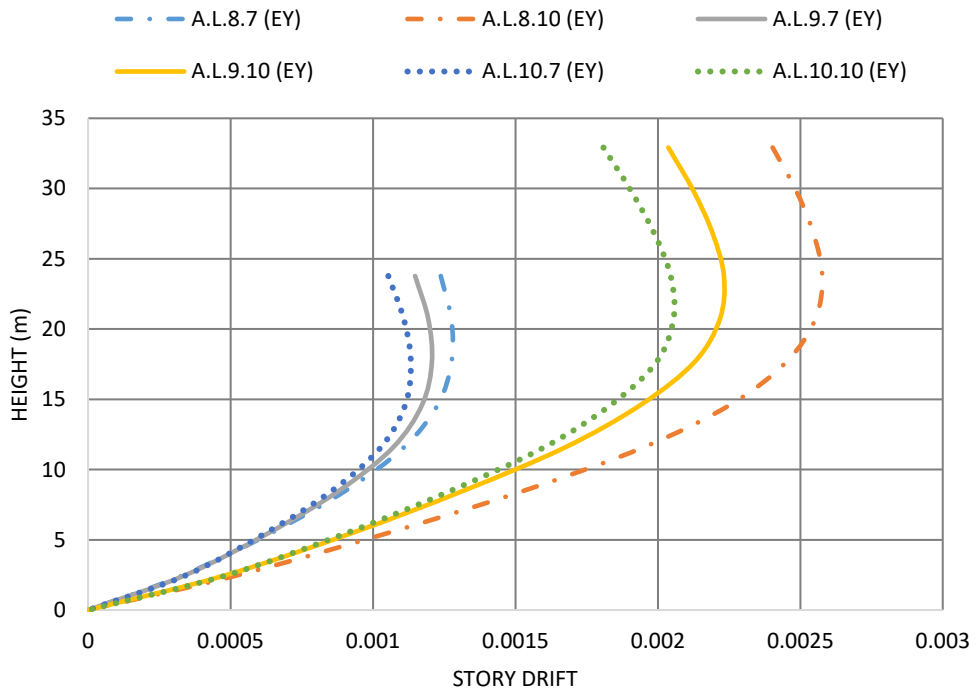
(d)

Figure 4.13: Height vs. Lateral Displacement (Type A) (a) Layered Shell (X-Direction), (b) Layered Shell (Y- Direction), (c) Thick Shell (X- Direction), (d) Thick Shell (Y- Direction)

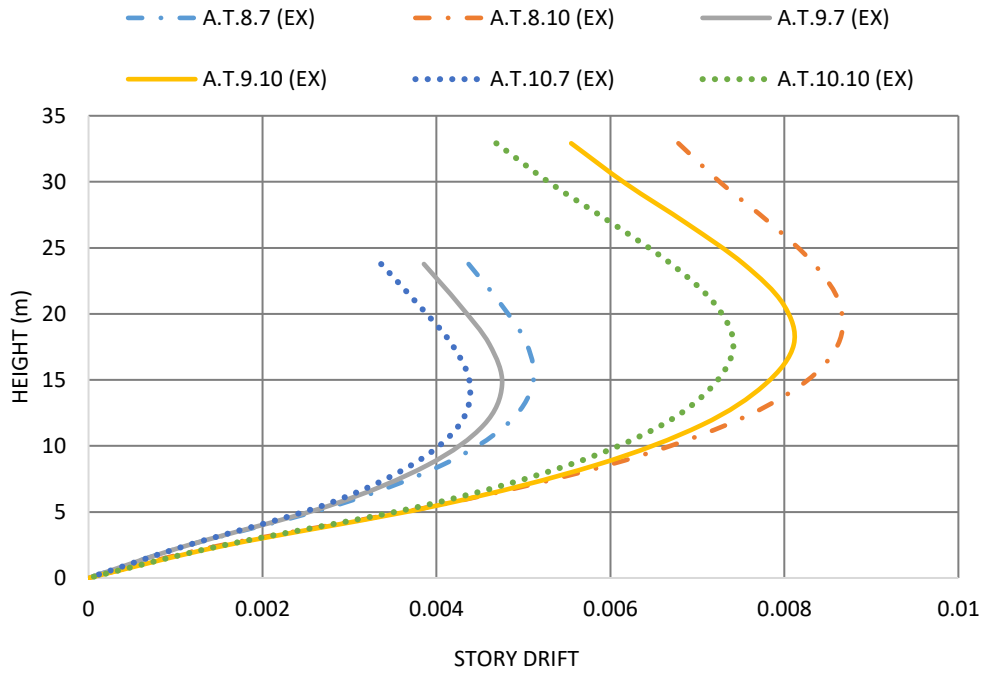
Figure 4.13 illustrates height vs. lateral displacement plot of type A models in consideration. As slab thickness increases, the lateral displacement observed decreases. Moreover, the 7 story buildings show less lateral displacement than the 10 story buildings. The thick shell models show more lateral displacement than the layered shell models. Model type B and C show similar results.



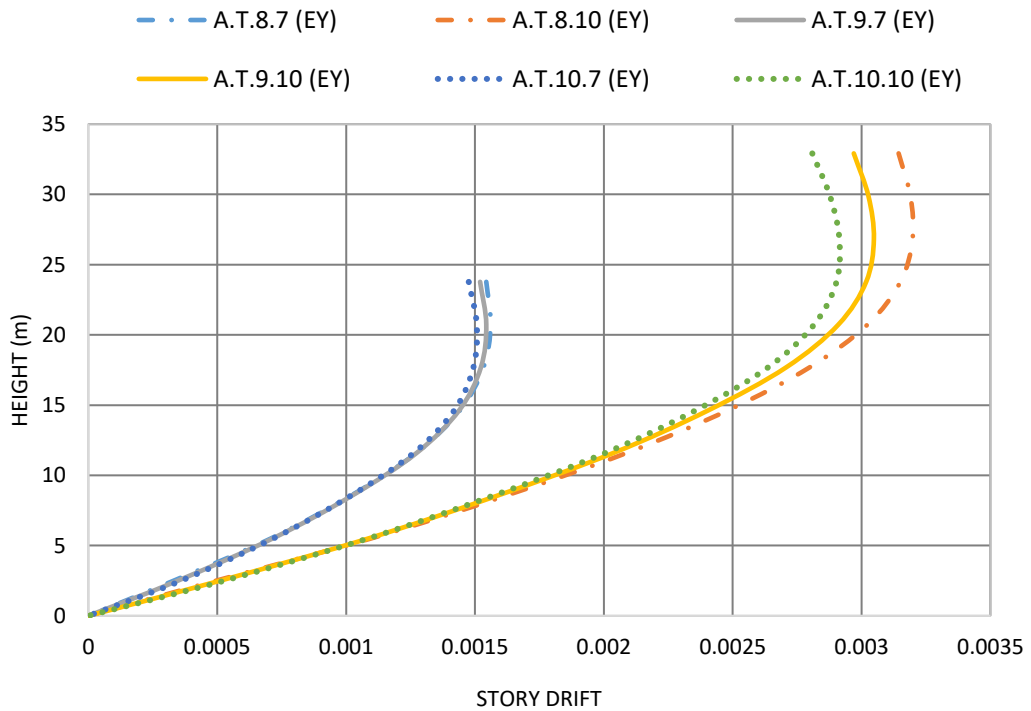
(a)



(b)



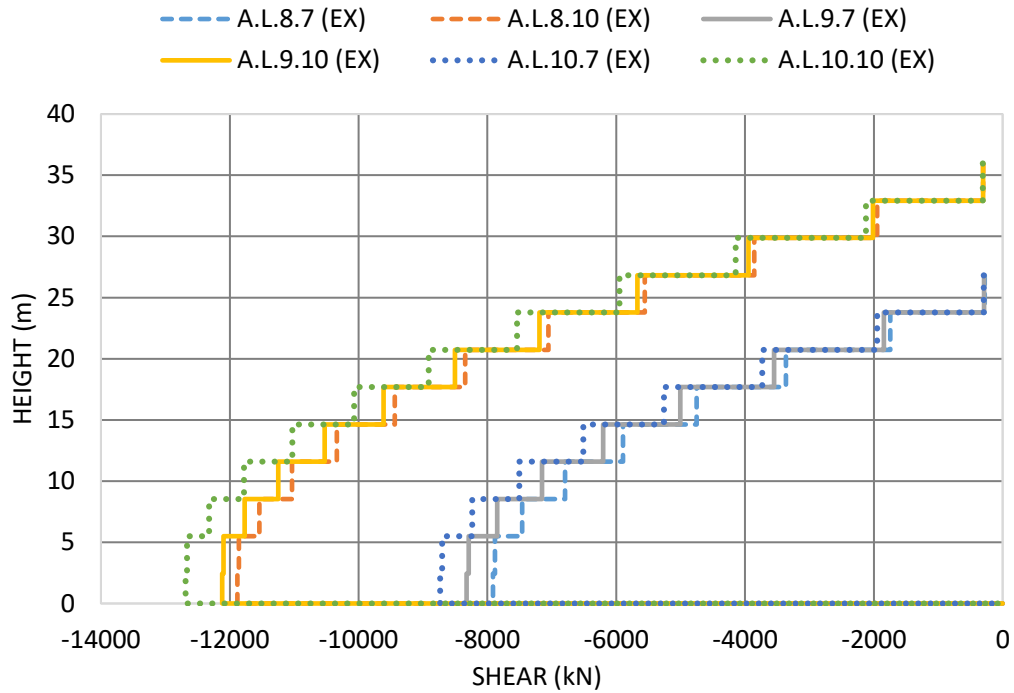
(c)



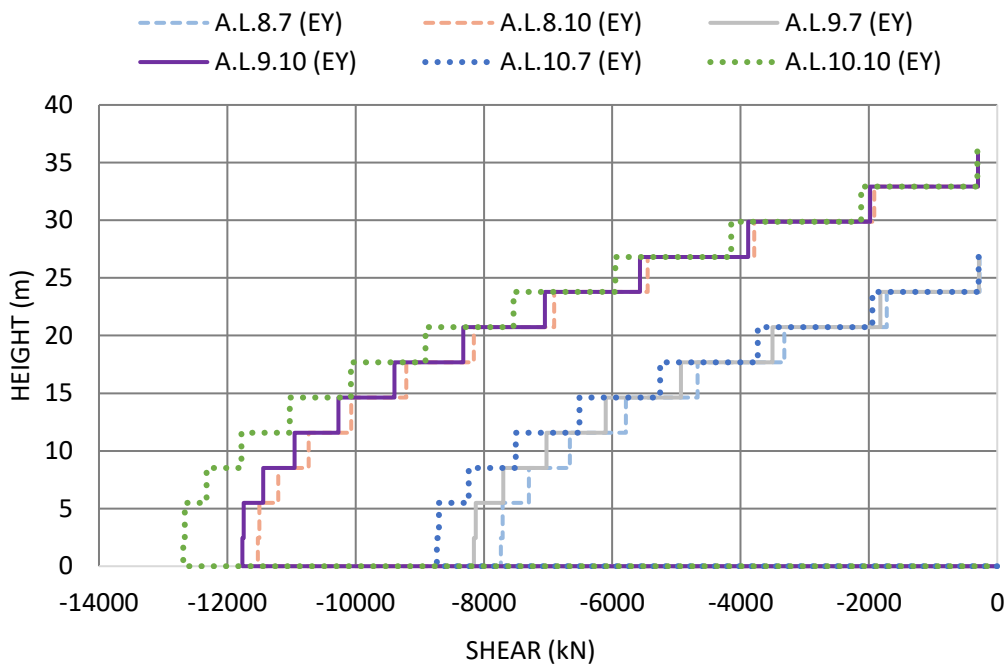
(d)

Figure 4.14: Height vs. Story Drift (Type A) (a) Layered Shell (X- Direction), (b) Layered Shell (Y- Direction), (c) Thick Shell (X- Direction), (d) Thick Shell (Y- Direction)

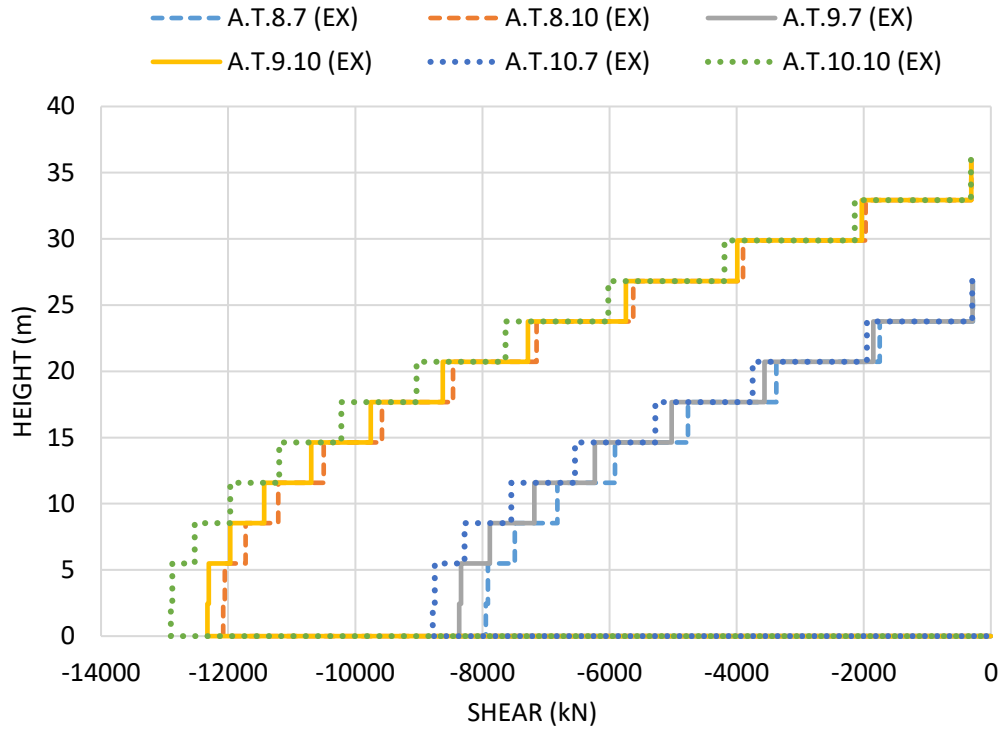
Figure 4.14 is an illustration of height vs story drift plot of type A models in consideration. As slab thickness increases, the story drift observed decreases. Moreover, the 7 story buildings show less lateral drift than the 10 story buildings. The thick shell models show more inter story drift than the layered shell models. Model type B and C show similar results.



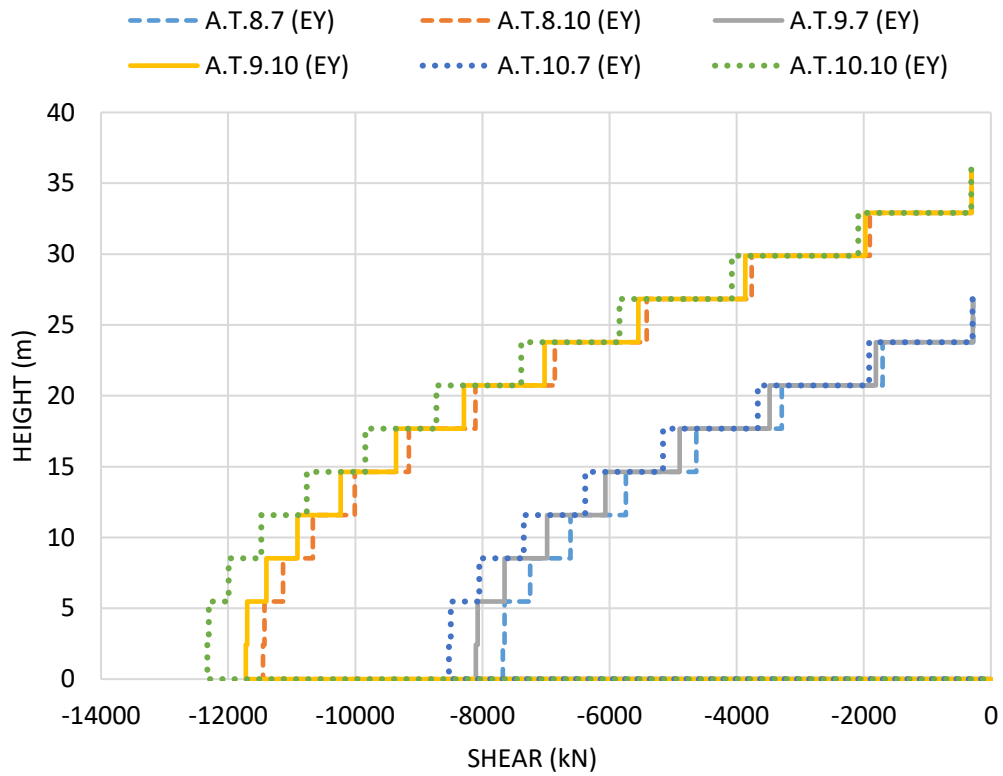
(a)



(b)



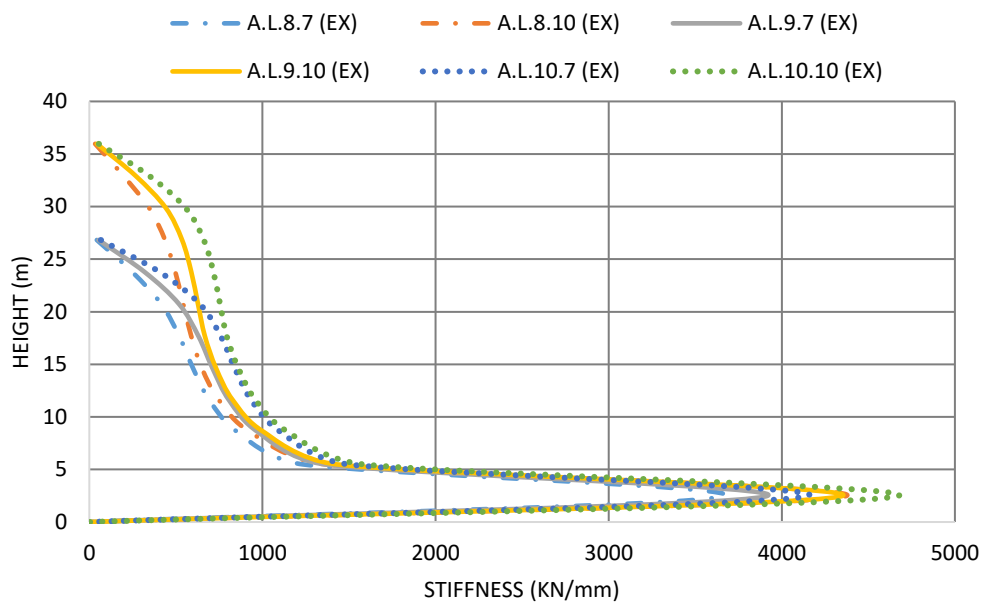
(c)



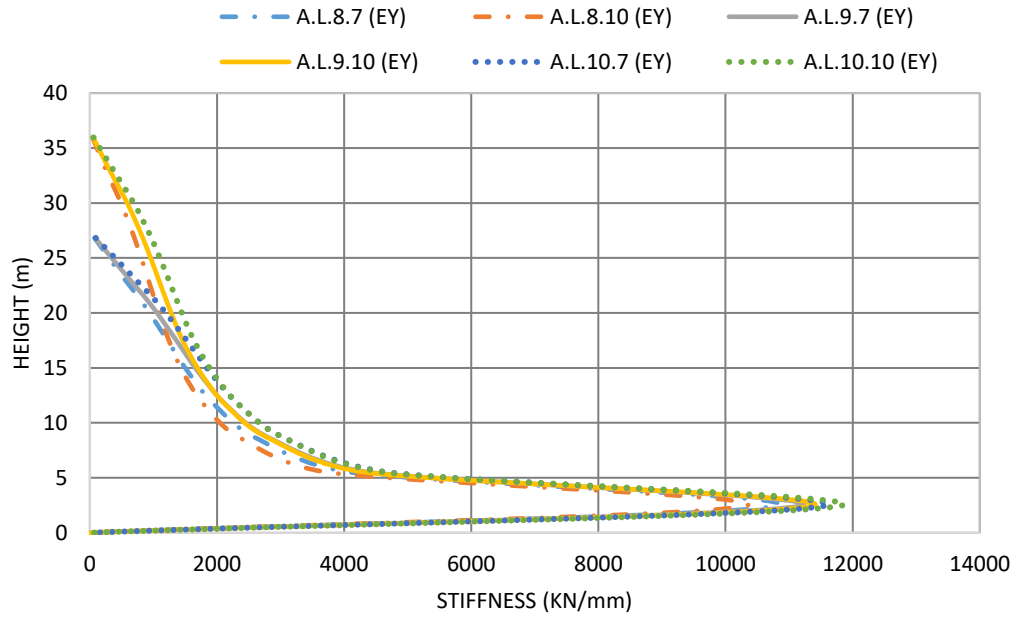
(d)

Figure 4.15: Height vs. Story Shear (Type A) (a) Layered Shell (X- Direction), (b) Layered Shell (Y- Direction), (c) Thick Shell (X- Direction), (d) Thick Shell (Y- Direction)

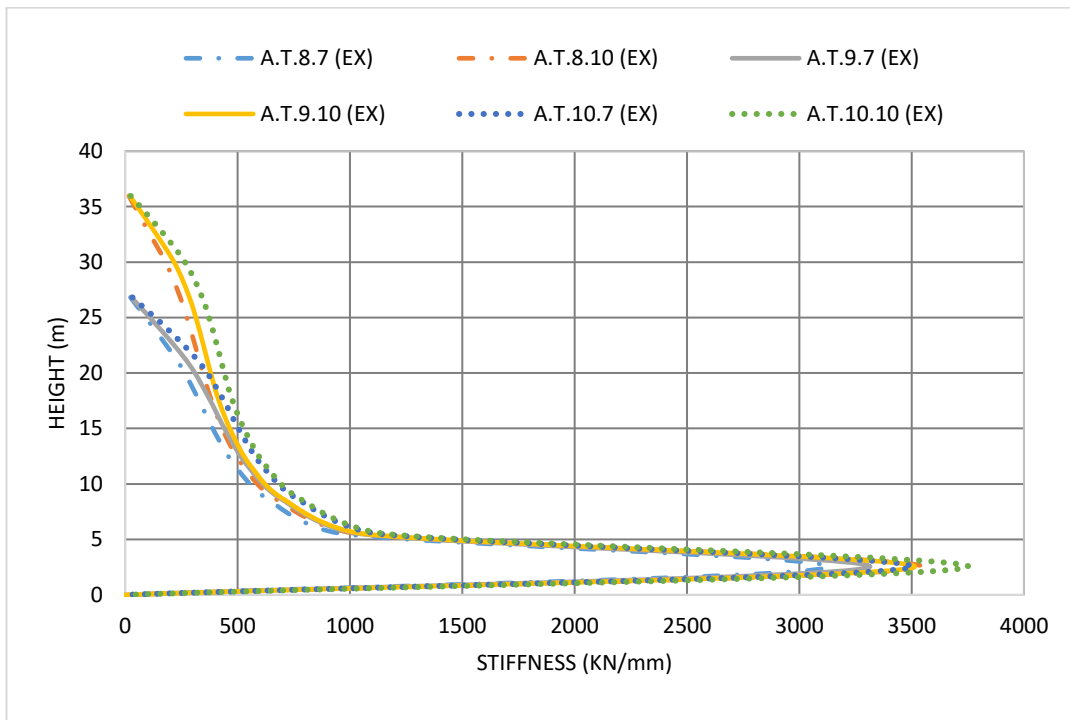
Figure 4.15 shows height vs story shear plot of type A models into consideration. The story shear observed increases with the increase of slab thickness. Moreover, the 7 story buildings show less lateral displacement than the 10 story buildings. The thick shell models carry slightly higher story shear than the layered shell models. Model type B and C show similar results. However, the larger floor area of model type A allows them to carry more shear than model type B and C.



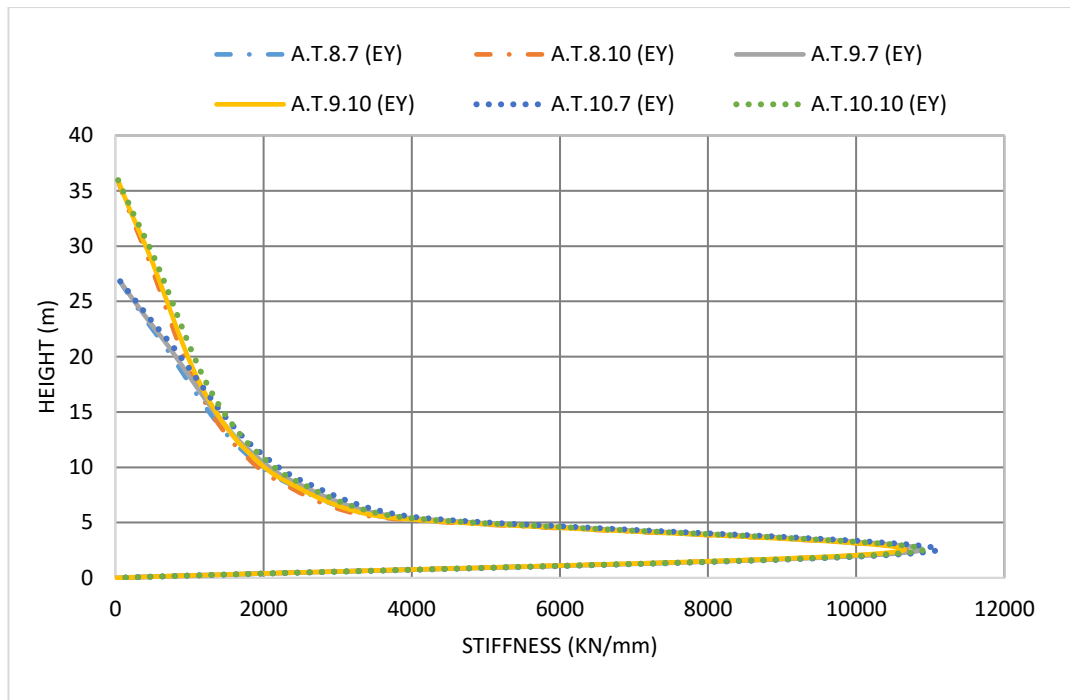
(a)



(b)



(c)



(d)

Figure 4.16: Height vs. Story Stiffness (Type A) (a) Layered Shell (X- Direction), (b) Layered Shell (Y- Direction), (c) Thick Shell (X- Direction), (d) Thick Shell (Y- Direction)

Figure 4.16 shows height vs. story stiffness plot of type A models. The story shear observed decreases with the increase of slab thickness. Moreover, the 7 story buildings are slightly stiffer than the 10 story buildings. All models are found to be stiffer in y-direction due to the favorable orientation of shear walls. The thick shell models show less story stiffness than the layered shell models. Model type B and C show similar results.

4.4 Structural Performance from Nonlinear Static Analysis

Comparison of structural performance from nonlinear static (pushover) analysis for layered shell and thick shell models have been summarized in this section.

4.4.1 Plastic Hinge

The following list presents the states of plastic hinges formed at performance point for all the structural systems under review. It can be seen that as story numbers are increased the number of plastic hinges with high magnitude of rotational angle increases. Number of plastic hinges formed are less in building with smaller dimension.

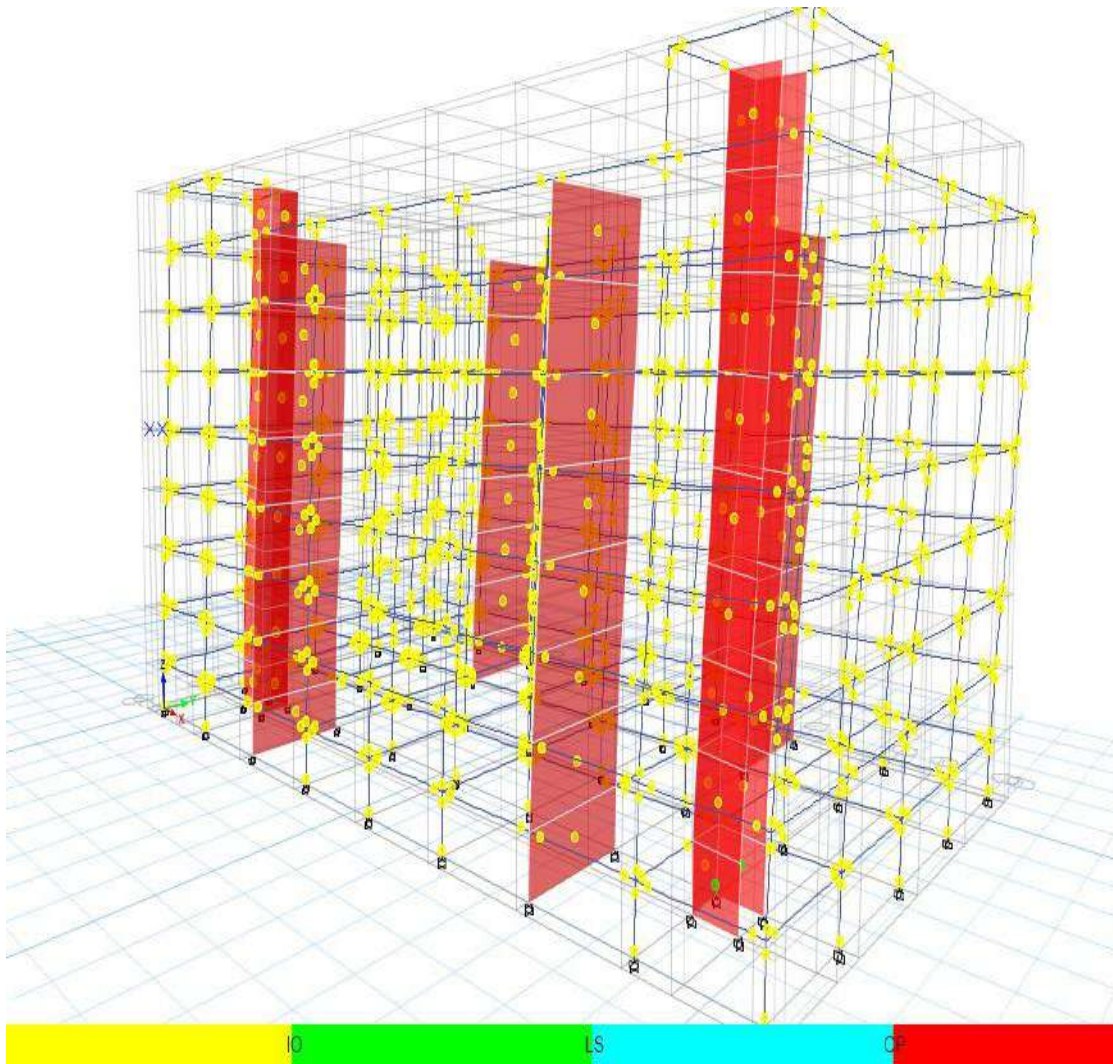


Figure 4.17: Plastic Hinge Formation at DBE Level Earthquake (Model A.L.9.7)

Figure 4.17 shows plastic hinge formation of a type A model (A.L.9.7) for pushover load in X-direction in case of MCE level earthquake. Most of the hinges formed are below the limit of immediate occupancy level. The other hinges are within life safety limit. No hinges fall beyond collapse prevention level.

Table 4.8: Plastic Hinge States at Target Displacement (Layered Shell)

Model ID	Direction	Top Displacement, δ (mm)	Base Force (kN)	A-IO	IO-LS	LS-CP	>CP	Total Hinges
A.L.8.7	X	228.78	14440.10	2221	1	0	0	2222
	Y	142.87	16278.94	2222	0	0	0	2222
A.L.8.10	X	232.30	11053.39	2960	0	0	0	2960
	Y	254.47	17638.72	2960	0	0	0	2960

Model ID	Direction	Top Displacement, δ (mm)	Base Force (kN)	A-IO	IO-LS	LS-CP	>CP	Total Hinges
A.L.9.7	X	214.17	16392.79	2220	2	0	0	2222
	Y	155.50	19974.71	2218	4	0	0	2222
A.L.9.10	X	230.00	12686.07	2964	0	0	0	2964
	Y	200.57	19556.58	2964	0	0	0	2964
A.L.10.7	X	200.46	18384.67	2220	2	0	0	2222
	Y	164.25	23689.43	2218	4	0	0	2222
A.L.10.10	X	227.88	15117.67	2960	0	0	0	2960
	Y	209.31	23040.89	2960	0	0	0	2960
B.L.8.7	X	190.93	14260.55	1810	0	0	0	1810
	Y	127.73	17507.64	1810	0	0	0	1810
B.L.8.10	X	252.76	12724.16	2416	0	0	0	2416
	Y	212.35	17418.48	2416	0	0	0	2416
B.L.9.7	X	306.38	21061.74	1805	1	2	2	1810
	Y	216.41	26507.50	1802	2	2	4	1810
B.L.9.10	X	246.96	16618.79	2416	0	0	0	2416
	Y	185.23	21458.37	2416	0	0	0	2416
B.L.10.7	X	168.91	18087.02	1810	0	0	0	1810
	Y	121.37	22505.92	1808	2	0	0	1810
B.L.10.10	X	239.44	18710.66	2416	0	0	0	2416
	Y	178.03	24343.44	2416	0	0	0	2416
C.L.8.7	X	151.90	11019.98	1725	1	0	0	1726
	Y	138.22	14524.36	1726	0	0	0	1726
C.L.8.10	X	146.84	8123.60	2296	0	0	0	2296
	Y	208.94	15550.86	2296	0	0	0	2296
C.L.9.7	X	138.63	12409.50	1724	2	0	0	1726
	Y	132.92	15457.63	1726	0	0	0	1726
C.L.9.10	X	135.64	9370.37	2296	0	0	0	2296
	Y	221.26	18143.19	2296	0	0	0	2296

Model ID	Direction	Top Displacement, δ (mm)	Base Force (kN)	A-IO	IO-LS	LS-CP	>CP	Total Hinges
C.L.10.7	X	126.54	13825.70	1725	1	0	0	1726
	Y	136.45	19179.12	1726	0	0	0	1726
C.L.10.10	X	124.85	11047.57	2296	0	0	0	2296
	Y	216.31	21005.34	2296	0	0	0	2296

Table 4.8 shows plastic hinge states for layered shell models at target displacement. All hinges in type A and type C model stay within the acceptable (upto LS) limit. One type B model formed hinges beyond the CP (>CP) range.

Table 4.9: Plastic Hinge States at Target Displacement (Thick Shell)

Model ID	Direction	Top Displacement, δ (mm)	Base Force (kN)	A-IO	IO-LS	LS-CP	>CP	Total Hinges
A.T.8.7	X	249.09	12071.42	2221	1	0	0	2222
	Y	147.54	16041.60	2222	0	0	0	2222
A.T.8.10	X	251.82	8034.39	2960	0	0	0	2960
	Y	246.24	17943.54	2960	0	0	0	2960
A.T.9.7	X	245.55	12946.90	2222	0	0	0	2222
	Y	151.06	15944.18	2222	0	0	0	2222
A.T.9.10	X	245.18	8990.20	2964	0	0	0	2964
	Y	241.75	19654.57	2964	0	0	0	2964
A.T.10.7	X	242.14	15009.66	2220	2	0	0	2222
	Y	150.81	17074.00	2222	0	0	0	2222
A.T.10.10	X	241.71	10585.68	2960	0	0	0	2960
	Y	238.77	21480.57	2960	0	0	0	2960
B.T.8.7	X	233.17	12355.46	1808	2	0	0	1810
	Y	140.43	14842.67	1810	0	0	0	1810
B.T.8.10	X	259.79	10290.58	2416	0	0	0	2416
	Y	221.47	16397.80	2416	0	0	0	2416
B.T.9.7	X	227.67	13520.63	1809	1	0	0	1810
	Y	140.33	16220.89	1810	0	0	0	1810
B.T.9.10	X	257.82	12432.19	2416	0	0	0	2416
	Y	207.48	17908.30	2416	0	0	0	2416
B.T.10.7	X	220.98	14766.76	1812	2	0	0	1814
	Y	139.97	17890.28	1794	0	0	20	1814
B.T.10.10	X	255.61	13973.12	2416	0	0	0	2416
	Y	206.11	19632.10	2416	0	0	0	2416
C.T.8.7	X	201.53	9484.85	1725	1	0	0	1726
	Y	134.15	13427.17	1726	0	0	0	1726
C.T.8.10	X	208.13	6186.53	2296	0	0	0	2296

Model ID	Direction	Top Displacement, δ (mm)	Base Force (kN)	A-IO	IO-LS	LS-CP	>CP	Total Hinges
	Y	221.87	14952.60	2296	0	0	0	2296
C.T.9.7	X	192.67	10764.51	1726	0	0	0	1726
	Y	134.08	14539.89	1726	0	0	0	1726
C.T.9.10	X	202.63	6929.56	2296	0	0	0	2296
	Y	228.99	14434.85	2292	0	0	4	2296
C.T.10.7	X	185.84	12314.72	1725	1	0	0	1726
	Y	134.05	16378.31	1726	0	0	0	1726
C.T.10.10	X	191.73	8060.98	2296	0	0	0	2296
	Y	226.28	16359.27	2296	0	0	0	2296

Table 4.9 shows plastic hinge states for thick shell models at target displacement. All hinges in type A model stay within the acceptable (upto LS) limit. One type B and one type C model formed hinges beyond the CP (>CP) range.

In all cases, the increase in number of stories increases the number of plastic hinges formed in the structure.

4.4.2 Base Shear and Maximum Top Displacement

This section summarizes the base shear and corresponding maximum top displacement calculated using displacement coefficient method (ASCE 41-13). The response spectrum is used following BNBC (2020).

Table 4.10: Base Shear and Corresponding Maximum Top Displacement (As Per ASCE 41-13)

EQ Direction	Building Height (m)	Layered Shell			Thick Shell		
		Model ID	Base Shear, V (kN)	Target Displacement, δ (mm)	Model ID	Base Shear, V (kN)	Target Displacement, δ (mm)
X	26.8224	A.L.8.7	14440.1	228.781	A.T.8.7	12071.42	249.089
Y	26.8224		16278.94	142.873		16041.6	147.544
X	35.9664	A.L.8.10	11053.39	232.295	A.T.8.10	8034.391	251.820
Y	35.9664		17638.72	254.470		17943.54	246.240
X	26.8224	A.L.9.7	16392.79	214.167	A.T.9.7	12946.9	245.553
Y	26.8224		19974.71	155.503		15944.18	151.062
X	35.9664	A.L.9.10	12686.07	229.996	A.T.9.10	8990.203	245.180
Y	35.9664		19556.58	200.571		19654.57	241.745
X	26.8224	A.L.10.7	18384.67	200.460	A.T.10.7	15009.66	242.137

EQ Direction	Building Height (m)	Layered Shell			Thick Shell		
		Model ID	Base Shear, V (kN)	Target Displacement, δ (mm)	Model ID	Base Shear, V (kN)	Target Displacement, δ (mm)
Y	26.8224		23689.43	164.249		17074	150.814
X	35.9664	A.L.10.10	15117.67	227.879	A.T.10.10	10585.68	241.710
Y	35.9664		23040.89	209.313		21480.57	238.767
X	26.8224	B.L.8.7	14260.55	190.933	B.T.8.7	12355.46	233.173
Y	26.8224		17507.64	127.733		14842.67	140.433
X	35.9664	B.L.8.10	12724.16	252.756	B.T.8.10	10290.58	259.788
Y	35.9664		17418.48	212.353		16397.8	221.474
X	26.8224	B.L.9.7	15499.93	177.796	B.T.9.7	13520.63	227.665
Y	26.8224		20246.8	124.981		16220.89	140.331
X	35.9664	B.L.9.10	16618.79	246.957	B.T.9.10	12432.19	257.823
Y	35.9664		21458.37	185.225		17908.3	207.479
X	26.8224	B.L.10.7	18087.02	168.913	B.T.10.7	14766.76	220.979
Y	26.8224		22505.92	121.372		17890.28	139.973
X	35.9664	B.L.10.10	18710.66	239.435	B.T.10.10	13973.12	255.613
Y	35.9664		24343.44	178.026		19632.1	206.114
X	26.8224	C.L.8.7	11019.98	151.898	C.T.8.7	9484.845	201.528
Y	26.8224		14524.36	138.218		13427.17	134.154
X	35.9664	C.L.8.10	8123.605	146.842	C.T.8.10	6186.529	208.131
Y	35.9664		15550.86	208.940		14952.6	221.869
X	26.8224	C.L.9.7	12409.5	138.635	C.T.9.7	10764.51	192.666
Y	26.8224		15457.63	132.923		14539.89	134.078
X	35.9664	C.L.9.10	9370.375	135.639	C.T.9.10	6929.564	202.627
Y	35.9664		18143.19	221.261		14434.85	228.990
X	26.8224	C.L.10.7	13825.7	126.540	C.T.10.7	12314.72	185.836
Y	26.8224		19179.12	136.450		16378.31	134.047
X	35.9664	C.L.10.10	11047.57	124.850	C.T.10.10	8060.983	191.729
Y	35.9664		21005.34	216.306		16359.27	226.280

The base shear and corresponding maximum top displacement calculated utilizing ASCE 41-13 (2013) code has been tabulated in Table 4.10. Higher stiffness in y-direction also causes lower displacement in the structures. Increase in building height increases the displacement of structures. Since the base shear capacity in layered shell models are higher than the corresponding thick shell models, the displacement is found to be less than the thick shell models.

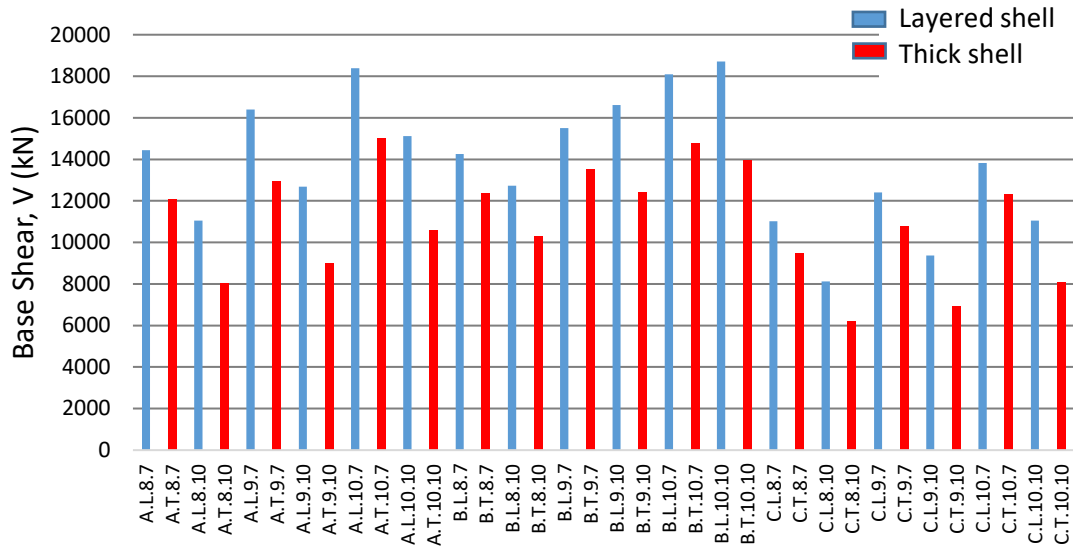


Figure 4.18: Base Shear Capacity Chart (X-Direction)

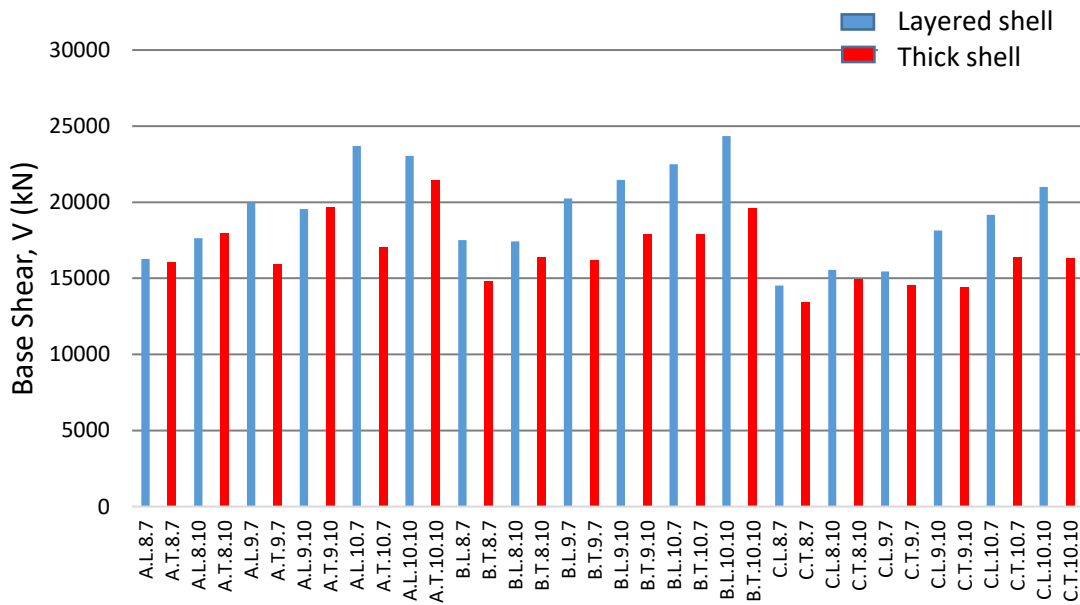
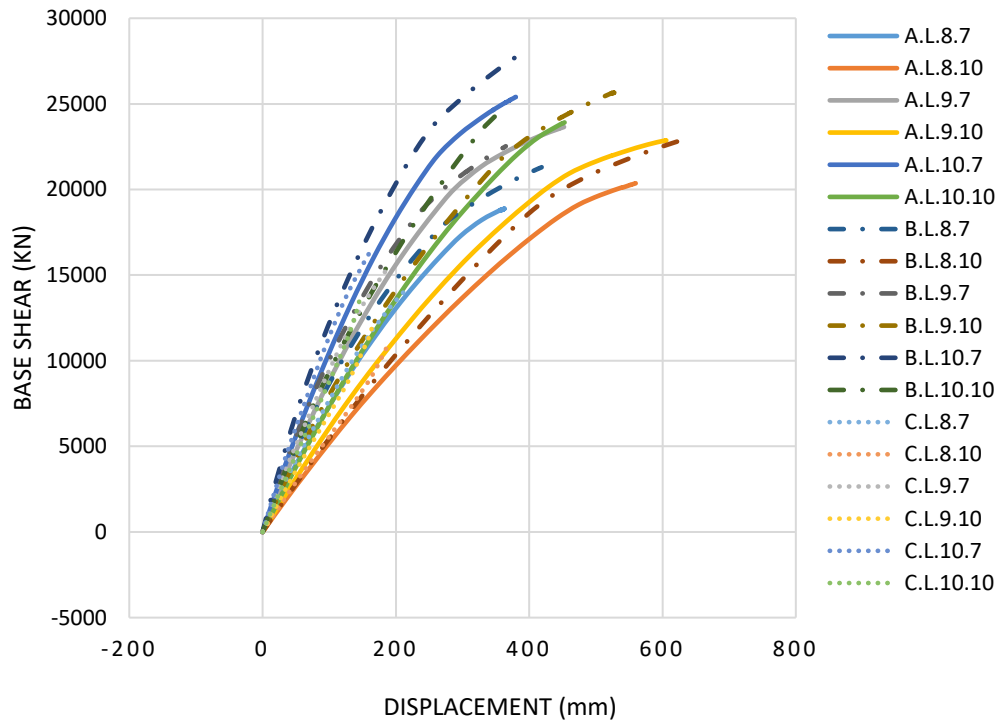


Figure 4.19: Base Shear Capacity Chart (Y-Direction)

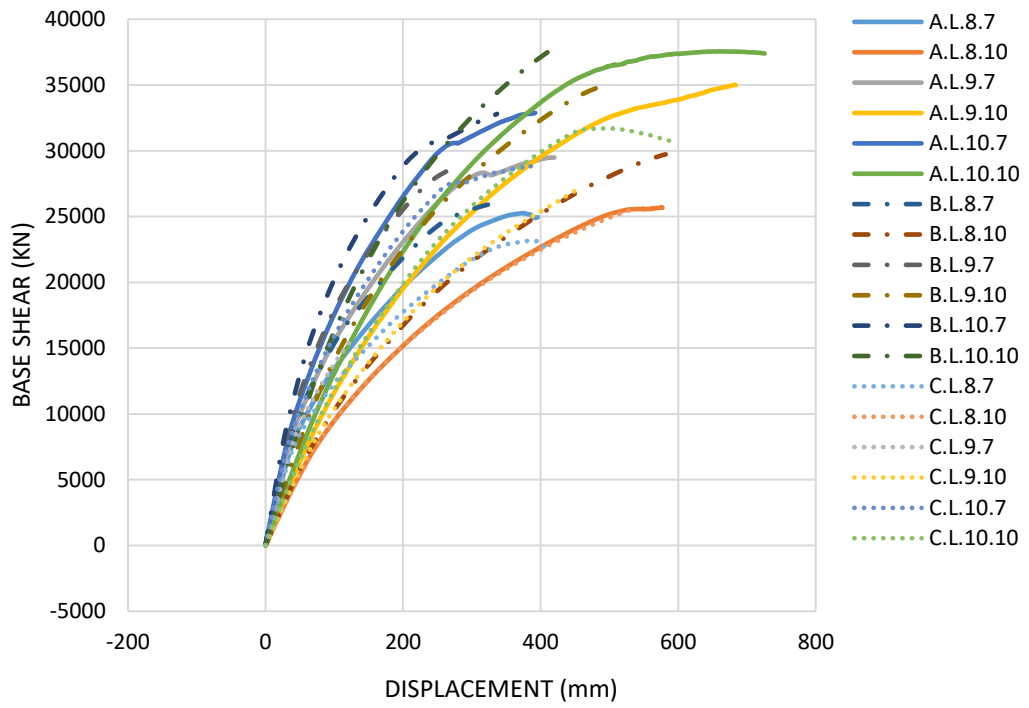
Figure 4.18 and Figure 4.19 have been added for better illustration of the base shear capacity. Since stiffness of the structures are higher along the y-direction, base shear capacity has also been found to be higher in all models. However, increase in building height reduces base shear capacity. Layered shell models exhibit higher base shear capacity than thick shell models.

4.4.3 Capacity curve

Capacity curve is the graphical illustration of base shear vs monitored displacement from nonlinear static pushover analysis. In ETABS 2016, capacity curve is derived following ASCE 41-13 NSP. From the capacity curves it can be seen that base shear capacity changes with height of the building, plan (aspect ratio) and also earthquake direction.

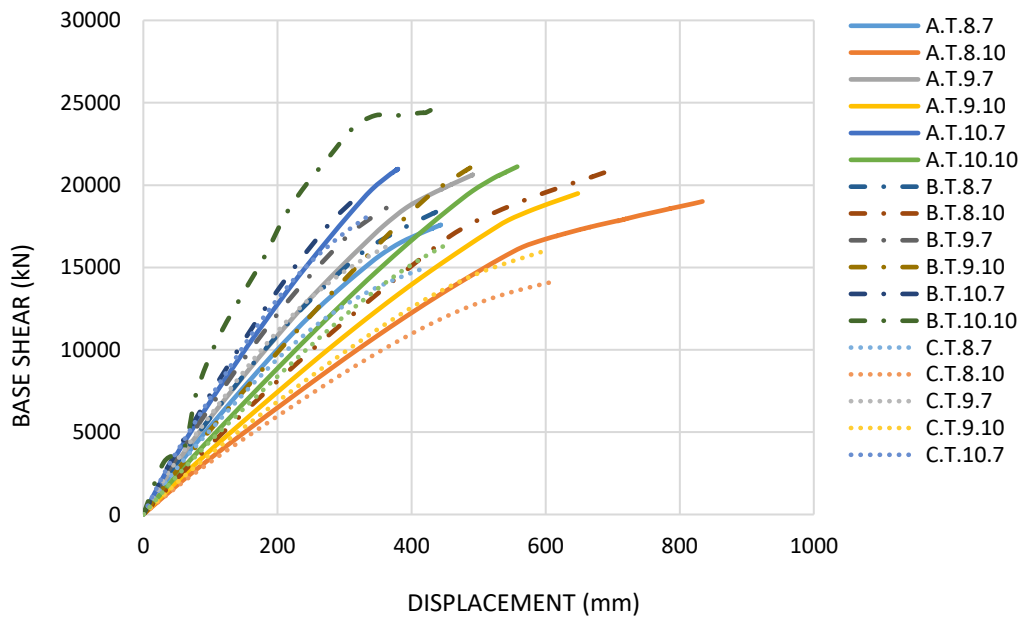


(a)

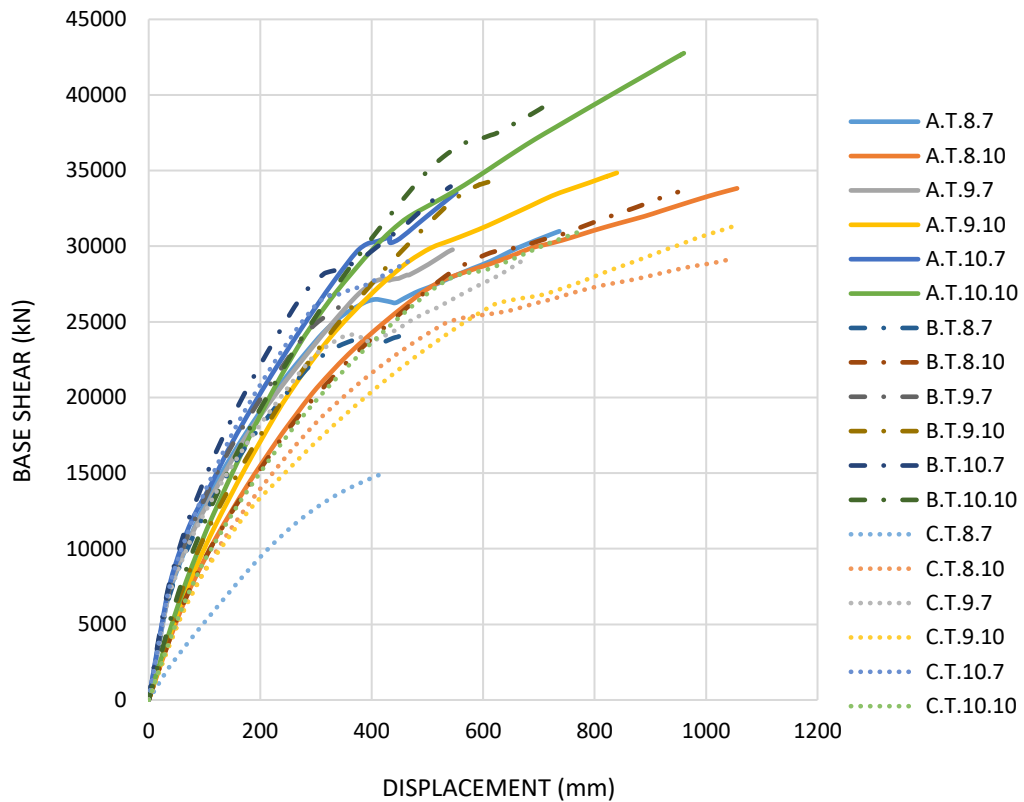


(b)

Figure 4.20: Capacity Curve (Base Shear vs. Displacement) for Layered Shell Models (a) X- Direction, (b) Y- Direction.



(a)



(b)

Figure 4.21: Capacity Curve (Base Shear vs. Displacement) for Thick Shell Models (a) X- Direction, (b) Y- Direction

Figure 4.20 represents capacity curve for layered shell models and Figure 4.21 represents capacity curve for thick shell models. The slopes of the y-direction curves are steeper than x-direction curves. That means the structure deforms less for same base shear in y-direction. This again proves the stiffness of the structure is higher in y-direction. The curves obtained for pushover in x-direction starts to flatten out for lower base shear than y-direction curves. It indicates that the structure deforms elastically in y-direction for higher base shear than x-direction. Nevertheless, no curves reached their peak strength as no curve is seen with negative slope.

The layered shell models produce smoother curve than thick shell models. The nonlinear material properties and series of interconnected layers with their own material properties and thickness in layered shell slabs show more realistic response of strength degradation of the structures while subjected to increasing lateral forces.

4.4.4 Slab Displacement at Different Earthquake Level

The slab displacement for all 36 models are calculated for Maximum Considered Earthquake (MCE), Design Based Earthquake (DBE) and Serviceability Earthquake (SE) level from target displacement obtained by following ASCE 41-13 (2013). The DBE level has been considered $2/3^{\text{rd}}$ of MCE level and SE has been taken to be $1/2$ of MCE level.

Table 4.11: Slab Displacement at Different Earthquake Level

EQ Direction	Building Height (m)	Layered Shell				Thick Shell			
		Model ID	Top Deflection at Target Displacement, δ (mm)			Model ID	Top Deflection at Target Displacement, δ (mm)		
			MCE	DBE	SE		MCE	DBE	SE
X	26.82	A.L.8.7	343.17	228.78	171.59	A.T.8.7	373.63	249.09	186.82
Y	26.82		214.31	142.87	107.15		221.32	147.54	110.66
X	35.97	A.L.8.10	348.44	232.30	174.22	A.T.8.10	377.73	251.82	188.86
Y	35.97		381.70	254.47	190.85		369.36	246.24	184.68
X	26.82	A.L.9.7	321.25	214.17	160.63	A.T.9.7	368.33	245.55	184.16
Y	26.82		233.25	155.50	116.63		226.59	151.06	113.30
X	35.97	A.L.9.10	344.99	230.00	172.50	A.T.9.10	367.77	245.18	183.89
Y	35.97		300.86	200.57	150.43		362.62	241.75	181.31
X	26.82	A.L.10.7	300.69	200.46	150.35	A.T.10.7	363.21	242.14	181.60
Y	26.82		246.37	164.25	123.19		226.22	150.81	113.11
X	35.97	A.L.10.10	341.82	227.88	170.91	A.T.10.10	362.57	241.71	181.28
Y	35.97		313.97	209.31	156.99		358.15	238.77	179.08
X	26.82	B.L.8.7	286.40	190.93	143.20	B.T.8.7	349.76	233.17	174.88
Y	26.82		191.60	127.73	95.80		210.65	140.43	105.33
X	35.97	B.L.8.10	379.13	252.76	189.57	B.T.8.10	389.68	259.79	194.84
Y	35.97		318.53	212.35	159.26		332.21	221.47	166.11
X	26.82	B.L.9.7	266.69	177.80	133.35	B.T.9.7	341.50	227.67	170.75
Y	26.82		187.47	124.98	93.74		210.50	140.33	105.25
X	35.97	B.L.9.10	370.44	246.96	185.22	B.T.9.10	386.73	257.82	193.37
Y	35.97		277.84	185.23	138.92		311.22	207.48	155.61
X	26.82	B.L.10.7	253.37	168.91	126.68	B.T.10.7	331.47	220.98	165.73
Y	26.82		182.06	121.37	91.03		209.96	139.97	104.98
X	35.97	B.L.10.10	359.15	239.44	179.58	B.T.10.10	383.42	255.61	191.71
Y	35.97		267.04	178.03	133.52		309.17	206.11	154.59

EQ Direction	Building Height (m)	Layered Shell				Thick Shell			
		Model ID	Top Deflection at Target Displacement, δ (mm)			Model ID	Top Deflection at Target Displacement, δ (mm)		
			MCE	DBE	SE		MCE	DBE	SE
X	26.82	C.L.8.7	227.85	151.90	113.92	C.T.8.7	302.29	201.53	151.15
Y	26.82		207.33	138.22	103.66		201.23	134.15	100.62
X	35.97	C.L.8.10	220.26	146.84	110.13	C.T.8.10	312.20	208.13	156.10
Y	35.97		313.41	208.94	156.71		332.80	221.87	166.40
X	26.82	C.L.9.7	207.95	138.63	103.98	C.T.9.7	289.00	192.67	144.50
Y	26.82		199.38	132.92	99.69		201.12	134.08	100.56
X	35.97	C.L.9.10	203.46	135.64	101.73	C.T.9.10	303.94	202.63	151.97
Y	35.97		331.89	221.26	165.95		343.49	228.99	171.74
X	26.82	C.L.10.7	189.81	126.54	94.90	C.T.10.7	278.75	185.84	139.38
Y	26.82		204.68	136.45	102.34		201.07	134.05	100.54
X	35.97	C.L.10.10	187.28	124.85	93.64	C.T.10.10	287.59	191.73	143.80
Y	35.97		324.46	216.31	162.23		339.42	226.28	169.71

Slab displacements at different earthquake level are presented in Table 4.11. The maximum displacement is found to be 1.1% of building height which is within reasonable limit.

4.4.5 Slab Performance Check

The calculated global acceptance limits of plastic rotation angle of slab for different performance levels as per ASCE 41-13 (2013) for all models are tabulated in Table 4.12.

Table 4.12: Modeling Parameters and Numerical Acceptance Limit for All Models

Model ID	Conditions		Modeling Parameters ^a			Acceptance Criteria ^a		
			Plastic Rotation Angle (Radians)	Residual Strength Ratio	Plastic Rotations Angle (Radians)			
					Performance Level			
						Secondary		
			a	b	c	IO	LS	CP
Condition i. Reinforced concrete slab-column connections^b								
	$(V_g/V_o)^c$	Continuity Reinforcement ^d						
A.L.8.7	0.00902	Yes	0.035	0.050	0.200	0.01	0.035	0.050
A.L.8.10	0.00975	Yes	0.035	0.050	0.200	0.01	0.035	0.050
A.L.9.7	0.00963	Yes	0.035	0.050	0.200	0.01	0.035	0.050

Model ID	Conditions		Modeling Parameters ^a			Acceptance Criteria ^a				
			Plastic Rotation Angle (Radians)		Residual Strength Ratio	Plastic Rotations Angle (Radians)				
						Performance Level				
								Secondary		
			a	b	c	IO	LS	CP		
Condition i. Reinforced concrete slab–column connections^b										
	(V _g /V _o) ^c	Continuity Reinforcement ^d								
A.L.9.10	0.00963	Yes	0.035	0.050	0.200	0.01	0.035	0.050		
A.L.10.7	0.01027	Yes	0.035	0.049	0.200	0.01	0.035	0.049		
A.L.10.10	0.01027	Yes	0.035	0.049	0.200	0.01	0.035	0.049		
B.L.8.7	0.00902	Yes	0.035	0.050	0.200	0.01	0.035	0.050		
B.L.8.10	0.01008	Yes	0.035	0.049	0.200	0.01	0.035	0.049		
B.L.9.7	0.00963	Yes	0.035	0.050	0.200	0.01	0.035	0.050		
B.L.9.10	0.01023	Yes	0.035	0.049	0.200	0.01	0.035	0.049		
B.L.10.7	0.01027	Yes	0.035	0.049	0.200	0.01	0.035	0.049		
B.L.10.10	0.01040	Yes	0.035	0.049	0.200	0.01	0.035	0.049		
C.L.8.7	0.00898	Yes	0.035	0.050	0.200	0.01	0.035	0.050		
C.L.8.10	0.00941	Yes	0.035	0.050	0.200	0.01	0.035	0.050		
C.L.9.7	0.00963	Yes	0.035	0.050	0.200	0.01	0.035	0.050		
C.L.9.10	0.00963	Yes	0.035	0.050	0.200	0.01	0.035	0.050		
C.L.10.7	0.01027	Yes	0.035	0.049	0.200	0.01	0.035	0.049		
C.L.10.10	0.01027	Yes	0.035	0.049	0.200	0.01	0.035	0.049		
A.T.8.7	0.00902	Yes	0.035	0.050	0.200	0.01	0.035	0.050		
A.T.8.10	0.00975	Yes	0.035	0.050	0.200	0.01	0.035	0.050		
A.T.9.7	0.00963	Yes	0.035	0.050	0.200	0.01	0.035	0.050		
A.T.9.10	0.00963	Yes	0.035	0.050	0.200	0.01	0.035	0.050		
A.T.10.7	0.01027	Yes	0.035	0.049	0.200	0.01	0.035	0.049		
A.T.10.10	0.01027	Yes	0.035	0.049	0.200	0.01	0.035	0.049		
B.T.8.7	0.00902	Yes	0.035	0.050	0.200	0.01	0.035	0.050		
B.T.8.10	0.01008	Yes	0.035	0.049	0.200	0.01	0.035	0.049		
B.T.9.7	0.00963	Yes	0.035	0.050	0.200	0.01	0.035	0.050		
B.T.9.10	0.01023	Yes	0.035	0.049	0.200	0.01	0.035	0.049		
B.T.10.7	0.01027	Yes	0.035	0.049	0.200	0.01	0.035	0.049		
B.T.10.10	0.01040	Yes	0.035	0.049	0.200	0.01	0.035	0.049		
C.T.8.7	0.00898	Yes	0.035	0.050	0.200	0.01	0.035	0.050		
C.T.8.10	0.00941	Yes	0.035	0.050	0.200	0.01	0.035	0.050		

Model ID	Conditions		Modeling Parameters ^a			Acceptance Criteria ^a		
			Plastic Rotation Angle (Radians)		Residual Strength Ratio	Plastic Rotations Angle (Radians)		
						Performance Level		
					Secondary			
			a	b	c	IO	LS	CP
Condition i. Reinforced concrete slab–column connections^b								
	(V _g /V _o) ^c	Continuity Reinforcement ^d						
C.T.9.7	0.00963	Yes	0.035	0.050	0.200	0.01	0.035	0.050
C.T.9.10	0.00963	Yes	0.035	0.050	0.200	0.01	0.035	0.050
C.T.10.7	0.01027	Yes	0.035	0.049	0.200	0.01	0.035	0.049
C.T.10.10	0.01027	Yes	0.035	0.049	0.200	0.01	0.035	0.049

Here, Gravity load (V_g) has been calculated using equation $V_g=1.2D+0.5L$ and Punching shear strength (V_o) has been calculated using equation $V_o= 4 \Phi \sqrt{f_c}'$.

It can be seen from Table 4.12 that for immediate occupancy structural performance level, all models have acceptable plastic rotation angle at 0.01 radian. The life safety acceptance limit is 0.035 radian and collapse prevention limit between 0.049 to 0.05 radian.

Table 4.13: Performance Level of Slab Based on Global Acceptance Limit (Layered Shell)

Model ID	EQ Direction	Plastic Rotation Angle, θ (rad)			Global Acceptance Limit			Performance Level (DBE)
					Immediate Occupancy (IO)	Life Safety (LS)	Collapse Prevention (CP)	
		MCE	DBE	SE				
A.L.8.7	X	0.013	0.009	0.006	0.01	0.035	0.050	IO
	Y	0.008	0.005	0.004	0.01	0.035	0.050	IO
A.L.8.10	X	0.010	0.006	0.005	0.01	0.035	0.050	IO
	Y	0.011	0.007	0.005	0.01	0.035	0.050	IO
A.L.9.7	X	0.012	0.008	0.006	0.01	0.035	0.050	IO
	Y	0.009	0.006	0.004	0.01	0.035	0.050	IO
A.L.9.10	X	0.010	0.006	0.005	0.01	0.035	0.050	IO
	Y	0.008	0.006	0.004	0.01	0.035	0.050	IO
A.L.10.7	X	0.011	0.007	0.006	0.01	0.035	0.049	IO
	Y	0.009	0.006	0.005	0.01	0.035	0.049	IO

Model ID	EQ Direction	Plastic Rotation Angle, θ (rad)			Global Acceptance Limit			Performance Level (DBE)
					Immediate Occupancy (IO)	Life Safety (LS)	Collapse Prevention (CP)	
		MCE	DBE	SE				
A.L.10.10	X	0.010	0.006	0.005	0.01	0.035	0.049	IO
	Y	0.009	0.006	0.004	0.01	0.035	0.049	IO
B.L.8.7	X	0.011	0.007	0.005	0.01	0.035	0.050	IO
	Y	0.007	0.005	0.004	0.01	0.035	0.050	IO
B.L.8.10	X	0.011	0.007	0.005	0.01	0.035	0.049	IO
	Y	0.009	0.006	0.004	0.01	0.035	0.049	IO
B.L.9.7	X	0.010	0.007	0.005	0.01	0.035	0.050	IO
	Y	0.007	0.005	0.003	0.01	0.035	0.050	IO
B.L.9.10	X	0.010	0.007	0.005	0.01	0.035	0.049	IO
	Y	0.008	0.005	0.004	0.01	0.035	0.049	IO
B.L.10.7	X	0.009	0.006	0.005	0.01	0.035	0.049	IO
	Y	0.007	0.005	0.003	0.01	0.035	0.049	IO
B.L.10.10	X	0.010	0.007	0.005	0.01	0.035	0.049	IO
	Y	0.007	0.005	0.004	0.01	0.035	0.049	IO
C.L.8.7	X	0.008	0.006	0.004	0.01	0.035	0.050	IO
	Y	0.008	0.005	0.004	0.01	0.035	0.050	IO
C.L.8.10	X	0.006	0.004	0.003	0.01	0.035	0.050	IO
	Y	0.009	0.006	0.004	0.01	0.035	0.050	IO
C.L.9.7	X	0.008	0.005	0.004	0.01	0.035	0.050	IO
	Y	0.007	0.005	0.004	0.01	0.035	0.050	IO
C.L.9.10	X	0.006	0.004	0.003	0.01	0.035	0.050	IO
	Y	0.009	0.006	0.005	0.01	0.035	0.050	IO
C.L.10.7	X	0.007	0.005	0.004	0.01	0.035	0.049	IO
	Y	0.008	0.005	0.004	0.01	0.035	0.049	IO
C.L.10.10	X	0.005	0.003	0.003	0.01	0.035	0.049	IO
	Y	0.009	0.006	0.005	0.01	0.035	0.049	IO

Table 4.13 shows all layered shell model slab performance levels according to global acceptance limits defined by ASCE 41-13 (2013). All models perform within immediate occupancy limit for DBE. Type A models show more rotation at target displacement than type B or type C models. Type C models have least rotation angle. All rotations up to MCE level earthquake stay within life safety limit.

Table 4.14: Performance Level of Slab Based on Global Acceptance Limit (Thick Shell)

Model ID	EQ Direction	Plastic Rotation Angle, θ (rad)			Global Acceptance Limit			Performance Level (DBE)
		MCE	DBE	SE	Immediate Occupancy (IO)	Life Safety (LS)	Collapse Prevention (CP)	
A.T.8.7	X	0.014	0.009	0.007	0.01	0.035	0.050	IO
	Y	0.008	0.006	0.004	0.01	0.035	0.050	IO
A.T.8.10	X	0.011	0.007	0.005	0.01	0.035	0.050	IO
	Y	0.010	0.007	0.005	0.01	0.035	0.050	IO
A.T.9.7	X	0.014	0.009	0.007	0.01	0.035	0.050	IO
	Y	0.008	0.006	0.004	0.01	0.035	0.050	IO
A.T.9.10	X	0.010	0.007	0.005	0.01	0.035	0.050	IO
	Y	0.010	0.007	0.005	0.01	0.035	0.050	IO
A.T.10.7	X	0.014	0.009	0.007	0.01	0.035	0.049	IO
	Y	0.008	0.006	0.004	0.01	0.035	0.049	IO
A.T.10.10	X	0.010	0.007	0.005	0.01	0.035	0.049	IO
	Y	0.010	0.007	0.005	0.01	0.035	0.049	IO
B.T.8.7	X	0.013	0.009	0.007	0.01	0.035	0.050	IO
	Y	0.008	0.005	0.004	0.01	0.035	0.050	IO
B.T.8.10	X	0.011	0.007	0.005	0.01	0.035	0.049	IO
	Y	0.009	0.006	0.005	0.01	0.035	0.049	IO
B.T.9.7	X	0.013	0.008	0.006	0.01	0.035	0.050	IO
	Y	0.008	0.005	0.004	0.01	0.035	0.050	IO
B.T.9.10	X	0.011	0.007	0.005	0.01	0.035	0.049	IO
	Y	0.009	0.006	0.004	0.01	0.035	0.049	IO
B.T.10.7	X	0.012	0.008	0.006	0.01	0.035	0.049	IO
	Y	0.008	0.005	0.004	0.01	0.035	0.049	IO
B.T.10.10	X	0.011	0.007	0.005	0.01	0.035	0.049	IO
	Y	0.009	0.006	0.004	0.01	0.035	0.049	IO
C.T.8.7	X	0.011	0.008	0.006	0.01	0.035	0.050	IO
	Y	0.008	0.005	0.004	0.01	0.035	0.050	IO
C.T.8.10	X	0.009	0.006	0.004	0.01	0.035	0.050	IO
	Y	0.009	0.006	0.005	0.01	0.035	0.050	IO
C.T.9.7	X	0.011	0.007	0.005	0.01	0.035	0.050	IO
	Y	0.007	0.005	0.004	0.01	0.035	0.050	IO

Model ID	EQ Direction	Plastic Rotation Angle, θ (rad)			Global Acceptance Limit			Performance Level (DBE)
					Immediate Occupancy (IO)	Life Safety (LS)	Collapse Prevention (CP)	
		MCE	DBE	SE				
C.T.9.10	X	0.008	0.006	0.004	0.01	0.035	0.050	IO
	Y	0.010	0.006	0.005	0.01	0.035	0.050	IO
C.T.10.7	X	0.010	0.007	0.005	0.01	0.035	0.049	IO
	Y	0.007	0.005	0.004	0.01	0.035	0.049	IO
C.T.10.10	X	0.008	0.005	0.004	0.01	0.035	0.049	IO
	Y	0.009	0.006	0.005	0.01	0.035	0.049	IO

Table 4.14 shows all thick shell model slab performance levels according to global acceptance limits defined by ASCE 41-13 (2013). All model performances are seen to be within immediate occupancy limit. Type A models show more rotation at target displacement than type B or type C models. Type C models have least rotation angle among all models. All rotations up to MCE level earthquake stay within life safety limit.

Comparison between Table 4.13 and Table 4.14 demonstrates that layered shell models show less rotation angle and safer performance level than thick shell models. The stiffness of the layered shell models contributes to the lower rotation of the slabs.

4.4.6 Punching Shear

This section discusses the punching shear analysis of layered shell and thick shell models for MCE, DBE and SE level earthquake and compares them with punching shear capacity of slabs. In this study, the top floor level of each model has been selected for the analysis of punching shear.

According to ACI 318-19 (2019), the lowest value obtained from the following three formulas has been considered as the punching shear stress capacity.

$$\Phi v_c = 0.17 \left(1 + \frac{2}{\beta} \right) \lambda \sqrt{f'_c} \quad (4.1)$$

$$\Phi v_c = 0.083 \left(\frac{\alpha_s d}{b_o} + 2 \right) \lambda \sqrt{f'_c} \quad (4.2)$$

$$\Phi v_c = 0.33 \lambda \sqrt{f'_c} \quad (4.3)$$

Where,

Φ_{v_c} = Punching shear stress capacity in MPa

f'_c = Concrete strength in MPa

λ = Lightweight factor, 1 for normal weight concrete

β = Ratio of long side to short side of the column

b_o = Punching perimeter

d = Effective depth of slab

α_s = 40 for interior columns, 30 for edge columns, 20 for corner columns

The punching stress observed in FE models at $d/2$ distance from column perimeter are compared with the stress capacity of slabs to understand the punching shear behavior in this study. Illustration of Model A.L.8.10 and Model A.T.8.10 punching shear pattern from ETABS are shown in Figure 4.22 and Figure 4.23 respectively. Stress observed for three levels of earthquake (MCE, DBE and SE) are shown around the column perimeter.

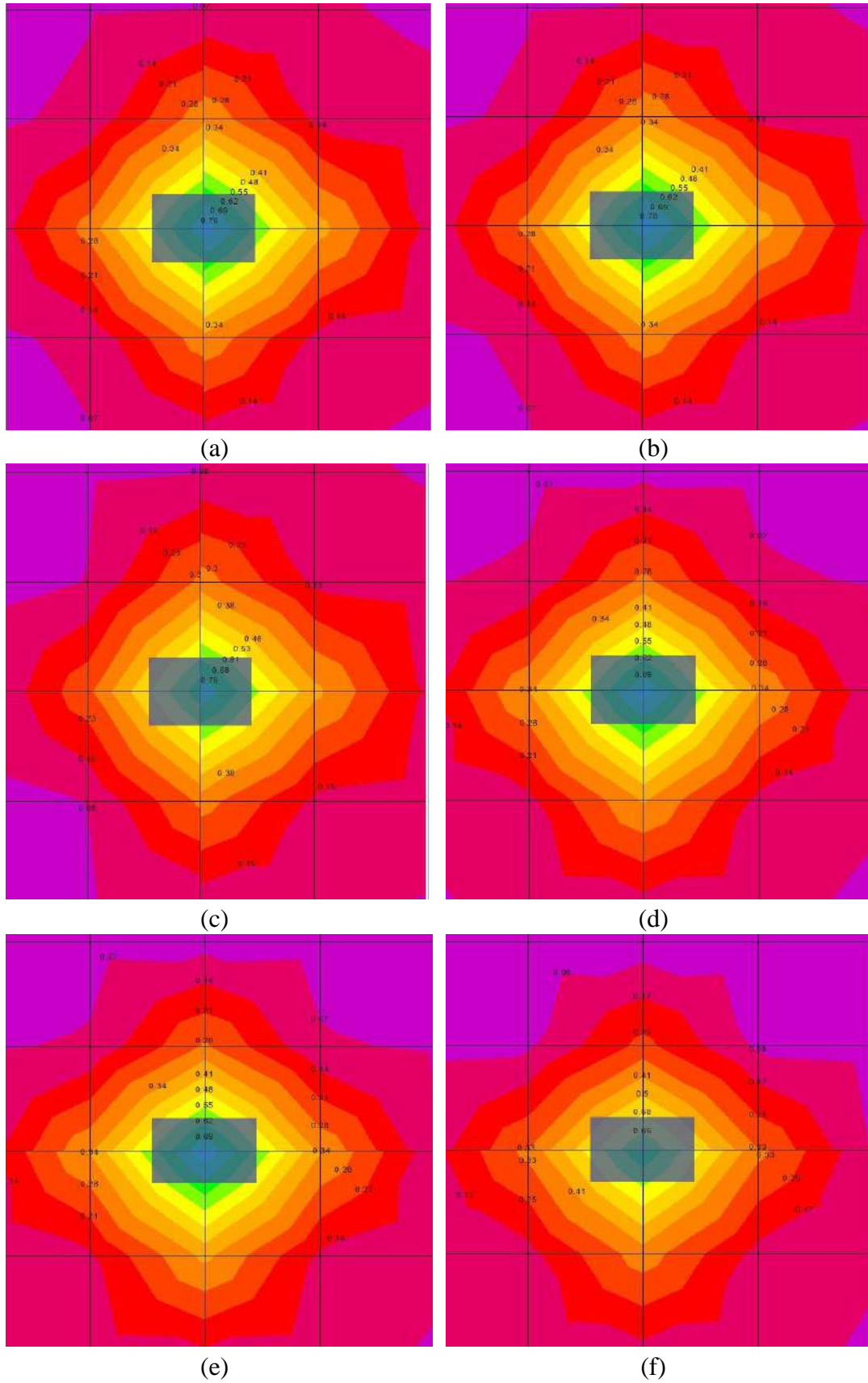


Figure 4.22: Punching Shear Results for Model A.L.8.10 (Layered Shell) (a) SE (X-Direction), (b) DBE (X-Direction), (c) MCE (X-Direction), (d) SE (Y-Direction), (e) DBE (Y-Direction), (f) MCE (Y-Direction)

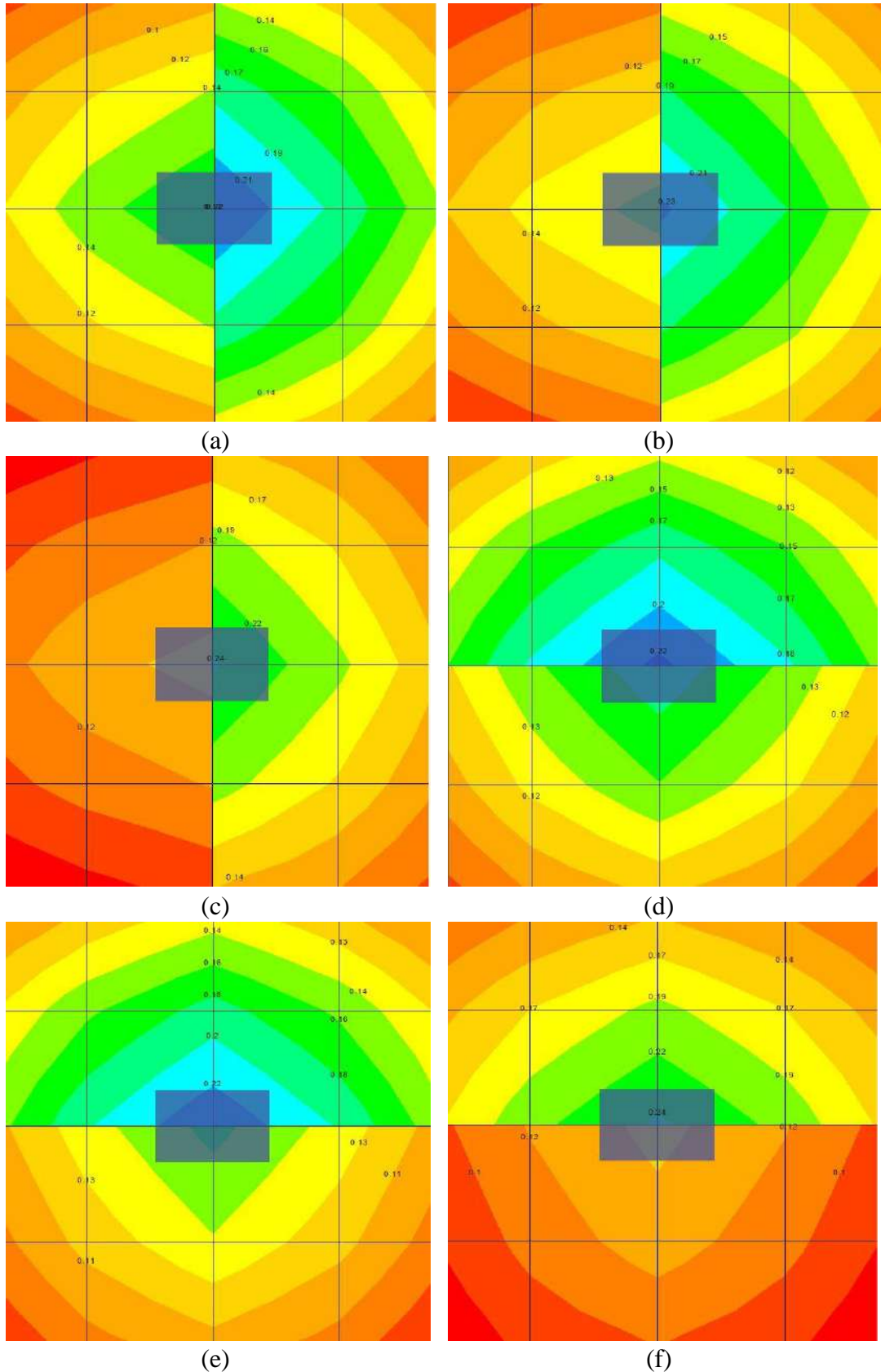


Figure 4.23: Punching Shear Results for Model A.T.8.10 (Thick Shell) (a) SE (X-Direction), (b) DBE (X-Direction), (c) MCE (X-Direction), (d) SE (Y-Direction), (e) DBE (Y-Direction), (f) MCE (Y-Direction)

Figure 4.22 shows the punching shear pattern captured in layered shell models and Figure 4.23 shows the punching shear pattern captured in thick shell models. The overall shear distribution is much higher in layered shell model than in thick shell. Both the layered shell and thick shell models captured higher stress in the considered pushover load direction. The summary results of all models are discussed below.

Table 4.15: Punching Shear for MCE Level Earthquake

Building Height (m)	Layered Shell					Thick Shell					Punching Shear Stress Capacity at d/2 (MPa)
	Model ID	Punching Shear Stress at d/2 (Nonlinear Model) (MPa)		Difference between Capacity and Observed Stress (%)		Model ID	Punching Shear Stress at d/2 (Nonlinear Model) (MPa)		Difference between Capacity and Observed Stress (%)		
		PX	PY	PX	PY		PX	PY	PX	PY	
26.82	A.L.8.7	0.664	0.692	40.75	38.25	A.T.8.7	0.236	0.219	78.93	80.51	1.121
35.97	A.L.8.10	0.643	0.645	37.99	37.76	A.T.8.10	0.228	0.225	77.96	78.34	1.037
26.82	A.L.9.7	0.639	0.656	43.19	41.70	A.T.9.7	0.242	0.227	78.49	79.84	1.126
35.97	A.L.9.10	0.656	0.662	41.68	41.14	A.T.9.10	0.240	0.235	78.72	79.16	1.126
26.82	A.L.10.7	0.615	0.641	45.32	43.06	A.T.10.7	0.249	0.236	77.84	79.07	1.126
35.97	A.L.10.10	0.642	0.656	42.98	41.71	A.T.10.10	0.244	0.242	78.30	78.50	1.126
26.82	B.L.8.7	0.695	0.758	38.02	32.41	B.T.8.7	0.223	0.213	80.09	81.00	1.121
35.97	B.L.8.10	0.670	0.700	33.23	30.28	B.T.8.10	0.231	0.223	76.96	77.81	1.003
26.82	B.L.9.7	0.668	0.665	40.63	40.90	B.T.9.7	0.226	0.229	79.94	79.67	1.126
35.97	B.L.9.10	0.643	0.702	39.24	33.71	B.T.9.10	0.227	0.225	78.57	78.79	1.059
26.82	B.L.10.7	0.650	0.736	42.23	34.56	B.T.10.7	0.255	0.243	77.36	78.44	1.126
35.97	B.L.10.10	0.628	0.598	43.50	46.21	B.T.10.10	0.247	0.245	77.77	77.99	1.111
26.82	C.L.8.7	0.686	0.718	39.02	36.18	C.T.8.7	0.243	0.218	78.43	80.64	1.126
35.97	C.L.8.10	0.674	0.719	37.30	33.16	C.T.8.10	0.231	0.224	78.50	79.15	1.075
26.82	C.L.9.7	0.651	0.649	42.18	42.32	C.T.9.7	0.267	0.224	76.24	80.11	1.126
35.97	C.L.9.10	0.644	0.688	42.83	38.86	C.T.9.10	0.238	0.233	78.85	79.31	1.126
26.82	C.L.10.7	0.621	0.654	44.81	41.92	C.T.10.7	0.254	0.233	77.39	79.32	1.126
35.97	C.L.10.10	0.637	0.675	43.37	40.03	C.T.10.10	0.255	0.245	77.33	78.24	1.126

Table 4.15 shows the punching shear results for Maximum Considered Earthquake (MCE). All type A and type B models have shown punching shear at MCE level. The results obtained from thick shell models show very small punching shear stress. Thick

shell models cannot capture nonlinear behavior of slab; thus, the stresses are below slab punching shear capacity by 76.24-80.64%. The layered shell models can capture material non linearity of concrete slab and due to the realistic multiple material layers, shows much higher stress than thick shell models. Nevertheless, the punching shear stress obtained by layered shell models are all below the slab punching shear stress capacity by 30.28-45.32%. This demonstrates no slab failure in punching shear at maximum considered earthquake level.

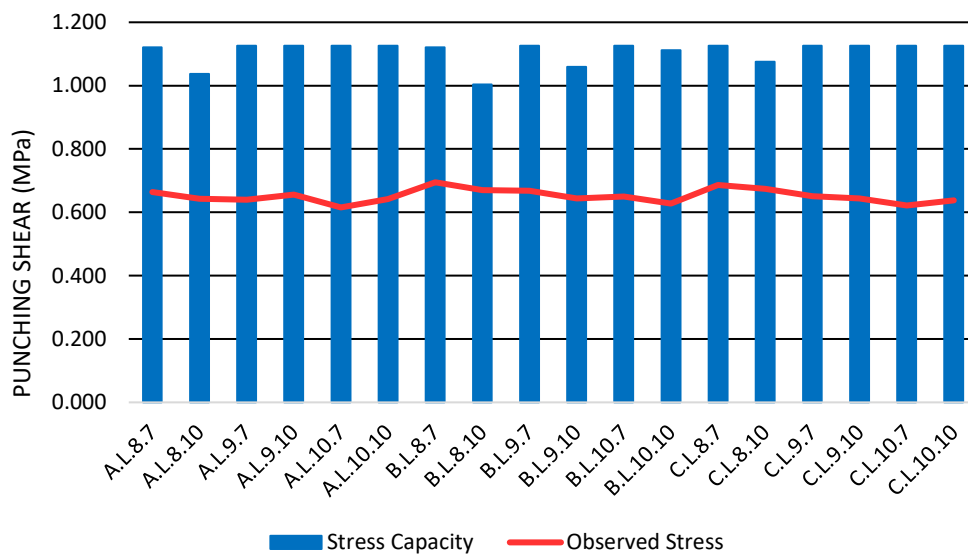


Figure 4.24: Punching Shear at MCE Level for Layered Shell Models (X-Direction)

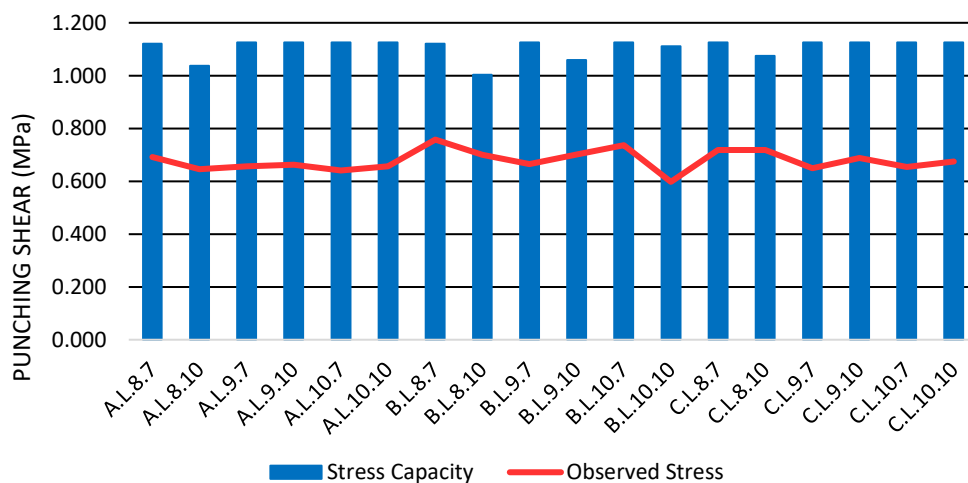


Figure 4.25: Punching Shear at MCE Level for Layered Shell Models (Y-Direction)

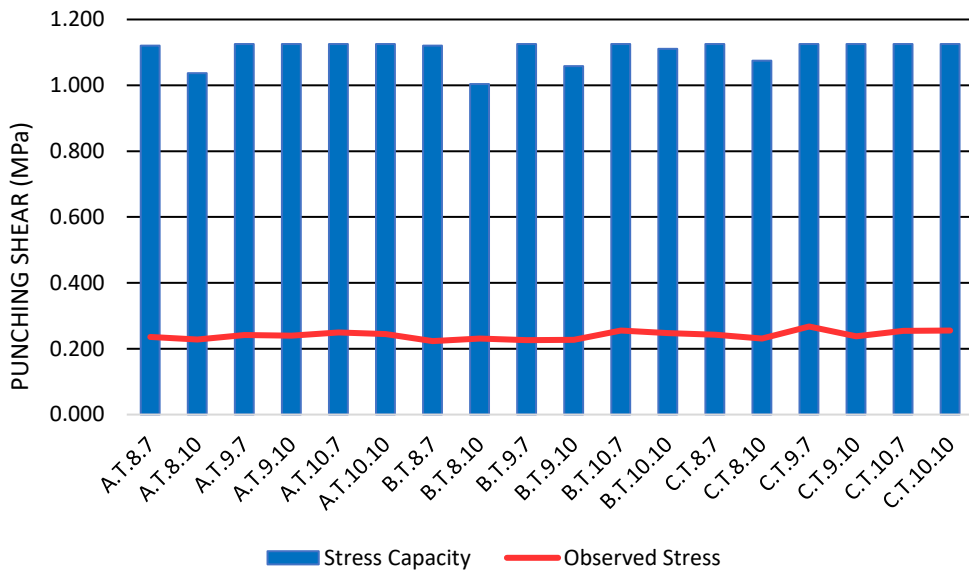


Figure 4.26: Punching Shear at MCE Level for Thick Shell Models (X-Direction)

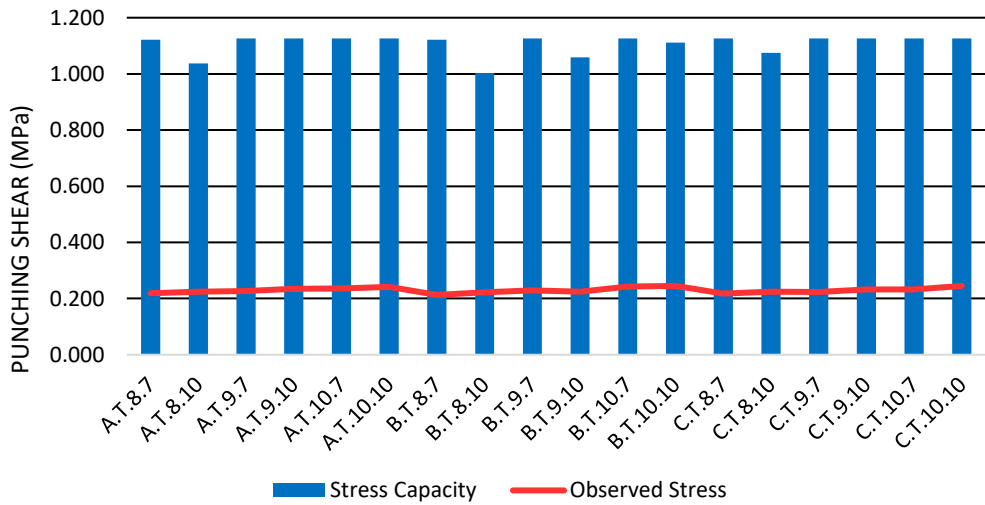


Figure 4.27: Punching Shear at MCE Level for Thick Shell Models (Y-Direction)

Figure 4.24, Figure 4.25, Figure 4.26 and Figure 4.27 shows the comparison of observed stress and punching shear capacity in graphical manner. The results of type B models undergo larger stress compared to capacity than type A or type C models.

Table 4.16: Punching Shear for DBE Level Earthquake

Building Height (m)	Layered Shell					Thick Shell					Punching Shear Stress Capacity at d/2 (MPa)
	Model ID	Punching Shear at d/2 (Nonlinear Model) (MPa)		Difference between Capacity and Observed Stress (%)		Model ID	Punching Shear at d/2 (Nonlinear Model) (MPa)		Difference between Capacity and Observed Stress (%)		
		PX	PY	PX	PY		PX	PY	PX	PY	
26.82	A.L.8.7	0.654	0.685	41.64	38.89	A.T.8.7	0.225	0.208	79.92	81.42	1.121
35.97	A.L.8.10	0.630	0.635	39.20	38.79	A.T.8.10	0.215	0.214	79.29	79.40	1.037
26.82	A.L.9.7	0.636	0.640	43.49	43.17	A.T.9.7	0.224	0.208	80.08	81.50	1.126
35.97	A.L.9.10	0.641	0.645	43.03	42.74	A.T.9.10	0.220	0.217	80.41	80.72	1.126
26.82	A.L.10.7	0.603	0.623	46.42	44.68	A.T.10.7	0.231	0.213	79.47	81.05	1.126
35.97	A.L.10.10	0.624	0.627	44.59	44.29	A.T.10.10	0.228	0.219	79.73	80.50	1.126
26.82	B.L.8.7	0.685	0.731	38.87	34.81	B.T.8.7	0.210	0.206	81.28	81.67	1.121
35.97	B.L.8.10	0.652	0.670	34.99	33.26	B.T.8.10	0.213	0.209	78.77	79.21	1.003
26.82	B.L.9.7	0.657	0.652	41.66	42.09	B.T.9.7	0.215	0.214	80.88	81.01	1.126
35.97	B.L.9.10	0.629	0.676	40.58	36.17	B.T.9.10	0.213	0.210	79.90	80.19	1.059
26.82	B.L.10.7	0.636	0.696	43.50	38.15	B.T.10.7	0.235	0.223	79.14	80.21	1.126
35.97	B.L.10.10	0.606	0.591	45.46	46.82	B.T.10.10	0.223	0.223	79.95	79.95	1.111
26.82	C.L.8.7	0.673	0.685	40.22	39.14	C.T.8.7	0.230	0.204	79.60	81.87	1.126
35.97	C.L.8.10	0.656	0.687	38.97	36.09	C.T.8.10	0.216	0.212	79.89	80.25	1.075
26.82	C.L.9.7	0.640	0.649	43.17	42.32	C.T.9.7	0.239	0.210	78.73	81.31	1.126
35.97	C.L.9.10	0.629	0.658	44.15	41.52	C.T.9.10	0.219	0.220	80.51	80.46	1.126
26.82	C.L.10.7	0.612	0.628	45.66	44.17	C.T.10.7	0.236	0.218	79.07	80.60	1.126
35.97	C.L.10.10	0.624	0.647	44.54	42.49	C.T.10.10	0.228	0.228	79.72	79.77	1.126

Table 4.16 shows the punching shear results for Design Based Earthquake (DBE). Similar to MCE, the results obtained from thick shell models show large difference from the slab punching shear capacity (78.73-81.67%). The punching shear stress observed by layered shell models are 33.26-46.82% lower than the calculated punching shear stress capacity.

Table 4.17: Punching Shear for SE Level Earthquake

Building Height (m)	Layered Shell					Thick Shell					Punching Shear Stress Capacity at d/2 (MPa)
	Model ID	Punching Shear at d/2 (Nonlinear Model) (MPa)		Difference between Capacity and Observed Stress (%)		Model ID	Punching Shear at d/2 (Nonlinear Model) (MPa)		Difference between Capacity and Observed Stress (%)		
		PX	PY	PX	PY		PX	PY	PX	PY	
26.82	A.L.8.7	0.647	0.671	42.30	40.14	A.T.8.7	0.215	0.203	80.80	81.88	1.121
35.97	A.L.8.10	0.579	0.582	44.14	43.85	A.T.8.10	0.209	0.210	79.81	79.73	1.037
26.82	A.L.9.7	0.620	0.631	44.95	43.94	A.T.9.7	0.217	0.198	80.69	82.40	1.126
35.97	A.L.9.10	0.579	0.638	48.51	43.35	A.T.9.10	0.210	0.209	81.31	81.45	1.126
26.82	A.L.10.7	0.598	0.613	46.84	45.58	A.T.10.7	0.218	0.206	80.60	81.68	1.126
35.97	A.L.10.10	0.611	0.618	45.67	45.07	A.T.10.10	0.205	0.209	81.78	81.39	1.126
26.82	B.L.8.7	0.681	0.708	39.28	36.85	B.T.8.7	0.206	0.197	81.66	82.40	1.121
35.97	B.L.8.10	0.644	0.655	35.82	34.70	B.T.8.10	0.205	0.202	79.55	79.85	1.003
26.82	B.L.9.7	0.581	0.642	48.37	42.94	B.T.9.7	0.212	0.205	81.15	81.77	1.126
35.97	B.L.9.10	0.620	0.645	41.45	39.05	B.T.9.10	0.206	0.202	80.58	80.90	1.059
26.82	B.L.10.7	0.628	0.668	44.19	40.68	B.T.10.7	0.221	0.211	80.38	81.25	1.126
35.97	B.L.10.10	0.599	0.573	46.09	48.42	B.T.10.10	0.211	0.209	80.99	81.17	1.111
26.82	C.L.8.7	0.655	0.670	41.82	40.50	C.T.8.7	0.218	0.200	80.67	82.25	1.126
35.97	C.L.8.10	0.649	0.676	39.62	37.09	C.T.8.10	0.209	0.205	80.58	80.90	1.075
26.82	C.L.9.7	0.623	0.640	44.65	43.14	C.T.9.7	0.222	0.201	80.26	82.17	1.126
35.97	C.L.9.10	0.618	0.647	45.12	42.54	C.T.9.10	0.214	0.210	80.98	81.38	1.126
26.82	C.L.10.7	0.603	0.614	46.39	45.40	C.T.10.7	0.219	0.205	80.58	81.81	1.126
35.97	C.L.10.10	0.613	0.637	45.57	43.42	C.T.10.10	0.221	0.212	80.41	81.19	1.126

Table 4.17 shows the punching shear results for Serviceability Earthquake (SE). Similar to MCE and DBE, the results obtained from thick shell models show 79.55-82.40% lower punching shear stress value than capacity of slab to resist punching. The punching shear stress observed by layered shell models are 34.70-48.51% lower than the punching shear capacity of the slabs.

All type A and type B models show displacement for MCE level earthquake only one of the type C layered shell models failed to show displacement for DBE level earthquake.

4.5 Remarks

The structural performance of the selected models has been analyzed through both linear static analysis (LSA) and nonlinear static analysis (NLSA). To validate the models, they have been compared with experimental and other finite element (FE) models. The FE models exhibited slightly higher stiffness than the experimental results, but the variation remained within acceptable limits. Notably, the punching shear stress observed in the layered shell FE models exceeded the capacity of the slabs, indicating strong agreement between the experiment and numerical model.

The results obtained from the linear static analysis of model type A have been presented and discussed in this study. The thick shell model displayed more displacement than the layered shell model, which can be attributed to the higher stiffness seen in the layered shell slabs due to considering distinct stiffness properties of each layer. Additionally, the favorable orientation of shear walls in the Y-direction contributed to the higher stiffness and lower displacement in Y-direction.

A comparison of the nonlinear behavior of model types A, B and C has been provided, considering parameters like the number of stories, slab thickness, and slab shell type. Most of the hinges formed were within the limits of immediate occupancy and life safety levels, with none falling beyond collapse prevention level. However, the increase in the number of stories led to poorer seismic performance, as number of total hinges formed in the LS-CP range and beyond CP range increases. Nonlinear static analysis revealed that layered shell models exhibited higher base shear capacity, indicating better seismic resistance. Layered shell models produced smoother capacity curves than thick shell models due to their nonlinear material properties and interconnected layers with distinct material properties and thickness. The global acceptance limit for slab performance confirmed that layered shell slabs exhibited lower plastic rotation and safer performance than thick shell slabs. The punching shear stress capacity of the slabs calculated using the prescribed code formula was much higher than the observed stress in various earthquake levels for both layered and thick shell models. Layered shell models provided a more realistic representation of the calculated stress compared to thick shell slabs.

Based on the findings, it can be concluded that although layered shell elements exhibit higher stiffness, the punching shear stress obtained from layered shells provides a more realistic representation for flat plate structures.

Chapter 5

CONCLUSIONS AND RECOMMENDATIONS

5.1 Conclusions

The performance of dual system flat plate structure with shear walls has been analyzed in this study for seismic loading. Two types of shell elements have been used here to model the slab - layered shell and thick shell. Upon performing linear static analysis in ETABS, nonlinear behaviors of the structures have been assessed by nonlinear static (pushover) analysis.

The present study aims to give an insight to a preferable analytical modelling technique for seismic design using layered shell element. The major findings and conclusions of the research are summarized below:

- i. From linear static analysis it can be seen that maximum top displacement is higher in thick shell models than layered shell ones. Similar trend holds for story drift. This is pertinent to the layered shell models higher stiffness than thick shell models.
- ii. From linear static analysis it can be seen that story shear at base is slightly higher in thick shell models than layered shell ones, which contradicts the smaller displacement seen in layered shell models. But nonlinear static analysis based on ASCE 41-13 overturns the findings of LSA – layered shell models exhibit higher base shear capacity indicating better seismic resistance.
- iii. Structures are stiffer along the direction of the shear walls, as such have a larger base shear capacity and smaller deflections in that direction.
- iv. Increasing number of stories lead to poor seismic performance, as number of total hinges formed in the LS-CP range and beyond CP range increases.
- v. The layered shell models produce smoother capacity curve than thick shell models. The nonlinear material properties and series of interconnected layers with their own material properties and thickness in layered shell slabs are capable of demonstrating more realistic response of strength degradation of the structures while subjected to increasing lateral forces.
- vi. Global acceptance limit for slab performance confirms layered shell slabs exhibit lower plastic rotation and safer performance than thick shell slabs.

- vii. The punching shear stress capacity of the slabs calculated using code prescribed formula is much higher than the observed stress in MCE, DBE and SE level earthquake in both layered and thick shell models. Layered shell models show more realistic representation of the stress calculated than thick shell slab.

Overall, the above findings contribute to a better understanding of the behavior of thick and layered shell structures under seismic loading conditions and can inform future design and construction practices. By using layered shell element punching shear behavior may be modelled in seismic analysis of flat plate structures.

5.2 Recommendations for Future Study

There is plenty of room for research following this study. Some recommendations for future study are presented below:

- i. Comprehensive study could be performed taking into account the effect of soft stories.
- ii. Since the buildings under consideration had no vertical or plan irregularities, how such irregularities may affect the seismic performance of buildings need to be studied.
- iii. Performance of flat plate shear wall structural systems should be assessed placing shear walls along both directions.
- iv. The effect of foundation flexibility or soil structure interaction can be incorporated in future study for determining more realistic structural performance.
- v. Only thick shell models have been compared with layered shell slabs to compare seismic performance. Thin shell models may also be included for comparison.
- vi. Experimental study could be conducted alongside software modelling to compare the results.

REFERENCES

- ACI 318-19. (2019). *Building Code Requirements for Structural Concrete and Commentary*, American Concrete Institute, Farmington Hills, MI.
- ASCE 41-13. (2013). *Seismic Evaluation and Retrofit of Existing Buildings*, American Society of Civil Engineers, Reston, Virginia, USA.
- ASCE 41-17. (2017). *Seismic Evaluation and Retrofit of Existing Buildings*, American Society of Civil Engineers, Reston, Virginia, USA.
- Agrahari, S. (2019). *Nonlinear Finite Element Analysis of Punching Shear Behavior of Flat Slabs*, Master's Thesis, International Institute of Information Technology, Hyderabad, India.
- Alam, M. N. (2018). *Evaluation of Response Modification Factor for Shear wall-Flat plate Structural Systems*, M.Engg Thesis, Bangladesh University of Engineering and Technology, Dhaka, Bangladesh.
- ATC 40. (1996). *Seismic Evaluation and Retrofit of Concrete Buildings*, Applied Technology Council, Seismic Safety Commission, Redwood City, California.
- Bazant, Z. P., and Cao, Z. (1987). Size Effect in Punching Shear Failure of Slabs. *ACI Structural Journal*, 84(1), 44–53.
- BNBC. (2020). *Bangladesh National Building Code*. Housing and Building Research Institute.
- Coronelli, A. M. D., Tornaghi, M. L., and Pascu, L. M. I. R. (2022). Deformation Capacity Evaluation For Flat Slab Seismic Design. *Bulletin of Earthquake Engineering*, 20(3), 1619–1654.
- CSI (2016). *CSI Analysis Reference Manual*, Computers & Structures, Inc, USA.
- CSI (2023). *Shell Element Internal Forces Stresses Output Convention*, Computers and Structures, Inc. https://docs.csiamerica.com/help-files/csibridge/Output_Conventions/Shell_Element_Internal_Forces_Stresses_Output_Convention.htm [Last accessed on 11 May 2023].
- Drakatos, I., Muttoni, A., and Beyer, K. (2018). Mechanical Model for Drift-Induced Punching of Slab- Column Connections without Transverse Reinforcement. *ACI Structural Journal*, 115(2), 463–474.
- Elfgren, L. and Shah, S. P. (Eds.). (2005). *Analysis of Concrete Structures by Fracture Mechanics*. In *Proceedings of the International RILEM Workshop*. Chapman and Hall.
- Elstner, R. C., and Hognestad, E. (1956). *Shearing Strength of Reinforced Concrete Slabs*. *ACI Structural Journal*, 28(1), 29-58.
- Elwood , K. J. , Matamoros , A. B. , Wallace , J. W. , Lehman , D. E., H., J. A. , Mitchell , A. D. , Moore , M. A. , Valley , M. T. , Lowes , L. N., C., and C. D., and Moehle, J. P. (2007). *Earthquake Spectra*, 23(3), 493–523.
- FEMA 273. (1997). *NEHRP Guidelines For The Seismic Rehabilitation Of Buildings*, Federal Emergency Management Agency, Washington D.C.
- FEMA 355F. (2000). *State of the Art Report on Performance Prediction and Evaluation of Steel Moment-Frame Buildings*, Federal Emergency Management Agency, Washington, D.C.
- FEMA 356. (2000). *Prestandard and Commentary for the Seismic Rehabilitation of Buildings*,

- Federal Emergency Management Agency, Washington, D.C.
- FEMA 440. (2005). *Improvement of Nonlinear Static Seismic Analysis Procedures*, Federal Emergency Management Agency, Washington, D.C.
- Gardner, N. J. (1990). Relationship of the Punching Shear Capacity of Reinforced Concrete Slabs With Concrete Strength. *ACI Structural Journal*, 87(1), 66–71.
- Hand, F.R., Pecknold, D.V. and Schnobrich, W. C. (1973). Nonlinear Layered Analysis of RC Plates and Shells. *Journal of the Structural Division*, 99(7), 1491–1505.
- Hillerborg, A. (1956). Jämviksteori för armerade betongplattor (Equilibrium theory for concrete slabs). *Betong (Stockholm)*, 41(4), 171-182.
- Ismail, E.-S. I. M. (2018). Non-Linear Finite Element Analysis of Reinforced Concrete Flat Plates with Opening Adjacent to Column Under Eccentric Punching Loads. *HBRC Journal*, 14(3), 438–449.
- Islam, M. R. (2014). *Numerical Modelling of Slab-Column Joint of RC Flat Plates*, M.Sc. Thesis, Bangladesh University of Engineering and Technology.
- Issa, A. M., Salem, M. M., Mostafa, M. T., Hadhoud, H. M., and Ghith, H. H. (2019). Performance of Shear Reinforcement against Punching Shear Loads. *International Journal of Engineering and Advanced Technology*, 9(2), 841–850.
- Jafarian, N., and Raji, A. (2022). *Effect of Gravity Shear Ratio on Governing Failure Mode of Reinforced Concrete Slab-Column Connections*. 1–33.
- Kang, T. H.-K., and Wallace, J. W. (2006). Punching of Reinforced and Posttensioned Concrete Slab-Column Connections. *ACI Structural Journal*, 104(4), 531 – 540.
- Khan, W. R. (2018). *Assessment of Inelastic Performance of Flat Plate and Wide Beam Frames*, M.Engg Thesis, Bangladesh University of Engineering and Technology.
- Kim, J., Kim, T., and Choi, H. (2008). Performance Evaluation of Non-Seismic Designed Flat-Plate Structures. *ASCE Journal of Performance of Constructed Facilities*, 22(6), 356–363. https://doi.org/10.1061/_ASCE_0887-3828_2008_22:6_356
- Loo, Y. C., and Guan, H. (1997). Cracking and Punching Shear Failure Analysis of RC Flat Plates. *ASCE Journal of Structural Engineering*, 123(10), 1321–1330.
- Mahmoud, A. M. (2015). Finite Element Implementation of Punching Shear Behaviors in Shear-Reinforced Flat Slabs. *Ain Shams Engineering Journal*, 6(3), 735–754.
- Mahmud-Ul-Hasan, A. K. M. (2019). *Seismic Analysis of Cast-In-Situ Concrete Diaphragm With Opening Adjacent to Shear Wall in Wall-Frame Structural System*. [M.Sc. Thesis, Bangladesh University of Engineering and Technology]. BUET Institutional Repository.
- Mazhar, H., Najam, F. A., Ahmed, L., and Akram, H. Z. (2016). *Nonlinear Modeling and Analysis of RC Buildings using ETABS (version 2016 and onwards)*.
- NCEI Hazard Earthquake Search. (n.d.). <https://www.ngdc.noaa.gov/hazel/view/hazards/earthquake/search> [Last accessed on December 16, 2022]
- Nikolic-brzev, S., and Stojadinovic, B. (1999). Performance-Based Seismic Evaluation of Concrete Flat Slab Structures. *8th Canadian Conference on Earthquake Engineering*, 1999, 433–438.
- Nilson, Arthur H., Darwin, David, and Dolan, C. W. (2009). *Design of Concrete Structures* (14th edition), McGraw-Hill Book Co., Singapore.

- Polak, M. A. (1998). Modeling Punching Shear of Reinforced Concrete Slabs using Layered Finite Elements. *ACI Structural Journal*, 95(1), 71–80.
- Song, J. W., Song, J. G., Lee, Y. W., and Kim, G. W. (2012). Seismic Performance Of Flat Plate System with Shear Reinforcements. *The 15th World Conference on Earthquake Engineering, Lisboa*.
- T. J. Hughes. (2000). *The Finite Element Method: Linear Static and Dynamic Finite Element Analysis*.
- Taranath, B. S. (2004). *Wind and Earthquake Resistant Buildings*, CRC Press: Taylor & Francis Group, New York, USA.
- Wang, W., and Teng, S. (2008). Finite-Element Analysis of Reinforced Concrete Flat Plate Structures by Layered Shell Element. *Journal of Structural Engineering*, 134(12), 1862–1872.
- Zameeruddin, M., and Sangle, K. K. (2016). Review on Recent Developments in the Performance-Based Seismic Design of Reinforced Concrete Structures. *Istruc*, 6, 119–133.

APPENDIX A

MODEL DETAILS

A.1 Reinforcement Details

The reinforcement details of slab, beam, column and shear walls are presented here.

Table A.1.1 shows reinforcement details of slabs for all models.

Table A.1.1: Reinforcement Details of Slab

Model ID	Slab Thickness	Position	Reinforcement Detail
A.L.8.7	8 inch	All floors	16mm bar@5" c/c
A.L.8.10	8 inch	All floors	16mm bar@5" c/c
A.L.9.7	9 inch	All floors	16mm bar@5" c/c
A.L.9.10	9 inch	All floors	16mm bar@5" c/c
A.L.10.7	10 inch	All floors	16mm bar@5" c/c
A.L.10.10	10 inch	All floors	16mm bar@5" c/c
B.L.8.7	8 inch	All floors	16mm bar@6" c/c
B.L.8.10	8 inch	All floors	16mm bar@5" c/c
B.L.9.7	9 inch	All floors	16mm bar@6" c/c
B.L.9.10	9 inch	All floors	16mm bar@5" c/c
B.L.10.7	10 inch	All floors	16mm bar@7" c/c
B.L.10.10	10 inch	All floors	16mm bar@5" c/c
C.L.8.7	8 inch	All floors	16mm bar@5" c/c
C.L.8.10	8 inch	All floors	16mm bar@5" c/c
C.L.9.7	9 inch	All floors	16mm bar@5" c/c
C.L.9.10	9 inch	All floors	16mm bar@5" c/c
C.L.10.7	10 inch	All floors	16mm bar@5" c/c
C.L.10.10	10 inch	All floors	16mm bar@5" c/c
A.T.8.7	8 inch	All floors	16mm bar@5" c/c
A.T.8.10	8 inch	All floors	16mm bar@5" c/c
A.T.9.7	9 inch	All floors	16mm bar@5" c/c
A.T.9.10	9 inch	All floors	16mm bar@5" c/c
A.T.10.7	10 inch	All floors	16mm bar@5" c/c
A.T.10.10	10 inch	All floors	16mm bar@5" c/c
B.T.8.7	8 inch	All floors	16mm bar@6" c/c
B.T.8.10	8 inch	All floors	16mm bar@5" c/c
B.T.9.7	9 inch	All floors	16mm bar@6" c/c
B.T.9.10	9 inch	All floors	16mm bar@5" c/c
B.T.10.7	10 inch	All floors	16mm bar@7" c/c
B.T.10.10	10 inch	All floors	16mm bar@5" c/c
C.T.8.7	8 inch	All floors	16mm bar@5" c/c
C.T.8.10	8 inch	All floors	16mm bar@5" c/c
C.T.9.7	9 inch	All floors	16mm bar@5" c/c
C.T.9.10	9 inch	All floors	16mm bar@5" c/c
C.T.10.7	10 inch	All floors	16mm bar@5" c/c
C.T.10.10	10 inch	All floors	16mm bar@5" c/c

Table A.1.2 shows reinforcement details of beams for all models.

Table A.1.2: Reinforcement Details of Beam

Model ID	Beam Type	Size	Position	Reinforcement Detail
A.L.8.7	Grade Beam (GB)	12x15 in	BGB	Main bar : 8-16 mm bar Stirrup : 10 mm @ 10" c/c
	Floor Beam (FB)	12X18 in	All floors	Longitudinal bar : 8-16 mm bar Stirrup : 10 mm @ 10" c/c
A.L.8.10	Grade Beam (GB)	12x15 in	BGB	Main bar : 8-16 mm bar Stirrup : 10 mm @ 10" c/c
	Floor Beam (FB)	12X18 in	All floors	Longitudinal bar : 8-16 mm bar Stirrup : 10 mm @ 10" c/c
A.L.9.7	Grade Beam (GB)	12x15 in	BGB	Main bar : 8-16 mm bar Stirrup : 10 mm @ 10" c/c
	Floor Beam (FB)	12X18 in	All floors	Longitudinal bar : 8-16 mm bar Stirrup : 10 mm @ 10" c/c
A.L.9.10	Grade Beam (GB)	12x15 in	BGB	Main bar : 8-16 mm bar Stirrup : 10 mm @ 10" c/c
	Floor Beam (FB)	12X18 in	All floors	Longitudinal bar : 8-16 mm bar Stirrup : 10 mm @ 10" c/c
A.L.10.7	Grade Beam (GB)	12x15 in	BGB	Main bar : 8-16 mm bar Stirrup : 10 mm @ 10" c/c
	Floor Beam (FB)	12X18 in	All floors	Longitudinal bar : 8-16 mm bar Stirrup : 10 mm @ 10" c/c
A.L.10.10	Grade Beam (GB)	12x15 in	BGB	Main bar : 8-16 mm bar Stirrup : 10 mm @ 10" c/c
	Floor Beam (FB)	12X18 in	All floors	Longitudinal bar : 8-16 mm bar Stirrup : 10 mm @ 10" c/c
B.L.8.7	Grade Beam (GB)	12x15 in	BGB	Main bar : 8-16 mm bar Stirrup : 10 mm @ 10" c/c
	Floor Beam (FB)	12X18 in	All floors	Longitudinal bar : 8-16 mm bar Stirrup : 10 mm @ 10" c/c
B.L.8.10	Grade Beam (GB)	12x15 in	BGB	Main bar : 8-16 mm bar Stirrup : 10 mm @ 10" c/c
	Floor Beam (FB)	12X18 in	All floors	Longitudinal bar : 8-16 mm bar Stirrup : 10 mm @ 10" c/c
B.L.9.7	Grade Beam (GB)	12x15 in	BGB	Main bar : 8-16 mm bar Stirrup : 10 mm @ 10" c/c
	Floor Beam (FB)	12X18 in	All floors	Longitudinal bar : 8-16 mm bar Stirrup : 10 mm @ 10" c/c
B.L.9.10	Grade Beam (GB)	12x15 in	BGB	Main bar : 8-16 mm bar Stirrup : 10 mm @ 10" c/c
	Floor Beam (FB)	12X18 in	All floors	Longitudinal bar : 8-16 mm bar Stirrup : 10 mm @ 10" c/c

Model ID	Beam Type	Size	Position	Reinforcement Detail
B.L.10.7	Grade Beam (GB)	12x15 in	BGB	Main bar : 8-16 mm bar Stirrup : 10 mm @ 10" c/c
	Floor Beam (FB)	12X18 in	All floors	Longitudinal bar : 8-16 mm bar Stirrup : 10 mm @ 10" c/c
B.L.10.10	Grade Beam (GB)	12x15 in	BGB	Main bar : 8-16 mm bar Stirrup : 10 mm @ 10" c/c
	Floor Beam (FB)	12X18 in	All floors	Longitudinal bar : 8-16 mm bar Stirrup : 10 mm @ 10" c/c
C.L.8.7	Grade Beam (GB)	12x15 in	BGB	Main bar : 8-16 mm bar Stirrup : 10 mm @ 10" c/c
	Floor Beam (FB)	12X18 in	All floors	Longitudinal bar : 8-16 mm bar Stirrup : 10 mm @ 10" c/c
C.L.8.10	Grade Beam (GB)	12x15 in	BGB	Main bar : 8-16 mm bar Stirrup : 10 mm @ 10" c/c
	Floor Beam (FB)	12X18 in	All floors	Longitudinal bar : 8-16 mm bar Stirrup : 10 mm @ 10" c/c
C.L.9.7	Grade Beam (GB)	12x15 in	BGB	Main bar : 8-16 mm bar Stirrup : 10 mm @ 10" c/c
	Floor Beam (FB)	12X18 in	All floors	Longitudinal bar : 8-16 mm bar Stirrup : 10 mm @ 10" c/c
C.L.9.10	Grade Beam (GB)	12x15 in	BGB	Main bar : 8-16 mm bar Stirrup : 10 mm @ 10" c/c
	Floor Beam (FB)	12X18 in	All floors	Longitudinal bar : 8-16 mm bar Stirrup : 10 mm @ 10" c/c
C.L.10.7	Grade Beam (GB)	12x15 in	BGB	Main bar : 8-16 mm bar Stirrup : 10 mm @ 10" c/c
	Floor Beam (FB)	12X18 in	All floors	Longitudinal bar : 8-16 mm bar Stirrup : 10 mm @ 10" c/c
C.L.10.10	Grade Beam (GB)	12x15 in	BGB	Main bar : 8-16 mm bar Stirrup : 10 mm @ 10" c/c
	Floor Beam (FB)	12X18 in	All floors	Longitudinal bar : 8-16 mm bar Stirrup : 10 mm @ 10" c/c
A.T.8.7	Grade Beam (GB)	12x15 in	BGB	Main bar : 8-16 mm bar Stirrup : 10 mm @ 10" c/c
	Floor Beam (FB)	12X18 in	All floors	Longitudinal bar : 8-16 mm bar Stirrup : 10 mm @ 10" c/c
A.T.8.10	Grade Beam (GB)	12x15 in	BGB	Main bar : 8-16 mm bar Stirrup : 10 mm @ 10" c/c
	Floor Beam (FB)	12X18 in	All floors	Longitudinal bar : 8-16 mm bar Stirrup : 10 mm @ 10" c/c
A.T.9.7	Grade Beam (GB)	12x15 in	BGB	Main bar : 8-16 mm bar Stirrup : 10 mm @ 10" c/c
	Floor Beam (FB)	12X18 in	All floors	Longitudinal bar : 8-16 mm bar Stirrup : 10 mm @ 10" c/c

Model ID	Beam Type	Size	Position	Reinforcement Detail
A.T.9.10	Grade Beam (GB)	12x15 in	BGB	Main bar : 8-16 mm bar Stirrup : 10 mm @ 10" c/c
	Floor Beam (FB)	12X18 in	All floors	Longitudinal bar : 8-16 mm bar Stirrup : 10 mm @ 10" c/c
A.T.10.7	Grade Beam (GB)	12x15 in	BGB	Main bar : 8-16 mm bar Stirrup : 10 mm @ 10" c/c
	Floor Beam (FB)	12X18 in	All floors	Longitudinal bar : 8-16 mm bar Stirrup : 10 mm @ 10" c/c
A.T.10.10	Grade Beam (GB)	12x15 in	BGB	Main bar : 8-16 mm bar Stirrup : 10 mm @ 10" c/c
	Floor Beam (FB)	12X18 in	All floors	Longitudinal bar : 8-16 mm bar Stirrup : 10 mm @ 10" c/c
B.T.8.7	Grade Beam (GB)	12x15 in	BGB	Main bar : 8-16 mm bar Stirrup : 10 mm @ 10" c/c
	Floor Beam (FB)	12X18 in	All floors	Longitudinal bar : 8-16 mm bar Stirrup : 10 mm @ 10" c/c
B.T.8.10	Grade Beam (GB)	12x15 in	BGB	Main bar : 8-16 mm bar Stirrup : 10 mm @ 10" c/c
	Floor Beam (FB)	12X18 in	All floors	Longitudinal bar : 8-16 mm bar Stirrup : 10 mm @ 10" c/c
B.T.9.7	Grade Beam (GB)	12x15 in	BGB	Main bar : 8-16 mm bar Stirrup : 10 mm @ 10" c/c
	Floor Beam (FB)	12X18 in	All floors	Longitudinal bar : 8-16 mm bar Stirrup : 10 mm @ 10" c/c
B.T.9.10	Grade Beam (GB)	12x15 in	BGB	Main bar : 8-16 mm bar Stirrup : 10 mm @ 10" c/c
	Floor Beam (FB)	12X18 in	All floors	Longitudinal bar : 8-16 mm bar Stirrup : 10 mm @ 10" c/c
B.T.10.7	Grade Beam (GB)	12x15 in	BGB	Main bar : 8-16 mm bar Stirrup : 10 mm @ 10" c/c
	Floor Beam (FB)	12X18 in	All floors	Longitudinal bar : 8-16 mm bar Stirrup : 10 mm @ 10" c/c
B.T.10.10	Grade Beam (GB)	12x15 in	BGB	Main bar : 8-16 mm bar Stirrup : 10 mm @ 10" c/c
	Floor Beam (FB)	12X18 in	All floors	Longitudinal bar : 8-16 mm bar Stirrup : 10 mm @ 10" c/c
C.T.8.7	Grade Beam (GB)	12x15 in	BGB	Main bar : 8-16 mm bar Stirrup : 10 mm @ 10" c/c
	Floor Beam (FB)	12X18 in	All floors	Longitudinal bar : 8-16 mm bar Stirrup : 10 mm @ 10" c/c
C.T.8.10	Grade Beam (GB)	12x15 in	BGB	Main bar : 8-16 mm bar Stirrup : 10 mm @ 10" c/c
	Floor Beam (FB)	12X18 in	All floors	Longitudinal bar : 8-16 mm bar Stirrup : 10 mm @ 10" c/c

Model ID	Beam Type	Size	Position	Reinforcement Detail
C.T.9.7	Grade Beam (GB)	12x15 in	BGB	Main bar : 8-16 mm bar Stirrup : 10 mm @ 10" c/c
	Floor Beam (FB)	12X18 in	All floors	Longitudinal bar : 8-16 mm bar Stirrup : 10 mm @ 10" c/c
C.T.9.10	Grade Beam (GB)	12x15 in	BGB	Main bar : 8-16 mm bar Stirrup : 10 mm @ 10" c/c
	Floor Beam (FB)	12X18 in	All floors	Longitudinal bar : 8-16 mm bar Stirrup : 10 mm @ 10" c/c
C.T.10.7	Grade Beam (GB)	12x15 in	BGB	Main bar : 8-16 mm bar Stirrup : 10 mm @ 10" c/c
	Floor Beam (FB)	12X18 in	All floors	Longitudinal bar : 8-16 mm bar Stirrup : 10 mm @ 10" c/c
C.T.10.10	Grade Beam (GB)	12x15 in	BGB	Main bar : 8-16 mm bar Stirrup : 10 mm @ 10" c/c
	Floor Beam (FB)	12X18 in	All floors	Longitudinal bar : 8-16 mm bar Stirrup : 10 mm @ 10" c/c

Table A.1.3 demonstrates reinforcement details of beams for all models.

Table A.1.3: Reinforcement Details of Column

Model ID	Column Type	Size	Position	Reinforcement Detail
A.L.8.7	Column (C1)	24x30 in	Plinth level to roof	Longitudinal bar : 20-25 mm bar Stirrup : 10 mm @ 6" c/c
A.L.8.10	Column (C1)	28x38 in	Plinth level to roof	Longitudinal bar : 24-28 mm bar Stirrup : 10 mm @ 6" c/c
A.L.9.7	Column (C1)	24x30 in	Plinth level to roof	Longitudinal bar : 24-25 mm bar Stirrup : 10 mm @ 6" c/c
A.L.9.10	Column (C1)	24x36 in	Plinth level to 3rd floor	Longitudinal bar : 24-28 mm bar Stirrup : 10 mm @ 6" c/c
	Column (C2)	21x 33 in	4th floor to roof	Longitudinal bar : 14-28 mm bar Stirrup : 10 mm @ 6" c/c
A.L.10.7	Column (C1)	24x30 in	Plinth level to 3rd floor	Longitudinal bar : 24-25 mm bar Stirrup : 10 mm @ 6" c/c
A.L.10.10	Column (C1)	24x36 in	Plinth level to 4th floor	Longitudinal bar : 24-28 mm bar Stirrup : 10 mm @ 6" c/c
	Column (C2)	21x 33 in	5th floor to roof	Longitudinal bar : 14-28 mm bar Stirrup : 10 mm @ 6" c/c
B.L.8.7	Column (C1)	24x30 in	Plinth level to roof	Longitudinal bar : 20-25 mm bar Stirrup : 10 mm @ 6" c/c
B.L.8.10	Column (C1)	34x44 in	Plinth level to 4th floor	Longitudinal bar : 28-28 mm bar Stirrup : 10 mm @ 6" c/c
	Column (C2)	31x41 in	5th floor to roof	Longitudinal bar : 24-28 mm bar Stirrup : 10 mm @ 6" c/c

Model ID	Column Type	Size	Position	Reinforcement Detail
B.L.9.7	Column (C1)	24x30 in	Plinth level to roof	Longitudinal bar : 20-25 mm bar Stirrup : 10 mm @ 6" c/c
B.L.9.10	Column (C1)	34x44 in	Plinth level to 4th floor	Longitudinal bar : 28-28 mm bar Stirrup : 10 mm @ 6" c/c
	Column (C2)	31x41 in	5th floor to roof	Longitudinal bar : 24-28 mm bar Stirrup : 10 mm @ 6" c/c
B.L.10.7	Column (C1)	24x36 in	Plinth level to roof	Longitudinal bar : 24-28 mm bar Stirrup : 10 mm @ 6" c/c
B.L.10.10	Column (C1)	34x44 in	Plinth level to 3rd floor	Longitudinal bar : 28-28 mm bar Stirrup : 10 mm @ 6" c/c
	Column (C2)	31x41 in	4th floor to roof	Longitudinal bar : 24-28 mm bar Stirrup : 10 mm @ 6" c/c
C.L.8.7	Column (C1)	24x28 in	Plinth level to roof	Longitudinal bar : 24-25 mm bar Stirrup : 10 mm @ 6" c/c
C.L.8.10	Column (C1)	24x36 in	Plinth level to roof	Longitudinal bar : 24-28 mm bar Stirrup : 10 mm @ 6" c/c
C.L.9.7	Column (C1)	24x28 in	Plinth level to roof	Longitudinal bar : 24-25 mm bar Stirrup : 10 mm @ 6" c/c
C.L.9.10	Column (C1)	24x36 in	Plinth level to roof	Longitudinal bar : 24-28 mm bar Stirrup : 10 mm @ 6" c/c
C.L.10.7	Column (C1)	24x28 in	Plinth level to roof	Longitudinal bar : 24-25 mm bar Stirrup : 10 mm @ 6" c/c
C.L.10.10	Column (C1)	24x36 in	Plinth level to 4th floor	Longitudinal bar : 24-28 mm bar Stirrup : 10 mm @ 6" c/c
	Column (C2)	21x 33 in	5th floor to roof	Longitudinal bar : 14-28 mm bar Stirrup : 10 mm @ 6" c/c
A.T.8.7	Column (C1)	24x30 in	Plinth level to roof	Longitudinal bar : 20-25 mm bar Stirrup : 10 mm @ 6" c/c
A.T.8.10	Column (C1)	28x38 in	Plinth level to roof	Longitudinal bar : 24-28 mm bar Stirrup : 10 mm @ 6" c/c
A.T.9.7	Column (C1)	24x30 in	Plinth level to roof	Longitudinal bar : 24-25 mm bar Stirrup : 10 mm @ 6" c/c
A.T.9.10	Column (C1)	24x36 in	Plinth level to 3rd floor	Longitudinal bar : 24-28 mm bar Stirrup : 10 mm @ 6" c/c
	Column (C2)	21x 33 in	4th floor to roof	Longitudinal bar : 14-28 mm bar Stirrup : 10 mm @ 6" c/c
A.T.10.7	Column (C1)	24x30 in	Plinth level to 3rd floor	Longitudinal bar : 24-25 mm bar Stirrup : 10 mm @ 6" c/c
A.T.10.10	Column (C1)	24x36 in	Plinth level to 4th floor	Longitudinal bar : 24-28 mm bar Stirrup : 10 mm @ 6" c/c
	Column (C2)	21x 33 in	5th floor to roof	Longitudinal bar : 14-28 mm bar Stirrup : 10 mm @ 6" c/c
B.T.8.7	Column (C1)	24x30 in	Plinth level to roof	Longitudinal bar : 20-25 mm bar Stirrup : 10 mm @ 6" c/c

Model ID	Column Type	Size	Position	Reinforcement Detail
B.T.8.10	Column (C1)	34x44 in	Plinth level to 4th floor	Longitudinal bar : 28-28 mm bar Stirrup : 10 mm @ 6" c/c
	Column (C2)	31x41 in	5th floor to roof	Longitudinal bar : 24-28 mm bar Stirrup : 10 mm @ 6" c/c
B.T.9.7	Column (C1)	24x30 in	Plinth level to roof	Longitudinal bar : 20-25 mm bar Stirrup : 10 mm @ 6" c/c
B.T.9.10	Column (C1)	34x44 in	Plinth level to 4th floor	Longitudinal bar : 28-28 mm bar Stirrup : 10 mm @ 6" c/c
	Column (C2)	31x41 in	5th floor to roof	Longitudinal bar : 24-28 mm bar Stirrup : 10 mm @ 6" c/c
B.T.10.7	Column (C1)	24x36 in	Plinth level to roof	Longitudinal bar : 24-28 mm bar Stirrup : 10 mm @ 6" c/c
B.T.10.10	Column (C1)	34x44 in	Plinth level to 3rd floor	Longitudinal bar : 28-28 mm bar Stirrup : 10 mm @ 6" c/c
	Column (C2)	31x41 in	4th floor to roof	Longitudinal bar : 24-28 mm bar Stirrup : 10 mm @ 6" c/c
C.T.8.7	Column (C1)	24x28 in	Plinth level to roof	Longitudinal bar : 24-25 mm bar Stirrup : 10 mm @ 6" c/c
C.T.8.10	Column (C1)	24x36 in	Plinth level to roof	Longitudinal bar : 24-28 mm bar Stirrup : 10 mm @ 6" c/c
C.T.9.7	Column (C1)	24x28 in	Plinth level to roof	Longitudinal bar : 24-25 mm bar Stirrup : 10 mm @ 6" c/c
C.T.9.10	Column (C1)	24x36 in	Plinth level to roof	Longitudinal bar : 24-28 mm bar Stirrup : 10 mm @ 6" c/c
C.T.10.7	Column (C1)	24x28 in	Plinth level to roof	Longitudinal bar : 24-25 mm bar Stirrup : 10 mm @ 6" c/c
C.T.10.10	Column (C1)	24x36 in	Plinth level to 4th floor	Longitudinal bar : 24-28 mm bar Stirrup : 10 mm @ 6" c/c
	Column (C2)	21x 33 in	5th floor to roof	Longitudinal bar : 14-28 mm bar Stirrup : 10 mm @ 6" c/c

Table A.1.4 demonstrates reinforcement details of beams for all models.

Table A.1.4: Reinforcement Details of Shear Wall

Model ID	Shear Wall Thickness	Position	Reinforcement Detail
All model	203 mm (8 inch)	Plinth level to 4th floor	Longitudinal bar : 20 mm bar @ 100 mm c/c Horizontal bar : 16 mm @ 200 mm c/c
		5th floor to roof	Longitudinal bar : 20 mm bar @ 200 mm c/c Horizontal bar : 16 mm @ 200 mm c/c

APPENDIX B

DUAL SYSTEM CHECK

The frame capacity to resist seismic base shear for all model types are presented here.

Table B.1.1 shows total seismic base shear and maximum base shear resistance by frame capacity for all models.

Table B.1.1: Dual System Check

Model ID	Total Base Shear (kN)		Base Shear resistance capacity of column (kN)		Base Shear resistance capacity of column (%)	
	X-direction	Y-direction	X-direction	Y-direction	X-direction	Y-direction
A.L.8.7	-7642.81	-7642.80	-4400.80	-2444.87	57.58	31.99
A.L.8.10	-11250.23	-11250.24	-6493.71	-4329.14	57.72	38.48
A.L.9.7	-8060.95	-8060.94	-5039.32	-3488.74	62.52	43.28
A.L.9.10	-11521.62	-11521.58	-5547.13	-3328.25	48.15	28.89
A.L.10.7	-8479.10	-8479.08	-4902.57	-3268.35	57.82	38.55
A.L.10.10	-12117.49	-12117.49	-5845.06	-3507.06	48.24	28.94
B.L.8.7	-6134.41	-6134.41	-2621.82	-2039.21	42.74	33.24
B.L.8.10	-9236.86	-9236.87	-4845.21	-3523.81	52.46	38.15
B.L.9.7	-6454.59	-6454.59	-2765.90	-1843.93	42.85	28.57
B.L.9.10	-9692.82	-9692.81	-5095.99	-2779.60	52.57	28.68
B.L.10.7	-6855.55	-6855.55	-3928.44	-2618.94	57.30	38.20
B.L.10.10	-10148.78	-10148.76	-5832.83	-3888.51	57.47	38.32
C.L.8.7	-6020.17	-6020.16	-3378.03	-2251.99	56.11	37.41
C.L.8.10	-8554.78	-8554.78	-3658.61	-2439.06	42.77	28.51
C.L.9.7	-6230.18	-6230.18	-3554.45	-2369.64	57.05	38.03
C.L.9.10	-9003.55	-9003.55	-3860.55	-2573.71	42.88	28.59
C.L.10.7	-6572.71	-6572.72	-3758.74	-2505.86	57.19	38.13
C.L.10.10	-9375.02	-9375.02	-4027.72	-2685.16	42.96	28.64